Titre: Title:	A 2d Decoupled Hydro-Sedimentary Tool Using Total Load Approach
Auteur: Author:	Elodie Jesus Mellado Navarro
Date:	2025
Type:	Mémoire ou thèse / Dissertation or Thesis
Référence: Citation:	Mellado Navarro, E. J. (2025). A 2d Decoupled Hydro-Sedimentary Tool Using Total Load Approach [Thèse de doctorat, Polytechnique Montréal]. PolyPublie. https://publications.polymtl.ca/65831/

URL de PolyPublie: PolyPublie URL:	https://publications.polymtl.ca/65831/
Directeurs de recherche: Advisors:	Tew-Fik Mahdi
Programme: Program:	Génie civil

POLYTECHNIQUE MONTRÉAL
affiliée à l'Université de Montréal

A 2d decoupled hydro-sedimentary tool using total load approach

ELODIE JESUS MELLADO NAVARRO
Département des génies civil, géologique, et des mines

Thèse présentée en vue de l'obtention du diplôme de *Philosophiæ Doctor*
Génie civil

April 2025

POLYTECHNIQUE MONTRÉAL
affiliée à l'Université de Montréal

Cette thèse intitulée :

A 2d decoupled hydro-sedimentary tool using total load approach

présentée par **Elodie Jesus MELLADO NAVARRO**
en vue de l'obtention du diplôme de *Philosophiæ Doctor*
a été dûment acceptée par le jury d'examen constitué de :

Ahmad SHAKIBAEINIA, président
Tew-Fik MAHDI, membre et directeur de recherche
Elmira HASSANZADEH, membre
Ousmane SEIDOU, membre externe

DEDICATION

À Dieu, à ma famille, et mes amis,
à qui je dois tout. . .

ACKNOWLEDGEMENTS

Communication and mutual support are invaluable treasures that we, as human beings, possess. Throughout my journey, I have been fortunate to encounter individuals who dedicated their time to support me during some of the most challenging moments of my life. My doctoral experience has been filled with a range of emotions, and I would like to express my gratitude to those who have stood by me.

First and foremost, I want to thank my research director at the Université Polytechnique de Montréal, professor Tew-Fik Mahdi. His guidance and support allowed me complete this work. I sincerely appreciate the invaluable help and advice he provided, and I am deeply grateful for his mentorship.

I would also like to acknowledge the Natural Sciences and Engineering Research Council of Canada (NSERC) for partially funding this research.

I would like to express my sincere gratitude the members of the jury, for kindly agreeing to serve as reviewers of this work.

Finally, I want to express my heartfelt thanks to my parents and my sister. Without their continuous support, my presence here today would not have been possible.

I would like to extend a special thanks to my cousin Philippe as well as my friends and colleagues from Polytechnique for their support.

RÉSUMÉ

Le transport des sédiment est un phénomène complexe à être étudié en laboratoire en raison des nombreuses variables en interaction. La modélisation permet une compréhension plus approfondie de ce phénomène. Bien que plusieurs modèles de transport des sédiments soient disponibles sur le marché, ils sont souvent des modèles commerciales dont l'utilisateur n'a pas accès au code source, ce qui limite leur développement et de tester de nouvelles techniques.

La modélisation du transport des sédiments est essentielle pour prédire son impact sur la population et l'environnement lors d'interventions fluviales. Le développement de cet outil aidera donc les autorités locales à atténuer, prévenir, et contrôler les conséquences du transport des sédiments aux rivières.

Le modèle STR2D (Sediment Transport in Rivers in 2D) est la suite de Shallow Fluent, développée par l'institut d'accueil, dont un module de transport de sédiments a été ajouté. Il résout les équations bidimensionnelles régissant le transport hydro-sédimentaire de manière découplée, en utilisant l'approche de transport combinée. Il prend en compte les effets des flux secondaires, permettant ainsi de simuler des événements tels que des ruptures de barrages et des inondations. Le module hydrodynamique de STR2D est un modèle bidimensionnel en volumes finis qui sauvegarde les variables au centre des cellules. Les équations de conservation de masse et de continuité sont résolues à l'aide de l'algorithme itératif SIMPLE (Semi-Implicit Method for Pressure Linked Equations).

Les travaux actuels portent sur le développement de l'approche du transport combinée développée par Greimann. Cette approche utilise une équation d'advection-diffusion pour modéliser le transport en suspension et en charriage. Ceci lui permet d'utiliser moins de paramètres d'entrée et d'hypothèses que d'autres modèles de transport sédimentaire, ce qui la rend simple, pratique et performante.

Cette thèse présente la vérification, l'étalonnage et la validation de STR2D. Une vérification et validation numérique est realisée en utilisant le modèle SRH2D (Sedimentation and River Hydraulics—Two-Dimension Model), développé par le Bureau of Reclamation des États-Unis.

Un cas expérimental réalisé à l'Université de Zurich est utilisé pour calibrer et valider le modèle. La vérification numérique est simplifiée en utilisant une composition sédimentaire uniforme du lit.

La vérification numérique vise à évaluer la capacité de STR2D à modéliser un comportement similaire à celui d'un modèle existant et commercial tel que SRH2D. Deux scénarios seront

analysés. Le premier considère un écoulement entrant saturé de sédiments. Le second scénario considère que l'écoulement n'est pas saturé de sédiments. Les deux scénarios montrent une bonne similitude entre STR2D et SRH2D concernant l'évolution du lit et la concentration traversant le chenal.

Lors de la validation, quatre paramètres sédimentaires ont été étudiés pour évaluer leur impact sur la composition du lit : la condition entrante de l'écoulement, le *hiding-exposure effect*, la longueur d'adaptation et l'épaisseur de la couche active. Le processus d'étalonnage a permis de mieux comprendre l'influence de chacun de ces paramètres sur la composition du lit. La pente finale expérimentale du lit est de 0.24% tandis que SRH2D et STR2D ont simulé une pente finale à 0.233%. En conclusion, STR2d présente des résultats cohérents et comparables aux résultats expérimentaux. Les résultats nous laissent croire à l'efficacité d'utiliser STR2D à résoudre des problèmes d'ingénierie.

ABSTRACT

Sediment transport is a complex phenomenon that must be studied in a laboratory setting due to the numerous interacting variables. A deeper understanding of this phenomenon can be achieved through modeling. While several sediment transport models are commercially available, in which the source code is not available, which limits further development. Modeling sediment transport is important for predicting its impact on the population and the environment when river interventions are made.

Therefore, developing this tool will assist local authorities in mitigating the consequences of sediment transport. STR2D (Sediment Transport in Rivers in 2D) is an updated version of Shallow Fluent developed at the host institute, with an added sediment transport module. It solves two-dimensional hydro-sediment transport governing equations in a decoupled manner using the joint method. It considers secondary flow effects, enabling simulations of events like dam breaks and floodings. The hydrodynamic module of STR2D is a two-dimensional model using a collocated finite volume scheme. The continuity and the momentum equations are solved using the iterative Semi-Implicit Method for Pressure Linked Equations algorithm (SIMPLE).

The current work involves developing the joint method using one advection-diffusion equation to model suspended and bed loads. This approach uses fewer input parameters and hypotheses than most sediment transport models, thus rendering it simple, practical, and computationally efficient.

This thesis presents the verification, calibration, and validation of STR2D against SRH2D (Sedimentation and River Hydraulics—Two-Dimension Model), developed by the U.S. Bureau of Reclamation. These comparisons are based on numerical and experimental benchmarks performed at Zurich University.

The verification process aims to assess STR2D's capability to model behavior comparable to that of SRH2D in both non-equilibrium and equilibrium states. Therefore, the verification process simplified the experimental benchmark using uniform sediment as the bed composition. Two scenarios were performed in the verification analysis: one where sediment concentration is not injected at the inlet (representing a non-equilibrium state) and another where sediment is injected reaching water capacity (representing an equilibrium state). Both scenarios showed good agreement between STR2D and SRH2D regarding the bed change and the concentration traveling through the channel.

The validation process calibrated four sediment parameters: the inlet condition, the hiding-exposure effect, the adaptation length, and the active layer's thickness. The calibration process permitted to enhance the understanding of the influence of each over the bed composition and to ultimately be able to obtain results that correlate with the experimental results. The final experimental bed slope was measured as 0.24% and SRH2D and STR2D modeled a final slope of 0.233%. Overall, the results provide positive feedback on using STR2D to solve engineering problems.

TABLE OF CONTENTS

LIST OF TABLES

LIST OF FIGURES

LIST OF SYMBOLS AND ACRONYMS

Nomenclature

AD	Advection-Diffusion
2D	Two-dimensional
2DA	Two-dimensional depth-averaged
SMS	Surface-water Solution software
SF-Fluent	Name of the 2DA hydrodynamic module
STR2D	Sediment Transport in Rivers 2D
SWE	Shallow Water Equations
STE	Sediment Transport Equation
S_e	Source term of sediment transport governing equation
C^{n+1}	Intermediate sediment concentration for time step n+1
C^n	Depth-averaged real sediment concentration for time step n
β	Ratio of sediment-to-flow velocities
V_t	Depth-averaged flow velocity
h	Water height (m)
x, y	x and y directions
D	Mixing coefficients of sediments
f	Sediment transport mode parameter
σ	Porosity or sometimes p
ω_s	Sediment fall velocity
F	Fall velocity parameter
$\vec{u}$	Velocity vector
R_e	Reynold number
μ_t	Turbulent dynamic
g_s	Gravitational acceleration
γ_s	Specific weight of sediment
ν	Kinematic viscosity
d_{mean}	Geometric diameter
V_v	Volume of voids
V_t	Total volume (voids and sediment)
p	Porosity or σ
p	may refer also to bed-material gradation
γ_m	Dry specific weight

γ	Specific weight of water
N	Active layer calibration parameter
V_t	Magnitude of velocities in the x and y directions
V_s	Magnitude of sediment velocity
α	Sediment transport direction
V_t	Sediment velocity
β	Ratio of sediment velocity with respect to water velocity
κ	Von Karman coefficient
Z	Suspension parameter or refer to bed elevation
θ	Shields parameter
τ	Shear stress
s	Specific gravity or SG
ϕ	Ratio of $\frac{\theta}{\theta_r}$
δ^*	Direction of the bed shear stress of the flow with secondary flow
$\Delta\delta$	Deviation of bed shear stress relative to the streamline caused by the helical secondary flow only
C_f	Friction coefficient
$\alpha^{'}$	Coefficient for rough or smooth bed
ρ	Water density
ϵ	Calibration coefficient
AA	Temporary variable
BB	Temporary variable
L	Adaptation length
q	Unit discharge
ζ	Suspended sediment coefficient
ϖ	
η	Relative roughness heigth
C_{sl}	Model constant
E	Erosion flux
D	Deposition flux
t	Time
ϵ_s	Turbulent diffusivity of the sediment
m	Active layer thickness
a_0, a_j	Coefficients in the discretized equations
$C_{j,k}$	Volumetric flux at the cell face s_j

$CalParam$	Calibration parameter for coupling hydrodynamic and sediment modules
u_*	Shear velocity
R_c	Local radius of curvature flow streamlines or R
h_f	Hiding-exposure effect
Δ	Difference
cs	Control surface
cv	Control volume
$\forall$	Volume

Subscripts

n	Time step
sus	suspension load or s
bed	bed load or b
r	reference
t	total or tot
x	x-direction
y	y-direction
2	second
k	Sediment size class
50	50% finer
90	90% finer
w	water
geo	geometric

Superscripts

a	Active layer
$*$	Equilibrium state or eq
ref	reference

Softwares

SMS	Surface Water Solution
SRH-2D	Sedimentation and River Hydraulics in 2D

STR-2D	Sediment Transport in Rivers in 2D - Sediment Module presented in this thesis
TELEMAC-2D	Open TELEMAC-MASCARET SYSTEM

LIST OF APPENDICES

CHAPTER 1 INTRODUCTION

An increase in sediment of 460% has been reported since 1950 on the water surface due to anthropogenic activities [4, 5]. Flood seasons [6] and construction performed in sediment-laden rivers [7] contribute to the increased presence of sediment. This can decrease the reservoir's capacity and provoke a dam failure, as occurred at the Barlin dam in Taiwan in 2007 [4, 8]. Additionally, it can damage hydraulic equipment in hydropower plants, such as turbines, due to sediment abrasion, resulting in efficiency losses, frequent maintenance, and shutdowns of the hydropower plants [4]. Furthermore, it can negatively impact water quality and aquatic life, as per the regulation of the Minister of the Environment, the Fight Against Climate Change, Wildlife and Parks, which states that sediment suspension concentration should be lower than 25 g/l [7, 9]. Anthropogenic activities such as the construction of a dam alters the hydraulic condition of a river and becomes a sediment trap [10] which result in the reduction of sediment downstream and lead to : bank erosion for an extend of several kilometers downstream of the dam [11, 12] and the degradation of low-lands [5, 13]

Understanding the impact of sediment transport in hydraulics is important to help prevent issues that may arise from it. Modelling sediment transport in hydraulics can assess sediment-water quality and help prevent sediment-related problems. Sediment transport is a dynamic and complex process whose mechanisms are not yet fully understood.

There are three main ways, according to the literature, that sediment is transported: wash-load, suspended-load, and bed-load [14]. Wash-load consists of very fine particles, and its effect is negligible on the bed evolution; hence, it is normally ignored when modelling sediment transport [14]. There are typically two methods used to model sediment transport.

One method is called the two-layer approach (also known as the separation method [15]), in which the suspended load and the bed-load are modelled separately. Usually, the advection-diffusion equation [14] is employed for suspended load and the Exner equation [16,17], which is a mass-conservation equation, is used for the bed-load. Most models, such as Gaia, which is the sediment transport model of Telemac [18], Delft3D [19], and BASEMENT [20], use the two-layer method [16, 18, 21] to model sediment transport. The two-layer method primarily considers an equilibrium state occurring at the interface where both sediment governing equations interact [15,22]. According to [22], this is an acceptable hypothesis for experimental cases but is not applicable to engineering practices, as this hypothesis does not hold when a flood wave passes through. The separation method is computationally demanding [15,23,24] since it needs to solve several equations and it considers multiple parameters.

The other method is the joint method which lumps the bed load and suspended load together, referred to them as bed-material, and uses a single sediment transport governing equation, which can take the form of either an advection-diffusion equation or an Exner equation [15]. The joint method is considered to be less computationally intensive, although it sacrifices accuracy [15], as it does not model both sediment transport modes. A recent joint method developed by Greimann uses a depth-averaged sediment concentration made up of advection and diffusion terms. This method integrates a parameter called the sediment transport mode, f, which allows shifting between suspended load, mixed load, and bed-load; hence, it does not compromise accuracy compared to other joint methods. Therefore, a bidimensional sediment transport model called Sediment Transport in Rivers in 2D (STR2D) has been developed at Ecole Polytechnique de Montréal to further investigate the mechanisms of sediment transport using the joint method.

This thesis is divided into seven chapters followed by three appendices that the reader can refer for further information.

- Chapter 1 - Introduction: the present chapter.
- Chapter 2 - Literature review: This chapter explains the hydrodynamic and the sediment transport concepts, followed by an overview of existing 2d hydro-sedimentary models.
- Chapter 3 - Methodology: It presents the important steps of the proposed 2D numerical hydro-sedimentary transport model.
- Chapter 4 - Model presentation: This chapter presents the details of the steps presented in the methodology.
- Chapter 5 - Results and Discussion: This chapter presents the results of verifying STR2D with SRH2D, calibrating four sediment transport parameters using SRH2D, and validating both models against the experimental results conducted at Zurich University.
- Chapter 6 - General Discussion: This chapter goes over the model presented, and the more important insights.
- Chapter 7 - Conclusion and perspective: This chapter summarizes the completed work, highlights its limitations, and discusses the future work.
- Appendix A: STR2D input variables

- Appendix B: SMS User's Manual
- Appendix C: Mathematical proof of the real concentration computation

The main objective of this research is to develop a 2D decoupled hydro-sedimentary model called Sediment Transport in Rivers 2D (STR2D), which will enable the development of the sediment transport mode, f, developed by Greimann for sediment transport.

The specific objectives are as follow:

- Define an enhanced sediment transport mode parameter, f
- Develop a bed stratification representation of the riverbed considering active layer, δ_a
- Implement riverine parameters in STR2D model for non-uniform sediments such as adaptation length L_b, hiding-exposure effect h_f, and sediment class k
- Develop an algorithm of sediment material cell-node distribution

Greimann has developed an approach to model sediment transport using a sediment transport mode, f, in a depth-averaged sediment transport equation. This thesis proposes a 2D hydro-sedimentary model as a tool for continuing development on sediment transport, such as the implementation of an enhanced sediment transport mode, f.

CHAPTER 2 LITERATURE REVIEW

Water flow on a mobile bed tends to carry sediment particles. The first and second following sections will be dedicated to explain the physical properties of water flow and of sediment particles.

2.1 Sediment transport

2.1.1 Modes of sediment transport

According to the literature, water flow can transport sediments in three distinct ways: bed load, suspended load, and wash load. The latter is neglected because it has minimal impact on bed deformation. The bed load refers sediments transported near the bed. They can roll, jump, or even slide over the bed. On the other hand, the suspended load, are sediments that are generally suspended by the turbulence of the flow. Hence, most models uses different governing equations to model the different mode of sediment transport usually dividing the flow into two or more layers. The most common model uses the two layer approach.

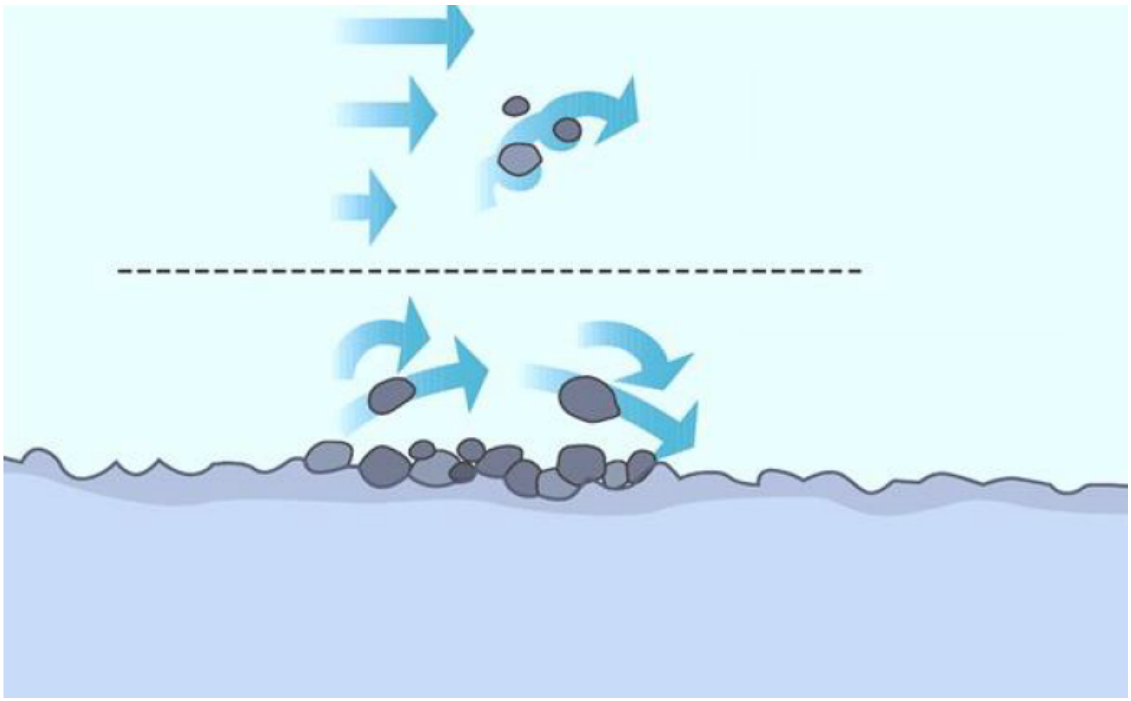

Figure 2.1 Modes of sediment transport: bed load and suspended load (adapted from [1])

2.1.2 Properties of sediment

Four sediment properties—size, density, shape, and fall velocity—are important for modeling sediment transport. Given the diverse shapes found in river beds, determining the size of particles is a complex task beyond mere diameter. Instead, other sediment properties, such as fall velocity, can better reflect the sediment size indirectly. A sediment grade scale [25] can help determine the sediment types, such as clay, silt, sand, gravel, cobbles, and boulders, based on a range of diameters. Moreover, among these sediment types, there exist distinct categories: cohesive and noncohesive sediments. Sand, gravel, cobbles, and boulders are noncohesive sediments, whereas clay and silt are considered cohesive sediments because they have a diameter equal to or less than 62.5 μm.

Sediment density, which depends on the type of rocks it originates from and its mineral composition, is the next key factor introduced. Clay minerals range from 2500 to 2700 kg/m^3. Other heavier minerals may have a density greater than 2850 kg/m^3. Quartz is the predominant mineral encountered in rivers; hence, the average density can be assumed to be 2650 kg/m^3 for practical purposes. Hence, a specific gravity of 2.65 is usually used.

The shape of sediment is a crucial determinant of its sediment-carrying velocity, fall velocity, bed load transport, and porosity. A flat particle, for instance, has a slower fall velocity and is more resistant to flow transport than a more rounded particle. The shape of a sediment can be characterized by sphericity, roundness, and shape factor. The shape factor, in particular, is highly practical for application. For natural particles, the shape factor typically falls between 0.6 and 0.7. A sphere, for instance, would have a shape factor of 1.0, while natural sands typically have a shape factor of 0.7 [26].

The fall velocity, ω_s, is the speed a sediment particle falls in a still water column. Several factors, including the Reynolds number, shape factor, sediment concentration, and turbulence, affect the fall velocity. For practical purposes, the fall velocity can be determined using a relation to the shape factor, water temperature, and sediment size as described by Lane and al. [26,27] or from empirical equations [28]. Equation 2.1 computes the fall velocity for gravel, sand and silt particles for diameter greater than 1 mm where F is equal to 0.79 for a water temperature between 10°C and 25°C. F is the fall velocity parameter, d is the sediment diameter, g is the gravitational acceleration, γ_s is the specific weight of sediment, and γ is the specific weight of water.

$$\omega_s = F \left[dg \left(\frac{\gamma_s - \gamma}{\gamma} \right) \right]^{\frac{1}{2}} \tag{2.1}$$

For smaller grain size Equation 2.2, F can take the following expression where ν is the kinematic viscosity.

$$F = \left(\frac{2}{3} + \frac{36\nu^2}{gd^3\left(\frac{\gamma_s}{\gamma} - 1\right)}\right)^{0.5} - \left(\frac{36\nu^2}{gd^3\left(\frac{\gamma_s}{\gamma} - 1\right)}\right)^{0.5} \tag{2.2}$$

The sediment velocity can take the following expression for particles sizes greater than 2.0 mm.

$$\omega_s = 3.32 * d^{\frac{1}{2}} \tag{2.3}$$

2.1.3 Bulk properties of sediment

Understanding the properties of a single sediment is essential to comprehend the properties of a group of sediment particles found in rivers of varying sizes and characteristics [29]. Samples are collected from the rivers under study and analyzed to examine their properties.

For such a study, a sieve analysis can be performed, in which, the samples are statistically analyzed, and the data can be presented in various ways to extract as much information about the sample. The cumulative frequency curve is a useful data representation used in sediment transport modeling to represent the bed composition, which has an S-shaped curve. On the ordinate axis, the percentage of sediment finer than a given size, while the sediment size is shown in the abscissa. This presentation of the data is useful to obtain information on the median size, d_{50} and d_{90}. The d_{50} can be used to compute the thickness of the active layer as mentioned earlier, or it can be used to compute the porosity of a sample. For example, the d_{90} is used to calculate the Manning coefficient for a sand mixture.

$$n = \frac{d_{90}^{1/6}}{26} \tag{2.4}$$

In modeling, the cumulative frequency curve also known as the gradation curve is divided in sediment classes, k. A sediment class is a range of diameter of sediment with a low and an upper boundary. The lower boundary can be expressed as d_{min} and the upper boundary as d_{max}. It is recommended to have more sediment classes for fine sediment than coarser sediment [23].

$$d_{min} = 2^a \tag{2.5}$$

$$d_{max} = 2^b \tag{2.6}$$

where d_{min} is the minimum diameter in the gradation curve and d_{max} is the maximum diameter. Hence, a and b can be computed. Then, it is possible to define the low and high boundaries of each class where N represent the number of classes. The following equations are guidelines to obtain the boundaries of sediment classes based on a logarithm space:

$$d_{low,k} = 2^{a+(k-1)\frac{b-a}{N}} \tag{2.7}$$

$$d_{up,k} = 2^{a+k\frac{b-a}{N}} \tag{2.8}$$

where N represents the number of classes and k the sediment class. Each sediment class are defined by its mean diameter and can be computed as follow [23]:

$$d_{mean,k} = \sqrt{d_{low,k} \star d_{up,k}} \tag{2.9}$$

Moreover, the gradation curve allows to obtain the percentage of sediment associated to a sediment class. It represents the amount of the sediment class in the sample which is also known as the volume of fraction.

Another parameter that can be extracted from the sample is the porosity. Porosity is the ratio of volume of void per unit volume of sediment where V_v is the volume of voids, V_t is the total volume (voids and sediment), and V_s is the volume of sediment. It allows to compute the volume of sediment deposition.

$$p = \frac{V_v}{V_t} = \frac{V_t - V_s}{V_t} = 1 - \frac{V_s}{V_t} \tag{2.10}$$

It is useful to convert from volume with voids and volume of sediment without voids.

$$V_t = \frac{V_s}{1-p} \tag{2.11}$$

There are empirical equation to compute the porosity of unconsolidated saturated material such as: [30]:

$$p = 0.245 + 0.14 * d_{50}^{-0.21} \tag{2.12}$$

where d_{50} is the median size in mm and applicable for diameters from 4×10^{-4} mm to 80 mm. P is the porosity. Equation 2.12 has been modified by Wu [31].

$$p = 0.13 + 0.21 * (d_{50} + 0.002)^{-0.21} \tag{2.13}$$

The porosity allows to compute parameters such as the dry specific weight γ_m as follow:

$$\gamma_m = \gamma G(1 - p) \tag{2.14}$$

where γ is the specific weight of water at 4°C, G is the specific gravity (by default 2.65) and p is the porosity of the sediment [23]. The specific weight is defined as the dry weight per unit volume of sediment. The specific weight of deposited material depends on consolidation and the size of the sediment. Consolidation is mostly important for reservoirs, whereas the initial specific weight, which depends on the size, provides a good approximation for rivers. The initial specific weight tends to increase as the sediment size increases [32].

2.1.4 Bed composition

Due to the change in vertical composition caused by historical sedimentation of the riverbed, it is convenient for models to divide the riverbed into several layers [14]. This way, if necessary, each layer can be specified with a different composition. Therefore, the user must initially specify the number of layers, the layer's thickness, the composition, and the elevation of each layer. The determination of the composition of the bed has already been discussed in the previous section through the use of sediment classes, porosity, and volume of fraction.

The uppermost layer is called the active layer and is also known as mixing layer by Wu [33]. The active layer is a layer that is actively and constantly interacting with the flow [24, 33]. It receives material from the flow when there is deposition and gives material to the flow when there is erosion. The active layer can also limit the erosion if it has given all its material which is known as availability limited [34]. In addition, the active layer can armor the bed when the flow carries the finest sediments and leaves the coarser sediments. When the flow is not strong enough to carry the material present in the active layer, it referred to as capacity limited. The thickness of the active layer is based on empirical equations as shown in Table 2.1, because it depends on the material. Therefore, the active layer's depth can be used as a calibration parameter by varying N.

Table 2.1 Empirical equations for Active Layer's Thickness

Empirical equations	Active layer thickness, δ_s
Van Rjin (1984)	$0.5*$ sand dune height
Bennett and Nordin	$N * d_{50}$
SRH2D	$N * d_{90}$

Throughout the simulation, the mass of the active layer remains unchanged. The layer beneath the active layer, also known as the second layer plays an indirect role but, as important as the active layer for the bed evolution. The purpose of the second layer, is to receive any excess material when there is deposition from the active layer, to keep its mass constant during the simulation. Furthermore, when there is erosion, the second layer provides the necessary amount of material when the active layer has been depleted, again to ensure the mass of the active layer remains constant at every time step.

Models differ in how the active layer behaves upon receiving material from deposition. In Wu [33], the newly deposited material is initially mixed with the active layer, and then the excess is mixed with the second layer. Hence, the active layer's composition, as well and the second layer's composition and thickness need to be updated. Similarly, Bennett and Nording also propose to initially mix the deposited material with the active layer. However, they recommend a layer beneath the active layer called the inactive deposition. The inactive deposition is not mixed with the layer forming the bed. In addition, the inactive deposition provides material to the active layer when needed, the other layer beneath will provide as well.

Sediment transport is the result of the dynamic interaction of water flow, sediment transport, and bed evolution [35]. Each of these categories have their own intrinsic characteristics which is influenced by the interaction with the other components.

2.1.5 Sediment transport capacity

The sediment transport capacity is the maximum amount of sediments that can be carried by a specific flow without eroding or depositing material unto the bed. When that maximum capacity is reached, the water flow is said to have reached its equilibrium state. Both the water flow and bed conditions have sediment transport capacity. Nonetheless, the water flow's sediment transport capacity depends on the local flow. The equilibrium state is a difficult state to attain for rivers and it is an idealised state can be obtained in controlled laboratory experiments. Rivers are normally in a non-equilibrium state, because of the change of flow and sediment conditions such as the water inflow and sediment inflow. However, rivers

are trying constantly to reach their equilibrium state. Table 2.2 presents some empirical equations computing the sediment transport capacity.

These sediment equations are continually updated. For instance, Meyer-Peter(1934) first developed the empirical equation and has been corrected to obtain the Meyer-Peter-Muller (1948)'s equation, then Meyer-Peter-Muller (2006) [36], and Meyer-Peter-Muller(2010) [37]. Some of the most used empirical sediment transport equations presented in Table 2.2 have their limitations due to the difficulty of controlling some parameters in the laboratory, the assumptions made, and their range of application.

Table 2.2 Sediment Transport Capacity Empirical Equations

Sediment Transport Equations	Finest Limit	Coarsest limit	Approach	Type
Meyer-Peter and Muller (1948)	NA	NA	NA	Bed load
Laursen (1958)	Clay	100	NA	Bed-material total load
Laursen-Madden(1993)	Clay	100	NA	Bed-material total load
Toffaleti (1969)	Sand	10	Einstein	Bed-material total load
Engelund and Hansen (1972)	Clay	10	Power	Bed-material total load
Ackers and White (1973)	Clay	100	Power	Bed-material total load
Ackers and White (1990))	Clay	100	Power	Bed-material total load
Yang (1973) + Yang (1984)	Clay	100	Power	Bed-material total load
Yang (1979) + Yang (1984)	Clay	100	Power	Bed-material total load
Yang et al. (1996)	Clay	100	Power	Bed-material total load
Ashida and Michiue (1972)	Clay	100	NA	NA
Parker(1990)	NA	NA	NA	Bed load
Brownlie (1981)	NA	NA	NA	Bed-material total load

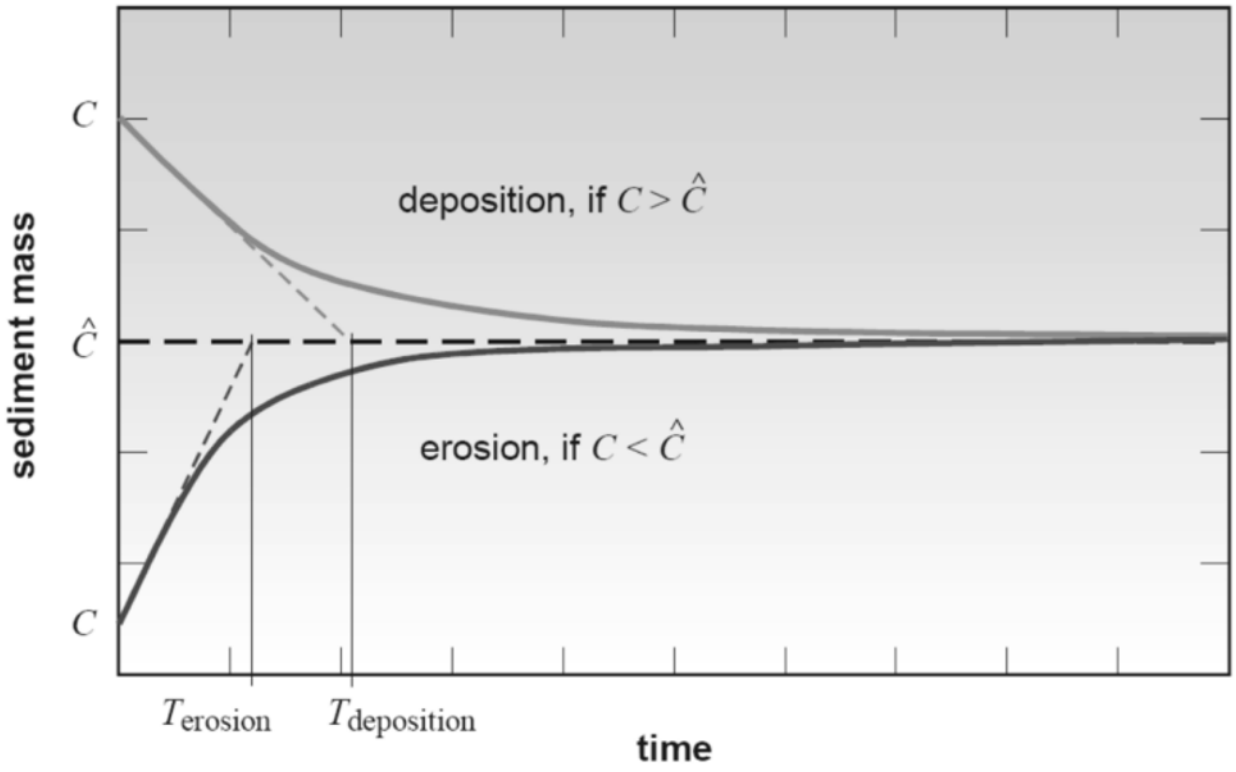

Figure 2.2 Temporal lag from non-equilibrium state to equilibrium state (adapted from [1])

2.1.6 Hiding-exposure effect

An alluvial bed consists of sediments of various sizes. Larger sediments on the riverbed are more likely to be transported by the water flow, while smaller particles can often be hidden beneath the larger ones. To address this, the concept of the hiding-exposure effect [38]—a coefficient included in the equilibrium sediment transport equation—is used. This factor reduces the bed shear stress for larger particles while increasing it for smaller ones. There are different empirical equations available to model this behavior. An empirical factor is added to account for this effect in the empirical sediment transport presented in Table 2.2.

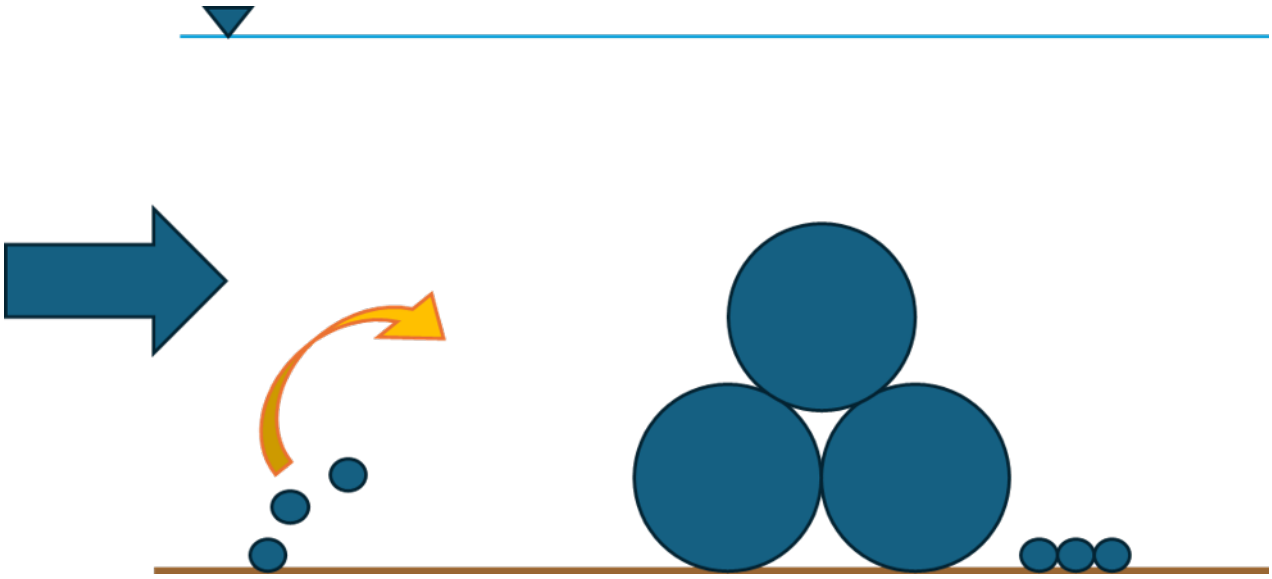

Figure 2.3 Hiding-exposure Effect

2.1.7 Secondary flows

River bends create secondary flows that affect sediment transport, as these sediments are influenced by both transverse and normal forces. The secondary flows increase the normal component of the bed shear stress. There are two ways to consider the secondary flows: gravitational and drag forces [39].

The transport direction models can be expressed this way:

$$\delta = \delta^* - \Delta\delta \tag{2.15}$$

where δ^* is the direction of the bed shear stress of the flow with secondary flow and $\Delta\delta$ is the deviation of the bed shear stress relative to the streamline caused by the helical secondary flow only.

The bed shear stress in the main flow direction used in Telemac is expressed as:

$$\tau_b = \frac{C_f}{2}\rho|\vec{u}|u \tag{2.16}$$

The bed shear stress of the flow used in the home code is as follow:

$$\tau_{bx} = \rho C_f u\sqrt{u^2+v^2} \tag{2.17}$$
$$\tau_{by} = \rho C_f v\sqrt{u^2+v^2} \tag{2.18}$$

where for Telemac $C_f = \frac{2gn^2}{h^{1/3}}$ and the home code $C_f = \frac{gn^2}{h^{1/3}}$.

$$|\tau_b| = \sqrt{(\tau_{bx})^2 + (\tau_{by})^2} \tag{2.19}$$

For telemac:

$$\tau^{sec_n} = \frac{C_f}{2}\rho\frac{Ah}{\alpha'}g|\vec{u}|\frac{1}{R} \tag{2.20}$$

For home code

$$\tau^{sec_n} = C_f\rho\frac{Ah}{\alpha'}g|\vec{u}|\frac{1}{R} \tag{2.21}$$

$$R_c = \frac{\alpha'|\vec{u}^2|}{g\partial Z_s/\partial n} = \frac{\alpha'|u|^3}{g(u\partial z_s/\partial y - v\partial z_z/\partial x)} \tag{2.22}$$

Its component:

$$\tau_x^{sec_n} = v\tau^{sec_n} \tag{2.23}$$
$$\tau_y^{sec_n} = -u\tau^{sec_n} \tag{2.24}$$

Its component:

$$\tau_x^{sec} = \tau_{bx} + \tau_x^{sec_n} \tag{2.25}$$
$$\tau_y^{sec} = \tau_{by} + \tau_y^{sec_n} \tag{2.26}$$

$$\cos\delta = \frac{\tau_x^{sec}}{|\tau^{sec}|} \tag{2.27}$$
$$\sin\delta = \frac{\tau_y^{sec}}{|\tau^{sec}|} \tag{2.28}$$

$$|\tau^{sec}| = \sqrt{(\tau_x^{sec})^2 + \left(\tau_y^{sec}\right)^2} \tag{2.29}$$

$$A = \frac{2\epsilon}{\kappa^2}\left(1 - \frac{\sqrt{g}}{\kappa C}\right) \tag{2.30}$$

The A used in the home code is

$$A = \frac{2}{\kappa^2}\left(1 - \frac{n\sqrt{g}}{\kappa h^{1/6}}\right) \tag{2.31}$$

$$AA = \sin\delta - \frac{1}{f(\theta)}\frac{\partial Z_b}{\partial y} \tag{2.32}$$

$$BB = \cos\delta - \frac{1}{f(\theta)}\frac{\partial Z_b}{\partial x} \tag{2.33}$$

$$norm = \sqrt{AA^2 + BB^2} \tag{2.34}$$

$$\sin\alpha = \frac{AA}{norm} \tag{2.35}$$

$$\cos\alpha = \frac{BB}{norm} \tag{2.36}$$

$$\tag{2.37}$$

$$\tan\alpha = \frac{\sin\alpha}{\cos\alpha} = \frac{AA}{BB} \tag{2.38}$$

Table 2.3 Summary of parameter A

Equation	A
Struiksma and al.	$\frac{2\epsilon}{\kappa^2}\left(1 - \frac{\sqrt{g}}{\kappa C}\right)$
Telemac	7.0
STR2D	$\frac{2}{\kappa^2}\left(1 - \frac{n\sqrt{g}}{\kappa h^{1/6}}\right)$

2.1.8 Two-layer approach

Most models use an advection-diffusion equation for the suspended load, which is applied from the water surface to the interface. The interface divides the suspended load and the bed load layers. Conversely, the Exner equation is applied to the bed; specifically, from the interface to the bed surface. The two governing equations has to consider a term source for the interaction between them at the interface. For example, it has to consider if a sediment was transported as a bed-load before is now transported as a suspended load or vice-versa.

This method assumes at the interface is at equilibrium state. This method is considered complex and slow.

2.1.9 Joint approach

Instead of adding hypotheses that impact the computation of the erosion and deposition, the present model uses the concept of joint method, which groups the bed load and suspended load which requires less hypotheses. The main reason this transport model was unpopular is that it could only be used for one sediment class. However, Greimann developed a way to consider several sediment classes [40].

$$\frac{\partial hC_k}{\partial t} + \frac{\partial(\cos\alpha_k)\beta_k V_t hC_k}{\partial x} + \frac{\partial(\sin\alpha_k)\beta_k V_t hC_k}{\partial y} = \frac{\partial}{x}\left(hf_k D_x \frac{\partial C_k}{\partial x}\right) + \frac{\partial}{y}\left(hf_k D_y \frac{\partial C_k}{\partial y}\right) + S_{e,k} \tag{2.39}$$

where $V_t = \sqrt{U^2 + V^2}$ is the magnitude of the velocities in the x and y directions, β_k represents the ratio of the sediment velocity, $V_{s,k}$, and the magnitude of the hydrodynamic velocity, V_t, α_k is called the sediment transport direction and D_x and D_y represent the mixing coefficient in the x and y directions.

In Equation 2.39, the sediment velocity, V_t is different from the total velocity V_k, but they are related by the parameter β, which is the ratio of these two velocities.

$$\beta_k = \frac{\sqrt{U_k^2 + V_k^2}}{\sqrt{U^2 + V^2}} = \frac{V_k}{V_t} \tag{2.40}$$

Furthermore, two distinct functions were developed in the laboratory for the bed and suspended load, β_{bed} and β_{sus}. There is a discontinuity in sediment velocity between bed load and suspended load layers. This issue is resolved by selecting the maximum of the two.

$$\beta_k = Max(\beta_{k,sus}; \beta_{k,bed}) \tag{2.41}$$

$$\beta_{k,bed} = \frac{U_*}{V_t} \frac{1.1\phi_k^{0.17}[1 - exp(-5\phi_k)]}{\sqrt{\theta_r}} \tag{2.42}$$

$$\beta_{k,sus} = 1 + \frac{u_\tau}{2\kappa V_t}[1 - exp(2.7Z)] \tag{2.43}$$

Equation 2.42 and Equation 2.43 are based on the assumption that the inertia of the sediment particle is not important. β_{bed} is a function where it is limited to $\phi < 20$ and is obtained

from a flume data from Francis and Hui [41,42] where the data ranges from $Z = 2$ to $Z = 50$. The function β_{sus} can be applied for $Z_{susp} < 1$ and it is based on the Rouse profile.

$$Z_k = \frac{w_s}{\kappa u_\tau} \tag{2.44}$$

The sediment transport mode parameter, f_k, a monotonically and non-linear function, makes the joint method unique in its approach to sediment transport modeling. This empirical factor can switch between the suspended and bed loads or vice versa without external interference. f_k varies between zero for pure bed load and one for pure suspended load. Hence, it can consider a mix load when the value is in between. However, the sediment transport mode parameter, f_k, is made of two functions developed in the laboratory for a rectangular channel eight feet long. In addition, it does not consider spatial and temporal lags from the transition of bed load to suspension load and vice versa.

$$f_k = min(1, 2.5e^{-Z}) \tag{2.45}$$

2.1.10 Bed evolution

A. Equilibrium and non-equilibrium states

Erosion and deposition are the main agents modifying the bathymetry of a river and are normally represented as a source term governing sediment transport equations as shown in Equation 2.46. These parameters are nonzero when the flow is in a non-equilibrium state. The sediment-water transport capacity, q^*_{tot}, can be compared to a bus with several seats, which depends on the sediment type and the flow condition. This parameter is determined through controlled laboratory experiments at an equilibrium, as discussed in Section 2.1.5 and sediment transport equation are presented in Table 2.2. When the flow is carrying less than its sediment-water transport capacity, q_{tot}, the flow will try to reach its equilibrium state by eroding the bed and the source term is negative. On the other hand, when the flow is carrying more than its capacity, q_{tot}, then sediments are deposited and the source term is positive. The source term is thus the rate of erosion for a sediment class, k, to achieve the equilibrium state.

$$S_{e,k} = \frac{1}{L_{tot}}(q^*_{tot} - q_{tot}) \tag{2.46}$$

where q^*_{tot} represents the sediment-water capacity at equilibrium and q_{tot} represents the actual total load transport rates. Previous sediment transport models assumed the sediment transport model to be at equilibrium state for rivers which is not representative of the reality.

The flow takes time and space to shift from a non-equilibrium state to equilibrium and it is considered through the use of an adaptation length. There are many empirical adaptation length equations depending on the type of sediments (sand or gravel). For suspended load the adaptation length is calculated in Equation 2.47.

$$L_{sus} = \frac{Uh}{\alpha w_s} = \frac{\zeta Uh}{\omega_s} \tag{2.47}$$

ζ was suggested by Han(1980) and He(1990) and varies between 0.25 to 1.0. Armanini(1988) proposed Equation 2.48.

$$\zeta = \eta + (1-\eta)exp(-1.5\eta^{-\frac{1}{6}}\varpi/u_\tau) \tag{2.48}$$

where $\eta = 33exp(-1-\kappa V_t/u_\tau)$. However, Equation 2.48 needs additional numerical and laboratory experiments to be validated.

SRH2D considers ζ to be a constant value.

The literature presents different values for the bed load adaptation length for L_{bed} because this parameter depends on the dominant bed form that influences the sediment transport. Consequently, the magnitude of this parameter can differ depending on whether the analysis is conducted in a laboratory or in a river.

Table 2.4 Empirical equations for adaptation length for bed load

Dominant bed forms	Adaptation length for bed load
Sand dune	5 to 10 times depth flow
Alternate bars	6.3 * channel width
Numerical	Grid spacing should be several times smaller than the adaptation length (1 to 2 times the grid spacing)

Philips and Sutherland provides another relationship for the adaptation length for bed load which depends on the critical shear stress.

$$L_{bed} = C_{sl}(\theta - \theta_c)d \tag{2.49}$$

where θ_c is equal to 0.045 and C_{sl} is equal to 4000.

According to the literature [15], the total load adaptation length, L_{tot} can be the maximum value between the adaptation length for bed load and the suspended load.

$$L_{tot} = \max(L_{bed}, L_{sus}) \tag{2.50}$$

Armanini and Di Silvio has proposed the following relation for the total adaptation length.

$$L_{tot} = \zeta V_t h / w_s \tag{2.51}$$

Or, it can be a weighted-average as proposed by Greimann [40]which allows to consider the mix load.

$$L_{tot} = (1 - f_k) L_{bed} + f_k * \zeta V_t h / w_s \tag{2.52}$$

2.2 Hydrodynamic

The Eulerian approach considers a control volume that is fix in time, in space and nondeforming and that a flux may enter or leave it. A control volume is a finite region of space which contains many fluid particles, fluid properties and characteristics which are normally average values [2]. It is a way to simplify by approximate a domain to answer engineering problems. The conservation of mass allows to track the fluid that goes through a control volume. Equation 2.53 is the conservation of mass equation expressed for a control volume.

$$\frac{\partial}{\partial t} \int_{cv} \rho d\forall + \int_{cs} \rho \vec{V} \cdot \vec{n} dA = 0 \tag{2.53}$$

where $\forall$ is the volume of the control volume; $\vec{V}$ is the vector of velocity; and A is one surface of the control volume. The first term from Equation 2.53 represents the mass accumulated in the control volume. The second term represents the mass flowrate that passes through the control volume.

A control volume is represented as a small and stationary cube element which is made of six control surfaces. In the x direction it is noted as Δx, Δy, and Δz.

$$\frac{\partial}{\partial t} \int_{cv} \rho d\forall \approx \frac{\partial \rho}{\partial t} \Delta x \Delta y \Delta z \tag{2.54}$$

where ρ is the water density. At the center of the element, it contains the fluid density ρ and the velocity in the x, y, and z directions which is denoted as u, v, and w respectively as

shown in Figure 2.4.

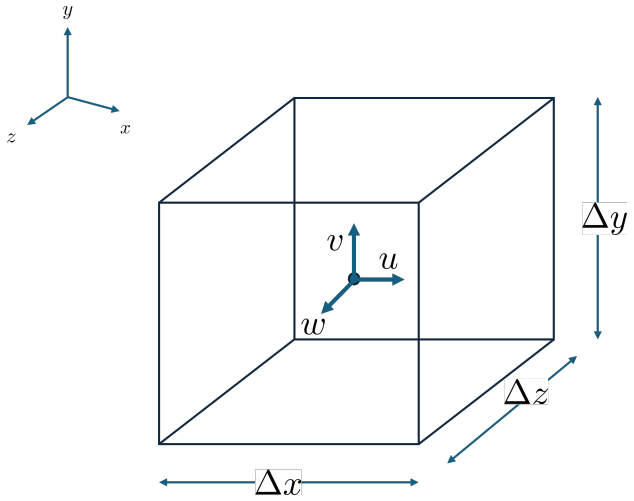

Figure 2.4 Differential element to develop the conservation mass equation [2]

As shown in Figure 2.5, the mass rate per unit area at the center of the cell is represented on the right face and on the left face.

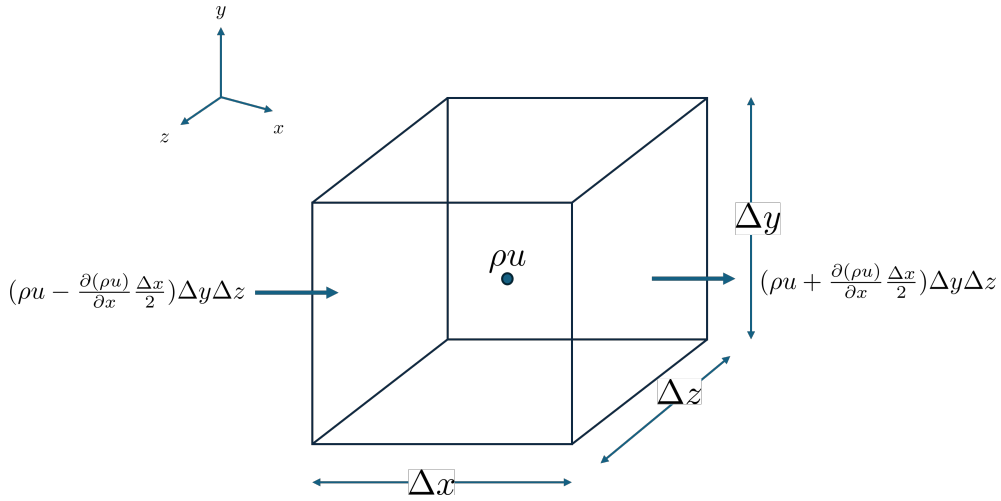

Figure 2.5 Example of the continuity equation in the x direction [2]

The result of these both expressions give:

$$\left[\rho u + \frac{(\rho u)}{\partial x}\frac{\Delta x}{2}\right]\Delta y \Delta z - \left[\rho u - \frac{(\rho u)}{\partial x}\frac{\Delta x}{2}\right]\Delta y \Delta z = \frac{\partial(\rho u)}{\partial x}\Delta x \Delta y \Delta z \tag{2.55}$$

This is done also for the y and z directions and it is obtained the conservation of mass equation as follow:

$$\frac{\partial \rho}{\partial t} + \frac{\partial \rho u}{\partial x} + \frac{\partial \rho v}{\partial y} + \frac{\partial \rho w}{\partial z} = 0 \tag{2.56}$$

There are two types of forces to consider: force from the weight of the control volume itself (F_b) and forces of the interaction of the control volume with its environment.

$$\frac{\partial}{\partial t}\int_{cv} \vec{V}\rho d\forall + \int_{cs} \vec{V}\rho\vec{V}\cdot\vec{n}dA = \sum \vec{F} \tag{2.57}$$

$$\Delta\vec{F}_b = \Delta m\vec{g} \tag{2.58}$$

where m is the mass of the control volume. The forces acting on the control surface by the environment are divided into two forces: shear (parallel) and normal forces.

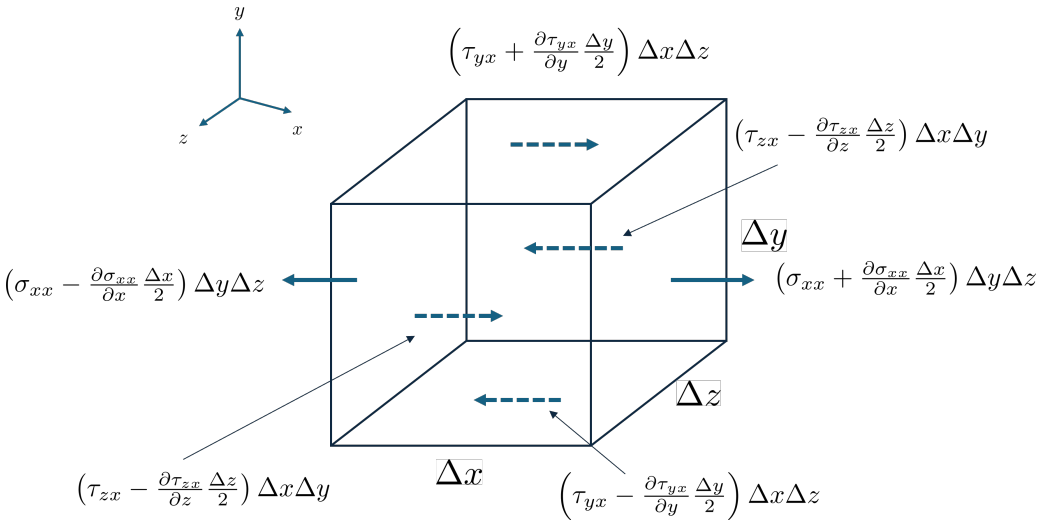

Figure 2.6 Example of the momentum equation in the x direction

In the x direction, it get the resultant force expressed as follow:

$$\Delta F_{sx} = \left(\frac{\partial \sigma_{xx}}{\partial x} + \frac{\partial \tau_{yx}}{\partial y} + \frac{\partial \tau_{zx}}{\partial z}\right)\Delta x\Delta y\Delta z \tag{2.59}$$

$$\rho g_x + \frac{\partial \sigma_{xx}}{\partial x} + \frac{\partial \tau_{yx}}{\partial y} + \frac{\partial \tau_{zx}}{\partial z} = \rho\left(\frac{\partial u}{\partial t} + u\frac{\partial u}{\partial x} + v\frac{\partial u}{\partial y} + w\frac{\partial u}{\partial z}\right) \tag{2.60}$$

$$\rho g_y + \frac{\partial \tau_{xy}}{\partial x} + \frac{\partial \sigma_{yy}}{\partial y} + \frac{\partial \tau_{zx}}{\partial z} = \rho\left(\frac{\partial v}{\partial t} + u\frac{\partial v}{\partial x} + v\frac{\partial v}{\partial y} + w\frac{\partial v}{\partial z}\right) \tag{2.61}$$

$$\rho g_z + \frac{\partial \tau_{xz}}{\partial x} + \frac{\partial \tau_{yz}}{\partial y} + \frac{\partial \sigma_{zz}}{\partial z} = \rho \left(\frac{\partial w}{\partial t} + u\frac{\partial w}{\partial x} + v\frac{\partial w}{\partial y} + w\frac{\partial w}{\partial z} \right) \tag{2.62}$$

where σ is the normal stress and τ is the shear stress; and u, v, and w are the x, y, and z components of velocity. To incorporate the viscous effects, the following stress-deformation relationships must be considered. These are the relationships for the normal stresses:

$$\sigma_{xx} = -p + 2\mu\frac{\partial u}{\partial x} \tag{2.63}$$

$$\sigma_{yy} = -p + 2\mu\frac{\partial v}{\partial y} \tag{2.64}$$

$$\sigma_{zz} = -p + 2\mu\frac{\partial w}{\partial z} \tag{2.65}$$

These are the relationships for the shear stresses:

$$\tau_{xy} = \tau_{yx} = \mu \left(\frac{\partial u}{\partial y} + \frac{\partial v}{\partial x} \right) \tag{2.66}$$

$$\tau_{yz} = \tau_{zy} = \mu \left(\frac{\partial v}{\partial z} + \frac{\partial w}{\partial y} \right) \tag{2.67}$$

$$\tau_{zx} = \tau_{xz} = \mu \left(\frac{\partial w}{\partial x} + \frac{\partial u}{\partial z} \right) \tag{2.68}$$

where p is pressure.

They are implemented into Equation 2.60, Equation 2.61, and Equation 2.62 and are from now on called the Navier-Stokes equations.

$$\rho \left(\frac{\partial u}{\partial t} + u\frac{\partial u}{\partial x} + v\frac{\partial u}{\partial y} + w\frac{\partial u}{\partial z} \right) = -\frac{\partial p}{\partial x} + \rho g_x + \mu \left(\frac{\partial^2 u}{\partial x^2} + \frac{\partial^2 u}{\partial y^2} + \frac{\partial^2 u}{\partial z^2} \right) \tag{2.69}$$

$$\rho \left(\frac{\partial v}{\partial t} + u\frac{\partial v}{\partial x} + v\frac{\partial v}{\partial y} + w\frac{\partial v}{\partial z} \right) = -\frac{\partial p}{\partial y} + \rho g_y + \mu \left(\frac{\partial^2 v}{\partial x^2} + \frac{\partial^2 v}{\partial y^2} + \frac{\partial^2 v}{\partial z^2} \right) \tag{2.70}$$

$$\rho \left(\frac{\partial w}{\partial t} + u\frac{\partial w}{\partial x} + v\frac{\partial w}{\partial y} + w\frac{\partial w}{\partial z} \right) = -\frac{\partial p}{\partial z} + \rho g_z + \mu \left(\frac{\partial^2 w}{\partial x^2} + \frac{\partial^2 w}{\partial y^2} + \frac{\partial^2 w}{\partial z^2} \right) \tag{2.71}$$

The Navier-Stokes equations use simplified assumptions to model the motion of fluids. Most 2D models employ a version of the depth-averaged Shallow Water Equation, which is derived from the Navier-Stokes equation. The Navier-Stokes equations are considered to be the governing differential equations of motion for incompressible Newtonian fluids as expressed by Equation 2.72 and Equation 2.73.

$$\nabla \cdot \vec{V} = 0 \tag{2.72}$$

$$\rho \left(\frac{\partial \vec{V}}{\partial t} + \vec{V} \cdot \nabla \vec{V} \right) = -\nabla p + \rho \vec{g} + \mu \nabla^2 \vec{V} \tag{2.73}$$

Three-dimensional (3D) hydrodynamic modeling is important for comprehending various fluid dynamics phenomena, applicable in fields ranging from astrophysics to coastal engineering. However, a significant drawback is the high computational expense involved in 3D hydrodynamic simulations.

The depth-averaged continuity equation for two-dimensional flow is obtained by integrating Equation 2.72 [43].

$$\frac{\partial Z}{\partial t} + \frac{\partial (\bar{u}h)}{\partial x} + \frac{\partial (\bar{v}h)}{\partial y} = 0 \tag{2.74}$$

where Z is the water surface elevation, $\bar{u}$ and $\bar{v}$ are the mean values of u and v over the depth of the channel h.

The depth-averaged momentum equation for two-dimensional flow is obtained by integrating Equation 2.73 [43].

$$\frac{\partial}{\partial t}(\bar{u}h) + \frac{\partial}{\partial x}(\bar{u}^2 h) + \frac{\partial}{\partial y}(\bar{u}\bar{v}h) = (g_x + g_z \frac{\partial h}{\partial x})h - \frac{g}{C^2}\bar{u}\sqrt{\bar{u}^2 + \bar{v}^2} \tag{2.75}$$

$$\frac{\partial}{\partial t}(\bar{v}h) + \frac{\partial}{\partial x}(\bar{u}\bar{v}h) + \frac{\partial}{\partial y}(\bar{v}^2 h) = (g_y + g_z \frac{\partial h}{\partial y})h - \frac{g}{C^2}\bar{v}\sqrt{\bar{u}^2 + \bar{v}^2} \tag{2.76}$$

Based on spatial dimensions, hydrodynamic models can be classified as one-dimensional, two-dimensional, and three-dimensional models. Each dimensional model serves a specific purpose and is not superior to the others; its effectiveness relies on the application and available computational resources. A one-dimensional model can be represented in the longitudinal axis, while a two-dimensional model may be depth-averaged. Since most rivers, lakes, and estuaries possess a complex physical environment, distinct flow patterns, and different

dimensions may coexist in a single body of water [44]. Three-dimensional (3D) models are being used more frequently to tackle complex challenges related to fluid dynamics [45], structural interactions [46], and environmental impacts [47], as they can capture intricate flow patterns around obstacles, structures, and natural terrain. However, a significant drawback is the high computational expense involved in 3D hydrodynamic simulations. Rivers usually consist of islands, narrow channels, and meandering tributaries with intricate curvatures. They require a high grid resolution to represent the bathymetry accurately. However, 3D models may not produce sufficiently refined cells adequately to represent in the river width direction, which is typically limited to around five or fewer grid cells. In this context, 2D models can represent the bathymetry of a river better than 3D models, which are constrained by the number of grids [47].

In the early 1990s, the PC's processor became more powerful, allowing for an increase in 2D modeling in engineering applications such as flood control design [48], flood mapping [49],and river restoration [50]. As a result, there has been a decrease in 1D model usage. While a strong hydraulic background is essential for using hydraulic models, 1D modeling necessitates more assumptions from the modeller than 2D modeling [51]. 1D models are useful when the hydraulic system exhibits a 1D nature, such as when the flow is in one direction, the water surface elevation is constant across the cross section, there is minimal terrain slope, and the channel is prismatic, as in an irrigation canal [52]. A 1D model cannot be applied to rivers with wide floodplains and intricate curvatures for real-world hydraulics. On the other hand, 2D models provide a more comprehensive flow fields representation, capturing lateral flow variations and more complex hydraulic interactions [44, 51].

2.2.1 Numerical modeling

The following Table presents 2d hydro-sedimentary models in which their different features are compared.

Models	Unstructured mesh	Conservation of mass	Conservation of momentum	Supercritical flow	Unsteady Flow	Mobile Bed	Two-layer approach	Joint method	Decoupled	Opensource	Developer
GAIA	x	x	x	x	x	x	x		x	x	EDF
GSTARS4		x	x	x	x	x		x	x		Colorado State University
HEC-RAS	x	x	x	x	x	x		x	x		US Army Corps of Engineers
BASEMENT	x	x	x	x	x	x	x		x		ETH Zurich
Delft3D	x	x	x	x	x	x	x		x	x	Deltares
SRH2D	x	x	x	x	x	x		x	x		USBR
MIKE21	x	x	x	x	x	x	x		x		DHI
STR2D	x	x	x	x	x	x		x	x	x	Ecole Polytechnique de Montréal

Figure 2.7 Table summarizing 2D models

As observed in Table 2.7, GAIA, BASEMENT, Delft3d, and MIKE21 employ a two-layer approach [19, 20, 53] to solve sediment transport. While GAIA and Delft3D are both open source, BASEMENT and Mike21 are not. TELEMAC uses Fortran, like STR2D, and is a well-known and robust 2D hydrodynamic software. Thus, the developed sediment transport module presented in this thesis, STR2D, is implemented in TELEMAC to verify the stability of the newly developed sediment transport module before it is implemented in SF-Fluent. TELEMAC's governing equations will be presented in the following section. GSTARS4, HEC-RAS, and SRH2D employ the joint method [23, 24]. GSTARS4 uses an approach that does not rely on a mesh but instead employs the stream tube concept, with no sediment exchange between the stream tubes. SRH2D and HEC-RAS use the sediment transport mode parameter as STR2D, but HEC-RAS express the depth-averaged concentration equation differently than SRH2D. SRH2D does not place the sediment velocity ratio in the denominator, as HEC-RAS does; instead, it is in the convective terms which is also used in STR2D [14, 54]. SRH2D governing equations will be presented in the following section.

A. SRH2D version 3

SRH2D solves the following depth-averaged 2D equations [55]:

$$\frac{\partial h}{\partial t} + \frac{\partial h\bar{u}}{\partial x} + \frac{\partial h\bar{v}}{\partial y} = e \tag{2.77}$$

$$\frac{\partial h\bar{u}}{\partial t} + \frac{\partial h\bar{u}\bar{u}}{\partial x} + \frac{\partial h\bar{v}\bar{u}}{\partial y} = \frac{\partial hT_{xx}}{\partial x} + \frac{\partial hT_{yy}}{\partial y} - gh\frac{\partial z}{\partial x} - \frac{\tau_{bx}}{\rho} \tag{2.78}$$

$$\frac{\partial h\bar{v}}{\partial t} + \frac{\partial h\bar{u}\bar{v}}{\partial x} + \frac{\partial h\bar{v}\bar{v}}{\partial y} = \frac{\partial hT_{xy}}{\partial x} + \frac{\partial hT_{yy}}{\partial y} - gh\frac{\partial z}{\partial y} - \frac{\tau_{by}}{\rho} \tag{2.79}$$

where x and y represent the Cartesian coordinates; h is water depth; e is source term (excess of rainfall rate);t is time; $\bar{u}$ and $\bar{v}$ are depth-averaged velocity components of x and y directions; g is the gravitational acceleration; T_{xx}, T_{xy}, T_{yy} are the depth-averaged stresses due to turbulence and dispersion; $z = z_b + h$ is the water surface elevation; z_b is bed elevation;ρ is water density; and τ_{bx}, τ_{by} is bed shear stresses.

$$\tau_{bx} = \rho C_f \bar{u}\sqrt{\bar{u}^2 + \bar{v}^2} \tag{2.80}$$

$$\tau_{by} = \rho C_f \bar{v}\sqrt{\bar{u}^2 + \bar{v}^2} \tag{2.81}$$

where $C_f = gn^2/h^{1/3}$ and n is Manning's roughness coefficient.

SRH2D uses the Boussinesq's formulation to model the turbulence.

$$T_{xx} = 2(\mu_0 + \mu_t)\frac{\partial u}{\partial x} - \frac{2}{3}k \tag{2.82}$$

$$T_{xy} = (\mu_0 + \mu_t)\left(\frac{\partial u}{\partial y} + \frac{\partial v}{\partial x}\right) \tag{2.83}$$

$$T_{yy} = 2(\mu_0 + \mu_t)\frac{\partial u}{\partial x} - \frac{2}{3}k \tag{2.84}$$

where μ_0 represents the kinematic viscosity of water; μ_t is turbulent eddy viscosity; and k is turbulent kinetic energy.

The governing equations are discretized using the segregated finite-volume approach [56]. It uses arbitrarily shaped polygon (triangular or quadrilaterals) unstructured mesh. The dependent variables are store at the center of the element. The governing equations are solved using an iterative solution process which is SIMPLEC algorithm to solve the governing equations [57].

The sediment module has been already presented in Section 2.1.9.

B. TELEMAC and GAIA

Telemac uses a vertex-centered approach, where the dependent variables are stored at the nodes. The nodes are connected to construct the mesh, but a control volume is created around each node, producing a second mesh in which the hydrodynamic computations are performed, similar to a dual mesh [58]. TELEMAC-2d model solves the following hydrodynamic governing equations [59]:

$$\frac{\partial h}{\partial t} + \vec{u} \cdot \nabla(h) + h\nabla(\vec{u}) = S_h \tag{2.85}$$

$$\frac{\partial u}{\partial t} + \vec{u} \cdot \nabla u = -g\frac{\partial Z}{\partial x} + S_x + \frac{1}{h}\nabla(h\nu_t\nabla\vec{u}) \tag{2.86}$$

$$\frac{\partial v}{\partial t} + \vec{v} \cdot \nabla u = -g\frac{\partial Z}{\partial y} + S_y + \frac{1}{h}\nabla(h\nu_t\nabla\vec{v}) \tag{2.87}$$

where S_h is the source or sink of fluid; S_x and S_y are the source terms for wind, Coriolis force,

bottom friction, a source or sink term for momentum; u, v are the velocity components; and ν_t is the momentum coefficients.

TELEMAC is a hydrodynamic model featuring its own sediment transport module, known as GAIA. It computes separately the suspended load and bed load and allows the interaction between the loads through erosion flux and deposition flux at the interface (Z_{ref}). GAIA distinctly separates the sediment transport in the water column, near-bed, and the bed evolution. It computes the suspended sediment using an advection-diffusion equation as follow:

$$\frac{\partial hC}{\partial t} + \frac{\partial hUC}{\partial x} + \frac{\partial hVC}{\partial y} = \frac{\partial}{\partial x}\left(h\epsilon_s \frac{\partial C}{\partial x}\right) + \frac{\partial}{\partial y}\left(h\epsilon_s \frac{\partial C}{\partial y}\right) + E - D \tag{2.88}$$

where $E = w_s C_{eq}$ is the erosion flux, $D = w_s C_{Zref}$ is the deposition flux; w_s is the settling velocity; C_{Zref} is the near-bed concentration using a Rouse profile; and C_{eq} is the near-bed equilibrium concentration determined by an empirical formula for suspended load [18]. GAIA uses the Exner equation to solve the bed evolution by considering bed load, suspended load, or both modes simultaneously.

$$(1-\alpha)\frac{(\partial \rho z_b)}{\partial t} + \nabla \cdot Q_{m,b} = 0 \tag{2.89}$$

Equation 2.88 solved by GAIA, for the suspended load, will be modified as follow to compute the intermediate sediment concentration and the interface will be at the bed surface $Z_{ref} = Z_b$.

$$\frac{\partial hC}{\partial t} + \frac{\partial hUC}{\partial x} + \frac{\partial hVC}{\partial y} = \frac{\partial}{\partial x}\left(h\epsilon_s \frac{\partial C}{\partial x}\right) + \frac{\partial}{\partial y}\left(h\epsilon_s \frac{\partial C}{\partial y}\right) \tag{2.90}$$

CHAPTER 3 RESEARCH DESCRIPTION

This thesis presents a 2d hydro-sedimentary model called STR2D (Sediment transport in rivers 2D) using the joint method for modelling sediment transport in rivers. The literature review identified existing gaps and limitations in this method. Additionally, it explored the complex interactions among flow, sediment transport, and bed evolution. Overall, this research emphasizes the need for a tool that can provide a better understanding of sediment transport phenomenon. STR2D (Sediment Transport in Rivers in 2D) is an enhanced version of Shallow Fluent, developed at the host institute, which includes a sediment transport module applied for non-cohesive sediments. This model solves the two-dimensional hydro-sediment transport governing equations in a decoupled fashion, utilizing the joint method. It takes into account secondary flow effects, allowing for the simulation of events such as dam failures and flooding, and is able to model the spatial and temporal evolution of sediment concentration. The hydrodynamic module of STR2D employs a two-dimensional model utilizing a collocated finite volume scheme. The continuity and momentum equations are solved through the iterative Semi-Implicit Method for Pressure Linked Equations algorithm (SIMPLE) [60].

Greimann has developed an approach based on the joint method to model sediment transport using a parameter called sediment transport mode, f, in the depth-averaged sediment transport equation. This thesis proposes a 2D hydro-sedimentary model as a tool for continuing development on sediment transport, such as the implementation of an enhanced sediment transport mode, f.

The specific objectives as stipulated in the introduction are restated for completeness:

- Define an enhanced sediment transport mode parameter, f
- Develop a bed stratification representation of the riverbed considering active layer, δ_a
- Implement riverine parameters in STR2D model for non-uniform sediments such as adaptation length L_b, hiding-exposure effect h_f, and sediment class k
- Develop an algorithm of sediment material cell-node distribution

3.1 Contributions

A 2D decoupled hydro-sedimentary tool is developed using the joint method to be extended for river applications.

- Develop a new expression for sediment transport mode, f
- Determine the limitations of the joint method
- Compare with experimental data
- Use one mesh for hydrodynamic and bed evolution computations

3.2 Thesis Structure

This thesis follows a classical format. The introduction and the literature review present the concepts of sediment transport and the joint method, along with other existing methods and their respective limitations. The methodology section outlines the governing equations employed in the sediment transport module, detailing the processes of erosion and deposition. It also explains how the active layer is taken into account and describes the subroutine developed to redistribute material deposited from center cells to nodes.

The sediment transport model STR2D is subjected to a series of comparisons and validations to ensure its applicability for river systems. In the results section, an experimental benchmark involving a rectangular channel conducted by ETH Zurich University is used to verify and validate the developed code. First, STR2D is validated against a numerical benchmark using SRH2D (Sedimentation and River Hydraulics-2D), the only sediment transport model known to the author that employs the joint method developed by the U.S. Bureau of Reclamation. Comparisons are made between STR2D and SRH2D in terms of hydrodynamic behavior, bed evolution, and sediment concentration for uniform sediments. Secondly, STR2D is compared to an experimental benchmark that involves non-uniform sediments typically found in rivers. The discussion and conclusion sections outline necessary future steps for enhancing the model's capability to simulate sediment transport in river environments.

CHAPTER 4 METHODOLOGY

This research continues the development of a 2D depth-averaged hydrodynamic model called Shallow Fluent (SF-Fluent) [63]. This model is capable of simulating heat and vegetated rivers using innovative techniques [64]. This numerical model has been programmed in an oriented-based manner, allowing new modules to be added.

As illustrated in Figure 4.1, the SF-Fluent model is in yellow while the additions made in this research—specifically the preprocessing treatment, sediment transport module, and post-processing treatment—are shown in blue. The primary objective of this research is to incorporate and further develop a sediment transport module as described in the methodology section.

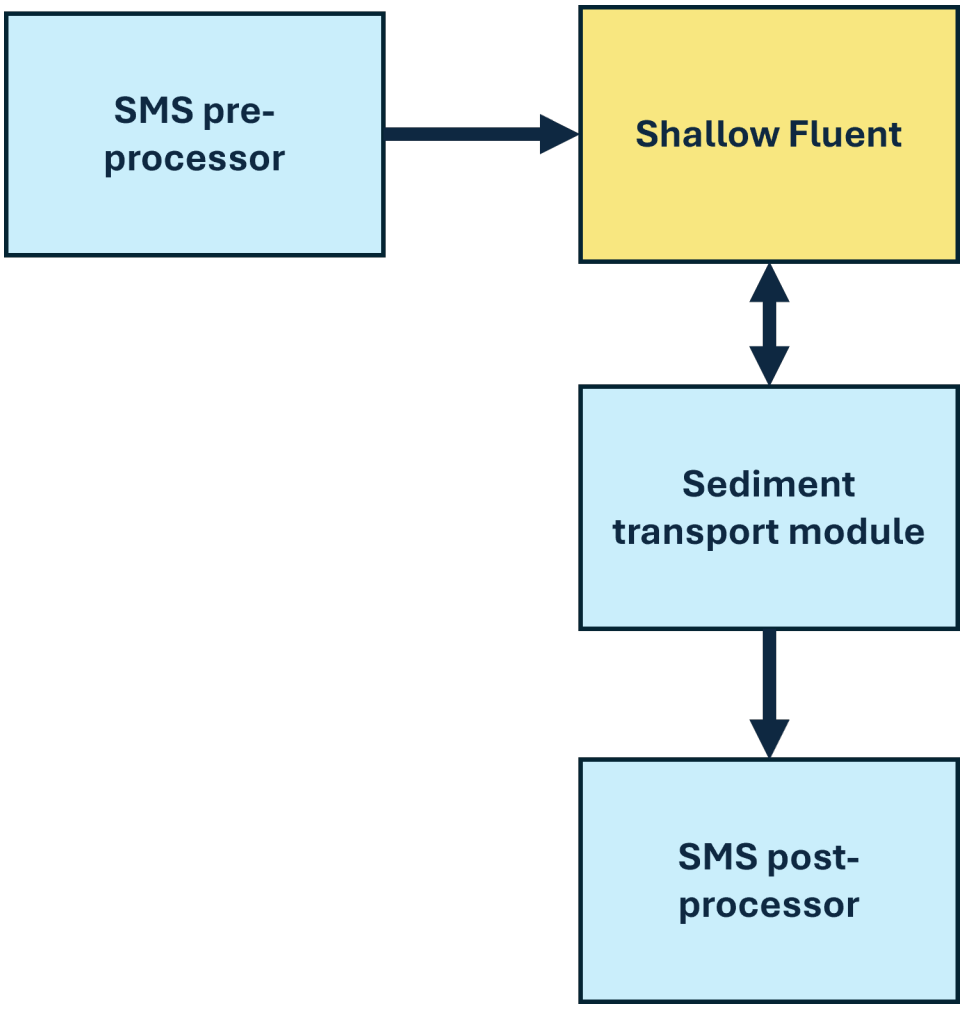

Figure 4.1 Existing SF-Fluent and Future extension to SF-Fluent

Previously, SF-Fluent used its own mesh format. To incorporate SMS (Surface-Water Modeling System) [65] into this research for pre- and post-treatment, a subroutine has been developed to read meshes from SMS in the .2dm format and to impose the boundary conditions. More detail on this subroutine can be found in Appendix **??**.

The code solves the sediment transport equation in a decoupled manner by first addressing the hydrodynamic variables, which are then provided to the sediment transport module. Using sediment properties, the module calculates the necessary additional hydraulic parameters to determine the hydraulic-sediment parameters. The depth-averaged concentration equation uses these hydraulic-sediment parameters, allowing for bed evolution computation.

Next, another subroutine developed and implemented in STR2D generates results in an ASCII text file that can be viewed in SMS. SMS serves as a powerful tool that enables users to visualize and analyze the results.

The next chapter details the different components illustrated in Figure 4.2.

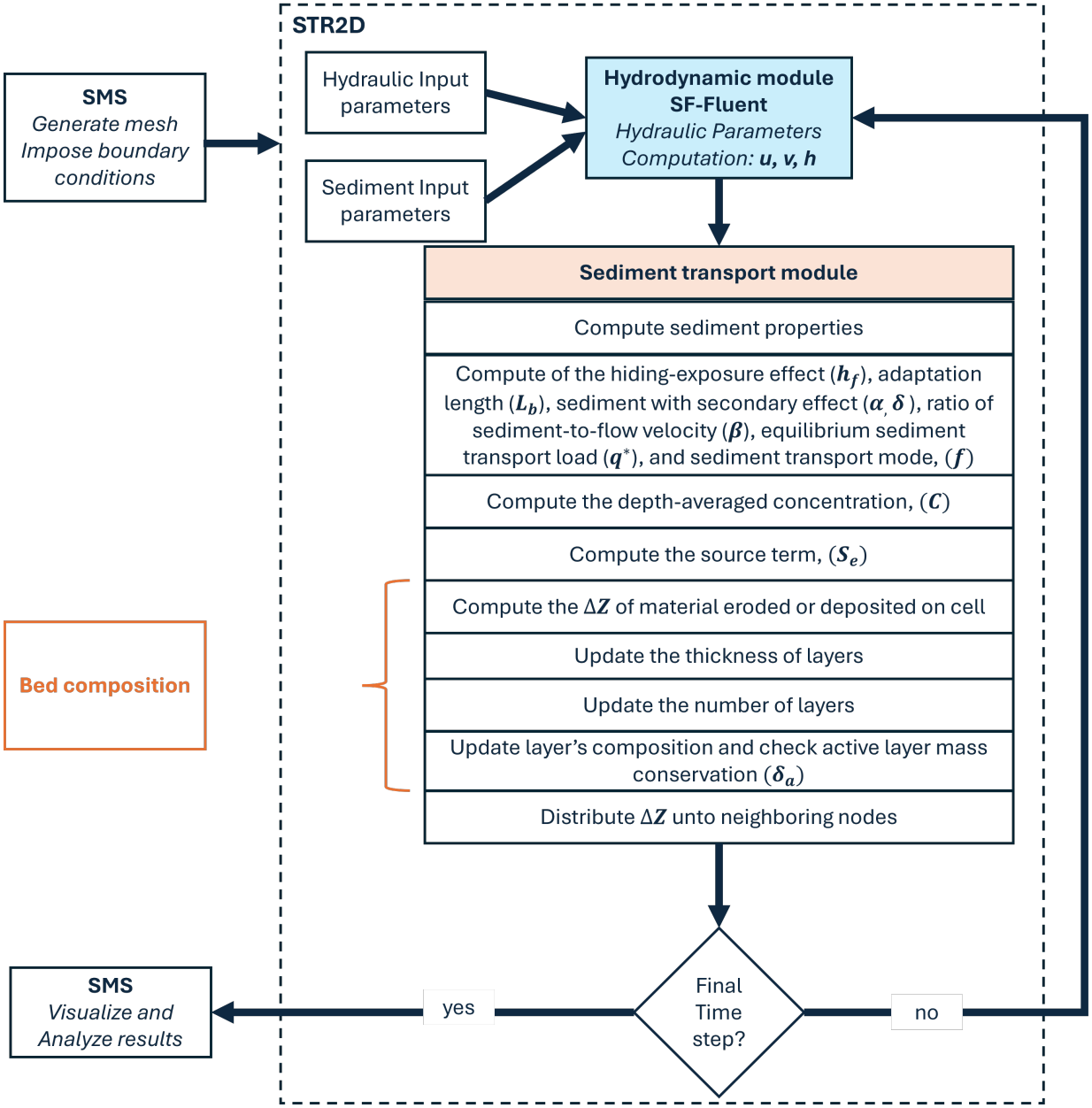

Figure 4.2 General Flowchart

CHAPTER 5 MODEL PRESENTATION

The hydrodynamic module is computed first and provides necessary information to the sediment transport module. If the water flow already carries sediment at its maximum capacity, no further sediment transport will occur. However, if sediment transport is taking place, the source term will determine whether the flow will erode or deposit material. A negative source term indicates deposition.

An additional step is considered when material is deposited on the bed. The second layer beneath the active layer may have its composition updated because the material can exceed the mass conservation of the active layer. Then, the active layer's composition is updated for erosion or deposition. If there is erosion, the proportion present changes due to the material leaving the active layer, and if there is deposition, newly deposited material alters the bed composition. In both processes, the second layer may change its thickness. When erosion occurs, the active layer may take material from the layer beneath to maintain its mass. When deposition occurs, excess material may be given to the layer beneath (second layer). The program continues until it reaches the final time step defined by the user. The sediment transport model is summarized in Figure 5.1.

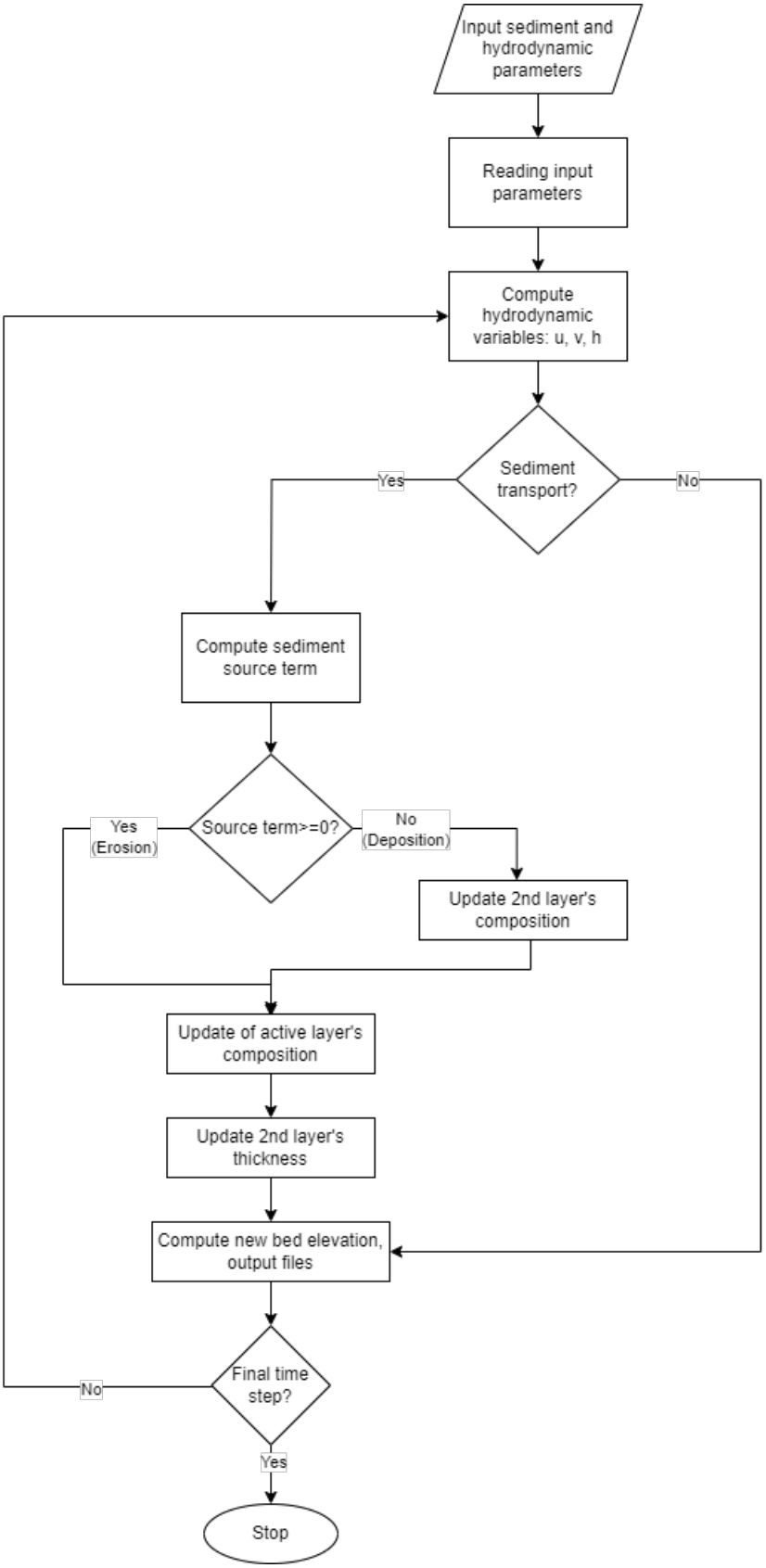

Figure 5.1 STR2D Flowchart

5.1 Hydrodynamic module

A 2D depth-averaged hydrodynamic model for incompressible flow in Fortran 90 language called SF-Fluent was developed at the host institute under the supervision of Professor Mahdi [3]. The model was built using subroutines and functions, allowing it to be extended to other applications such as sediment or contaminant transport in a decoupled way. Hence, this study aims at providing a numerical laboratory solver where new techniques can be tested and improved. The hydrodynamic module of STR2D is a two-dimensional model that uses a collocated finite volume scheme. It is capable of simulating both laminar and turbulent flows, and it can account for secondary flow effects, which allows the modeling of events such as dam breaks and floodings.

The continuity and the momentum equations are solved using the iterative Semi-Implicit Method for Pressure Linked Equations algorithm (SIMPLE) [60]. This algorithm couples the pressure and velocity fields, using the continuity equation as a pressure correction equation. This iterative process is presented in Figure 5.2. The advantage of using this iterative algorithm is being able to solve parabolic equations such as advection-diffusion. In addition, SF-Fluent solver uses triangular cells and stores the hydrodynamic variables at the cell-center.

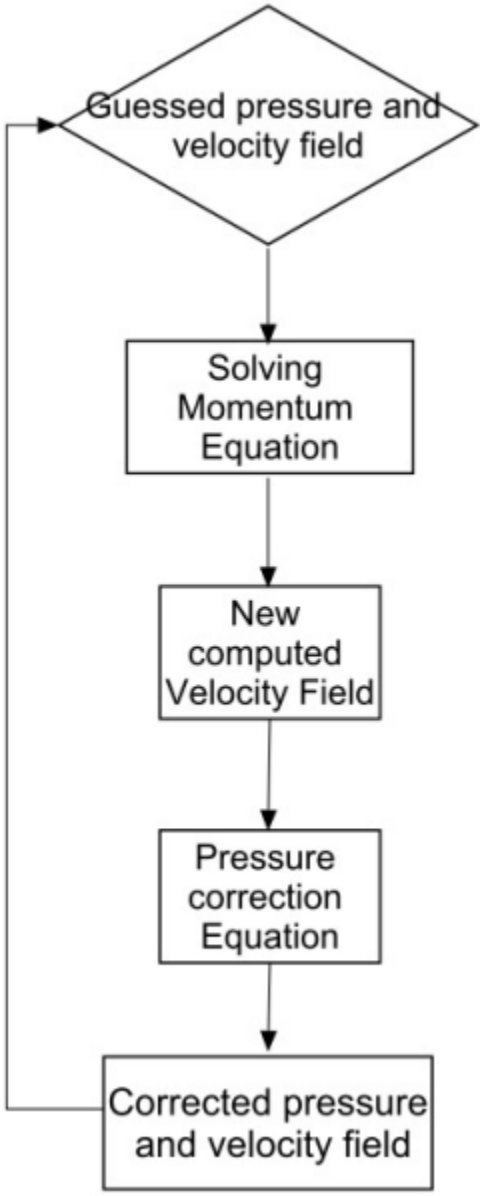

Figure 5.2 Simple algorithm used in SF-Fluent

The hydrodynamic governing equations are solved using an explicit iterative method called Semi-Implicit Method for Pressure Linked Equations (SIMPLE).

$$\nabla \cdot \vec{u} = 0 \tag{5.1}$$

$$\frac{\partial u}{\partial t} + \nabla \cdot (uu) = -\nabla P + \frac{1}{Re}\nabla \cdot ((1 + \mu_t \nabla u^T)) \tag{5.2}$$

where u is the velocity vector, Re is the Reynold number, μ_t is the turbulent dynamic viscosity, P is pressure and T is the transpose of a vector. The continuity equation is converted

into a pressure correction equation. Then, an initial guessed pressure and velocity fields are used to solve the momentum equations and the resulted velocity field is put back into the pressure correction equation to obtain corrected velocity and pressure fields. The algorithm checks if convergence is achieved. If it is not, then it continues to iterate until the preset residual criterion is obtained. The iterative solver is only applicable to unstructured mesh, which is preferred for modeling complex geometries such as rivers with irregular boundaries. The present solver uses triangular unstructured mesh. The collated finite volume scheme discretizes the governing equations and stores the dependent variables at the center of the cell.

The highlighted innovative techniques develop in SF-Fluent [63] are:

- An innovative way to prevent checkerboard pressure using a Multi-Block Local Triangulation
- A new way to express the depth-averaged governing equation to consider low water depth
- A new second order wetting-drying front
- A Total-Value Linearly Interpolation (TV-LI)
- New ways to express the hydrodynamic equations considering vegetation as porous media

5.2 Sediment transport module

If the sediment transport module is activated, the model will request input parameters for sediment transport. These parameters include:

- number of sediment classes
- upper and lower diameters for each sediment class
- number of layers
- thickness of the active layer
- thickness of each bed layer
- hiding-exposure effect

- adaptation length
- equilibrium sediment equation
- sediment properties (specific gravity, wet and dry bulk density)

These input parameters for the sediment transport equation allow for the computation of the d50 diameter (d_{50}), the d90 (d_{90}) diameter, the porosity (σ), and the fall velocity (ω). The sediment transport module also computes additional hydraulic parameters, including the flow magnitude (V_t), bed shear stress (τ_b), shear velocity (u_*), and local radius of curvature (R_c). The hydraulic parameters and the sediment properties allow for the computation of the hydraulic-sediment parameters from the depth-averaged concentration equation. Figure 5.3 illustrates how the hydraulic-sediment parameters depend on the hydraulic and sediment properties parameters.

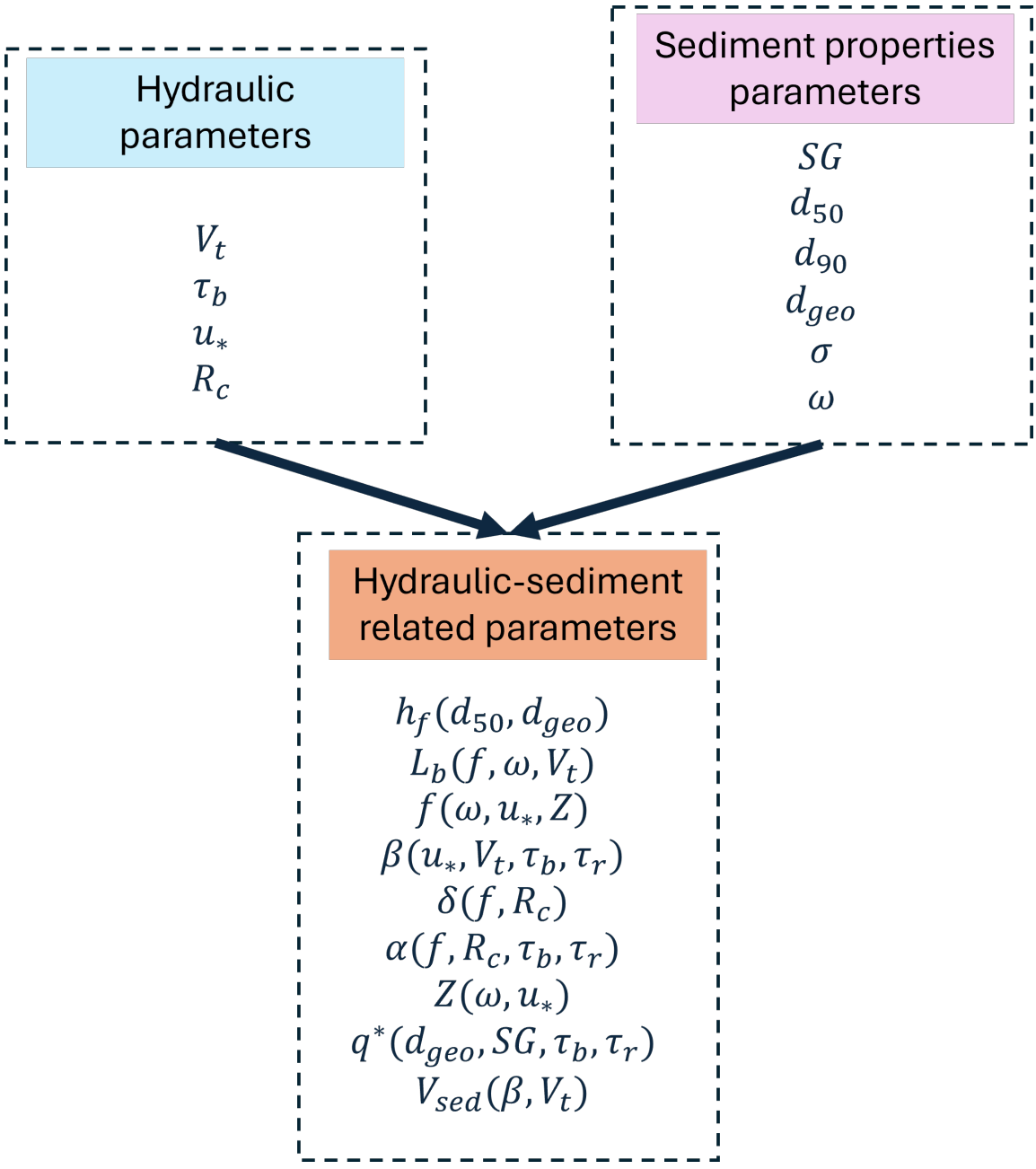

Figure 5.3 Sediment parameters Flowchart

5.2.1 Governing Equations of Sediment Transport Model

Equation 5.3 is solved using the fractional step method [66] and an intermediate concentration, C_k^{int}, is obtained [67]. The depth-averaged concentration equation is integrated over an unstructured triangular mesh as shown in Figure 5.4.

$$\frac{\partial hC_k}{\partial t}+\frac{\partial(\cos\alpha_k)\beta_k V_t hC_k}{\partial x}+\frac{\partial(\sin\alpha_k)\beta_k V_t hC_k}{\partial y}=\frac{\partial}{\partial x}\left(hf_k D_x\frac{\partial C_k}{\partial x}\right)+\frac{\partial}{\partial y}\left(hf_k D_y\frac{\partial C_k}{\partial y}\right) \quad (5.3)$$

where h is the water depth, C_k is the depth-averaged sediment concentration for each sediment class, α is the direction angle of the sediment transport (relative to the x axis), f is the transport mode parameter, and β is the velocity ratio, and D_x and D_y are mixing coefficient of suspended sediment in the x and y axis.

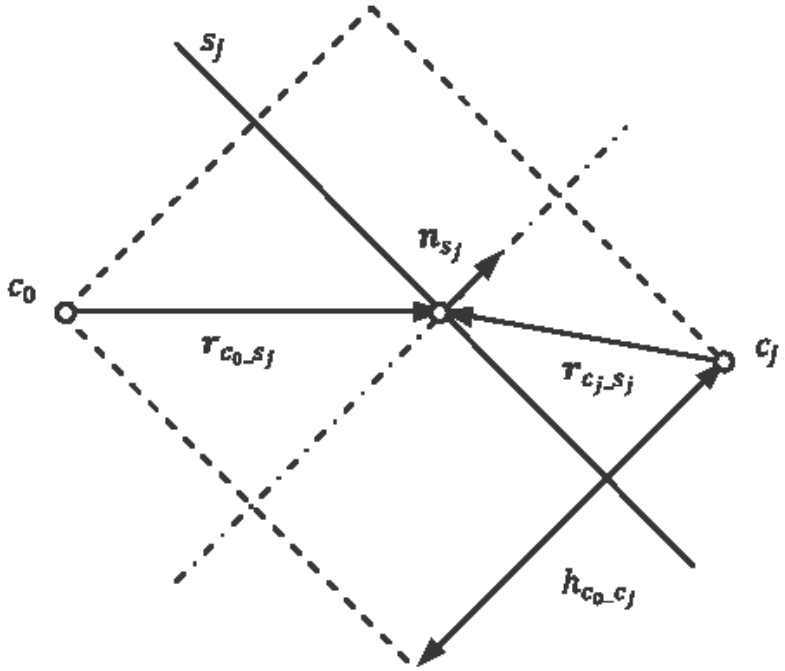

Figure 5.4 Geometrical notations used in discretized equations: central cell, c_0, neighboring cell, c_j, cell face, s_j, distance vector $\vec{r}$ [3]

The distance from the centroid of the central cell, c_0 and the cell face, s_f, is written as r_{c0_sj}. STR2D discretizes the convective terms using first order upwind scheme, solves the gradient at cell-center calculation using Green's Theorem, and uses the two point method to solve the gradient at the cell face. The discretized equation of the depth-averaged sediment

concentration for each sediment class, C_k, for a triangular mesh can be expressed as:

$$a_{0,k}C_{0,k} = \sum_{j=1}^{3} a_{j,k}C_{j,k} + S_{conv_k} + S_{diff_k} \tag{5.4}$$

$$\begin{aligned} a_{0,k} &= \frac{(hA)^{n+1}}{\Delta t} + \sum_{j=1}^{3}[[C_{s_j}, 0]] + diffusionterm & (5.5)\\ a_{j,k} &= [[-C_{s_j}, 0]] + diffusionterm & (5.6)\\ S_{conv_k} &= \frac{hA}{\Delta t}C_{j,k}^{n} + [[C_{s_j}, 0]]\nabla C \cdot \vec{r} & (5.7) \end{aligned}$$

The term $\nabla C \cdot \vec{r}$ varies its expression under two different conditions: 1) If the convective flux is equal to or greater than zero, then:

$$S_{conv_k} = \frac{(hA)^{n+1}}{\Delta t}C_{j,k}^{n} - [[C_{s_j}, 0]]\left(\frac{\partial C^{n+1}}{\partial x}r_{x,c0\_s_j} + \frac{\partial C^{n+1}}{\partial y}r_{y,c0\_s_j}\right) \tag{5.8}$$

2)If the convective flux is less than zero then:

$$S_{conv_k} = \frac{(hA)^{n+1}}{\Delta t}C_{j,k}^{n} + [[C_{s_j}, 0]]\left(\frac{\partial C^{n+1}}{\partial x}r_{x,cj\_s_j} + \frac{\partial C^{n+1}}{\partial y}r_{y,cj\_s_j}\right) \tag{5.9}$$

where h is the water depth, A is the area of the cell, r_{x,cj_s_j} and r_{y,cj_s_j} represent the x and y components of $\vec{r}$, $C_{0,k}$ represents the sediment concentration at the central cell for a sediment class k and $C_{j,k}$ at neighboring cells. S_{conv_k} is the convective source term, and S_{diff_k} represents the diffusion source term. $C_{s,j}$ represents the convective flux at the cell face, s_j, and can be written as follow:

$$C_{s_j} = u_{sed_k,s_j}(h_{s_j}s_{x,j}) + v_{sed_k,s_j}(h_{s_j}s_{y,j}) \tag{5.10}$$

where C_{s_j} is the flux convective, u_{sed_k} and v_{sed_k} are the sediment velocities in the x and y direction.

As in SRH2D [24], the mixing coefficients, D_x and D_y are set to zero. Hence, the diffusion terms are not solved.

$$S_{e,k} = \frac{1}{L_{t,k}}\left(q_{t,k}^{\star} - q_{t,k}\right) \tag{5.11}$$

$q_{t,k}^{\star}$ represents the sediment discharge at equilibrium state for a sediment class k which is

computed by one of the sediment equations shown in Table 2.2. $q_{t,k}$ is the actual sediment discharge. To consider the spatial lag to reach equilibrium state, $L_{t,k}$,an adaptation length is used and it can be used as a calibration parameter. The source term, $S_{e,k}$, expressed in Equation 5.11 is the ratio of the difference between the sediment discharge at equilibrium state $q^{\star}_{t,k}$ and the real discharge for sediment class k over the distance that it takes to reach the equilibrium state, also known as the adaptation length.

The real sediment discharge is a function of the real concentration C_k of sediment class k.

$$q_{t,k} = \beta_k V_t h C_k \tag{5.12}$$

Equation 5.13 [67] allows to link the source term with the intermediate concentration C_k^{int} obtained from solving Equation 5.3 and the real concentration C_k for sediment class k.

$$S_{e,k} = \frac{\partial hC}{\partial t} \approx \frac{(hC_k)^{n+1} - (hC_k^{int})}{\Delta t} \tag{5.13}$$

The actual concentration C_k^{n+1} present in the river can be computed by coupling Equation 5.11 and Equation 5.13 as shown in Equation 5.14. The derivation is found in Appendix B. Then, the source term, $S_{e,k}$, can be computed. The source term allows to compute the bed change as explained in Section 5.2.4.

$$C_k^{n+1} = \frac{\frac{\Delta t \times q^{\star}_{t,k}}{L_{t,k}} + C_k^{int} h^{int}}{\left(1 + \frac{\beta_k V_t \Delta t}{L_{t,k}}\right) h^{n+1}} \tag{5.14}$$

As summarized in Figure 5.5, the depth-averaged concentration equation is an advection-diffusion equation with a source term that accounts for bed changes. This equation is initially solved using the fractional step method by setting the source term to zero. The advection-diffusion equation without a source term is solved by discretizing it with a collocated finite volume scheme and subsequently solving it using the SIMPLE algorithm. Thus, the intermediate concentration is computed. Next, using Equation 5.11 and Equation 5.13, the real concentration is solved analytically for the next time step. The source term is calculated based on the real concentration for the next time step as presented in Appendix B. If the total source term, which is the sum of all sediment classes, k, is negative, the model indicates deposition. Conversely, if the total source term is positive, then there is erosion.

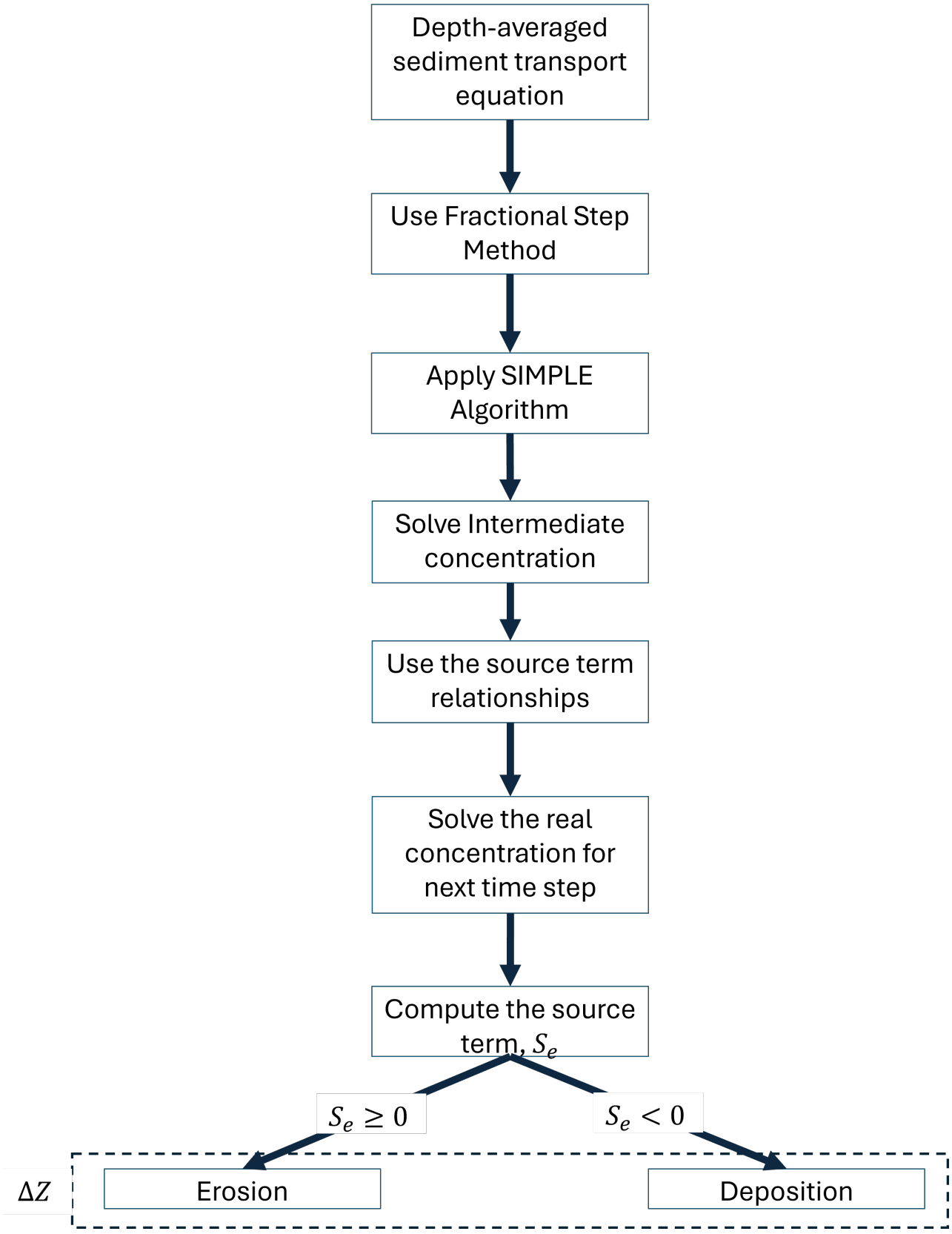

Figure 5.5 Concentration Computation Flowchart

5.2.2 Coupling

There are cases where sediments can travel slower than the flow. In those cases, one sediment time step is greater than the flow time step as shown in 5.6. The flow can undergo several time steps before considering sediment transport. STR2D provides the possibility to consider a constant parameter $CalParam$ which can be equal to or greater than 1.0.

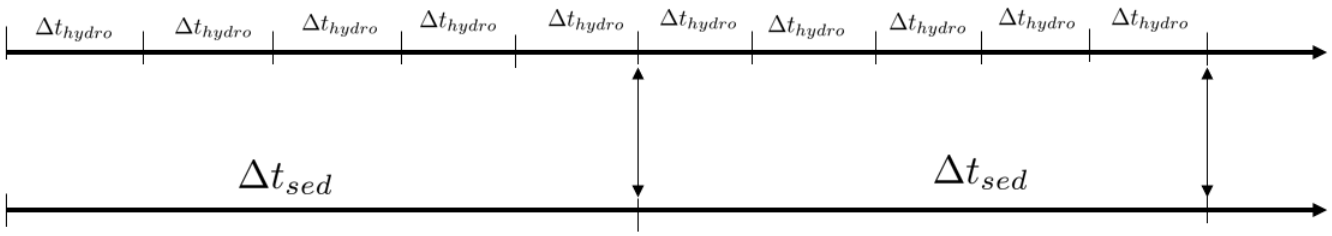

Figure 5.6 Coupling of the morpho-hydro-sedimentary module

$$\Delta t_{sed} = \Delta t_{hydro} * CalParam \tag{5.15}$$

5.2.3 River Bed Composition

A river bed is composed of different types and sizes of sediments which produce a non-uniform sediment composition. The input variables for STR2D are divided into four type of categories:

- sediment
- river's bed
- sediment transport
- bed evolution

The sediment category considers the sediment information present in the simulation: porosity, specific gravity, number of sediment class, and dry bulk density. In river's bed category, it considers the number of layers, the thickness of each layer, and the composition of each layers (gradation). Whereas in the sediment transport category, the fall velocity is considered. In addition, the bed evolution category considers the adaptation length for erosion, deposition, and total load.

Uniform sediment distributions are found in a controlled environment. STR2D can model the nonuniform sediment distribution using the concept of zones. Each zone can have different sediment distribution and are identified with an id.

River beds are generally modeled in a stratified manner layers. One layer can be composed of different sediments sizes which are divided in classes. A sediment class is a range of sediment diameter with an upper and lower limit. Usually, in the literature, one diameter represents the sediment range called the geometric diameter which is the square root of the product between the upper and lower diameter of the range.

The number of layers, thickness, and composition for each layer in a zone are defined at the beginning by the user. Figure 5.7 shows an example of how these parameters can vary between two different zones. The first zone is composed of two layers of different composition. The second zone is composed of three layers.

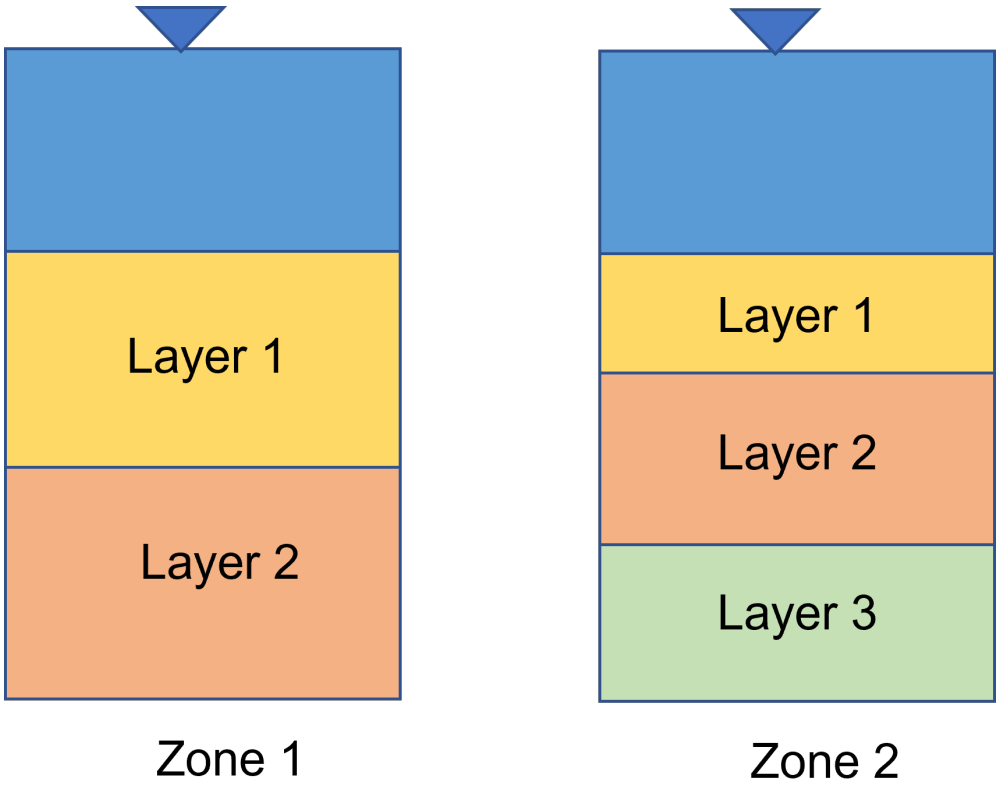

Figure 5.7 Zones initially defined

In addition, the thickness of the active layer must be provided by the user as well: in millimeters or as presented in Figure 2.1. The active layer will provide material for erosion and/or receive material from deposition. This layer is not a physical layer (real) but an

user-defined layer. It can be used as a calibration parameter.

The active layer is usually defined as part of the upper portion of the initially defined upper layer. Its composition depends on the thickness of the active layer and the layers' thickness defined. If the active layer's thickness δ_a^n has a thickness smaller than the layer at the surface, the active layer will be part of the initial upper layer. If the user defines initially, that the bed is composed of two layers. Then, the STR2D considers three layers with the active layer. The material composition of the active layer will be the same as the upper layer. On the other hand, if the active layer's thickness is greater than the first layer, then it composition will be a mix of the upper layer and the layer beneath it. The number of layer will be modified as shown in Figure 5.8 for Zone 2.

If the active layer is composed of two or more layers, its composition is computed weight-averaging the thickness of each layer along with their respective compositions.

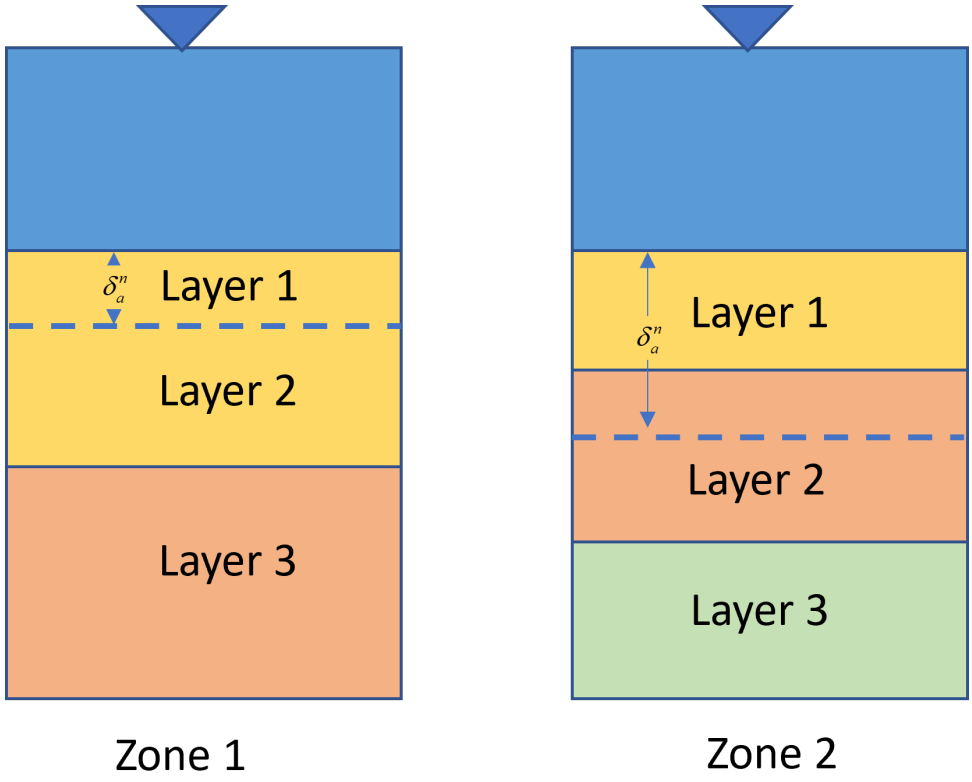

Figure 5.8 Zones considering active layer

When the active layer is considered, the upper layer is constantly interacting with the flow through erosion and deposition processes. Bed armouring is a phenomena that may happen when the erosion is limited. In this model, bed armouring may be considered in one of these two ways. First, the flow may have the capacity to erode different sediment k class present

in the active layer, but when the material available is less than the flow capacity, it is called "availability limited". Secondly, when there is just enough material for the flow to carry, then it is called "capacity limited" because it is limited by the flow capacity.

5.2.4 Bed Evolution Module

The source term and the bed change can be computed and updated analytically respectively as shown in Equations 5.16 and 5.17.

$$-S_{e,k} = (1 - \sigma_{ak})\frac{\partial Z_{b,k}}{\partial t} \tag{5.16}$$

When the source term is greater than zero, then the bed lowers (erosion), and when the source term is less than zero then the active layer receives material from deposition.

$$Z_{b,k}^{n+1} = \frac{-S_{e,k}\Delta t}{1 - \sigma_{ak}} + Z_{b,k}^{n} \tag{5.17}$$

Adding all the bed change for each sediment class k gives the total bed change in the river bed Z_b.

$$\sum Z_{b,k} = Z_b \tag{5.18}$$

Bedrock is another element that can limit the erosion process. The bedrock elevation is an important information to obtain because it is considered as the reference level below which no more erosion can occur. Whereas, the active layer is an user-defined layer: limits erosion and/or receives material from the deposition process.

In Figure 5.8 is an example of two zones in which on zone has initially two layers and the second layer it has three layers. Visually, the different colors show the different type of composition that the different layers are made of.

The layers' elevations can be computed once the bedrock elevation and the thickness of each layer is known as shown in Figure 5.9.

Each layers possesses an upper and bottom elevations used to monitor the erosion and deposition processes during the simulation for each layer. The upper layer, after undergoing erosion, may be completely eroded. In addition, it can indicate the availability of material; hence, the new bed elevation. On the other hand, in the case of deposition, it will be able to adjust the upper layers' elevations. If there is too much material in the upper layer (aka active layer) permitted due to the mass conservation defined initially, the amount of material in excess will be given to the layer below.

Water has a maximum capacity to transport sediments which is denoted as the sediment discharge $q^{\star}_{t,k}$ computed by one of the methods presented in Table 2.2 at equilibrium state. If the real sediment discharge $q_{t,k}$ is greater than $q^{\star}_{t,k}$ at equilibrium then the water can transport more and erosion will happen. If the opposite happens, then deposition will occur. The equations presented above in Section 6 is able to represent this concept of erosion and deposition processes. For instance, the source term in Equation 5.11 will be positive and there is a lowering of the bed happening according to Equation 5.17.

A. Active layer mass conservation

The mass of the active layer with no void m_a does not change through out the simulation but its composition may change by the presence of non-uniform sediment. Equation 5.19 and Equation 5.20 are the general equations that ensure mass conservation of the active layer expressed with no voids for erosion and deposition processes respectively. Recalling the erosion process explained at Section 2.1.10 (explaining the erosion process), the active layer maintains its mass by taking material from the layer beneath it. It is expressed so in Equation 5.19 by using $p_{2,k}$, the bed-material gradation of the second layer. If the second layer is completely eroded, the next layer will also be used to supply the necessary material to the active layer, and this process will be repeated as needed. As explained in earlier sections, the erosion can be limited by the active layer which is known as the availability limited. Furthermore, the active layer can also be limited if the user has specified a thickness of layer or a bedrock elevation.

On the other hand, if deposition process occurs, there is no need to take material from the material of the layer below. The newly deposited material is mixed with the active layer and the second layer, as shown in Figure 5.11. A similar procedure is followed by Bennett and Nordin [34] where the newly deposited material is mixed with the active layer and the exceeding material is given to the layer beneath (layer 2). The composition of the active layer has to be updated to consider the newly deposited material, $p_{a,k}$.

$$\frac{\partial m_a p_{ak}}{\partial t} = -S_{e,k} + p_{2,k} \sum_k S_{e,k} \tag{5.19}$$

$$\frac{\partial m_a p_{ak}}{\partial t} = -S_{e,k} + p_{a,k} \sum_k S_{e,k} \tag{5.20}$$

Equation 5.19 and Equation 5.20 are discretized and are represented by Equation 5.21 and Equation 5.22 respectively. They are used to update the active layer material, $p^{n+1}_{a,k}$. The

first term at the right hand side of Equation 5.21 and Equation 5.22, $m_{a,k}p^{n}_{a,k}$, represents the active layer's thickness with no void for a sediment class k at time step n. It is the thickness available at the active layer for sediment class k for erosion at time step n. The second term at the right hand side, of Equation 5.21 and Equation 5.22, $S_{e,k}\Delta t$, represents the erosion or deposition of an individual sediment class k unto the active layer. For instance, at any time step, the erosion can be the overall process happening but a sediment class can nevertheless still be subjected to deposition. The second term allows to consider that scenario. The composition of the active layer can change if newly material is deposited. The third term at the right hand side of Equation 5.21 and Equation 5.22, $p^{n+1}_{2,k}\sum_{1}^{k} S_{e,k}\Delta t$, represents the amount of material taken from the layer beneath the active layer when erosion occurs.

$$m_{a,k} = m_a p^{n+1}_{a,k} = m_{a,k}p^{n}_{a,k} - S_{e,k}\Delta t + p^{n}_{2,k}\sum_{1}^{k} S_{e,k}\Delta t \tag{5.21}$$

When overall deposition process happens, it uses $p^{n+1}_{a,k}$ instead of $p^{n+1}_{2,k}$. Figure 5.10 summarizes the procedure in which the active layer conserves its mass throughout the simulation when erosion occurs. The left image of Figure 5.10 shows the mass allocated for each sediment class in the active layer at time step n. The right image of Figure 5.10 represents when the upper layer is eroded but not completely. In addition, it shows the way the active layer does to maintain its mass by taking material from the layer beneath at time step $n+1$.

$$m_{a,k} = m_a p^{n+1}_{a,k} = m_{a,k}p^{n}_{a,k} - S_{e,k}\Delta t + p^{n+1/2}_{a,k}\sum_{1}^{k} S_{e,k}\Delta t \tag{5.22}$$

Depending on the amount received or taken from the active layer, the thickness of the layer beneath the active layer is changing during the simulation and its composition during deposition process.

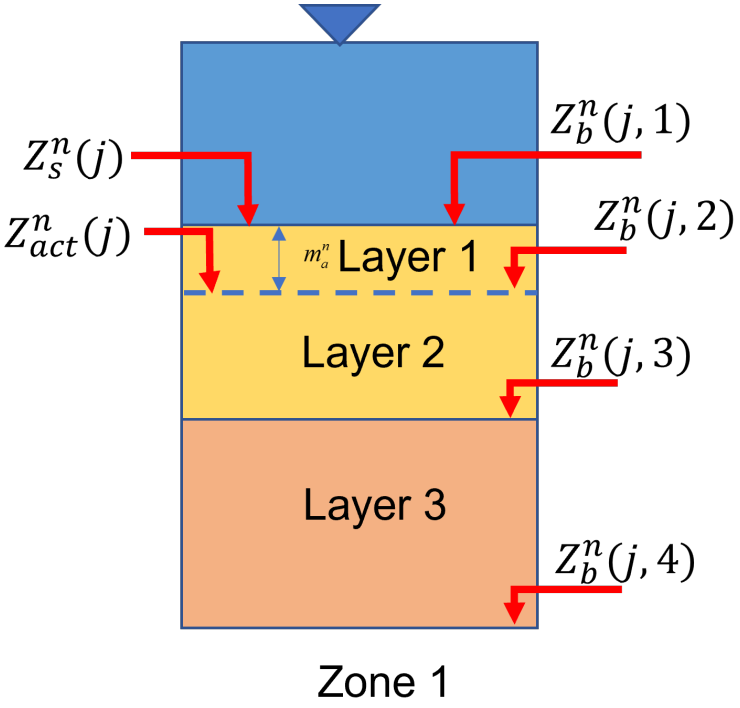

(a)

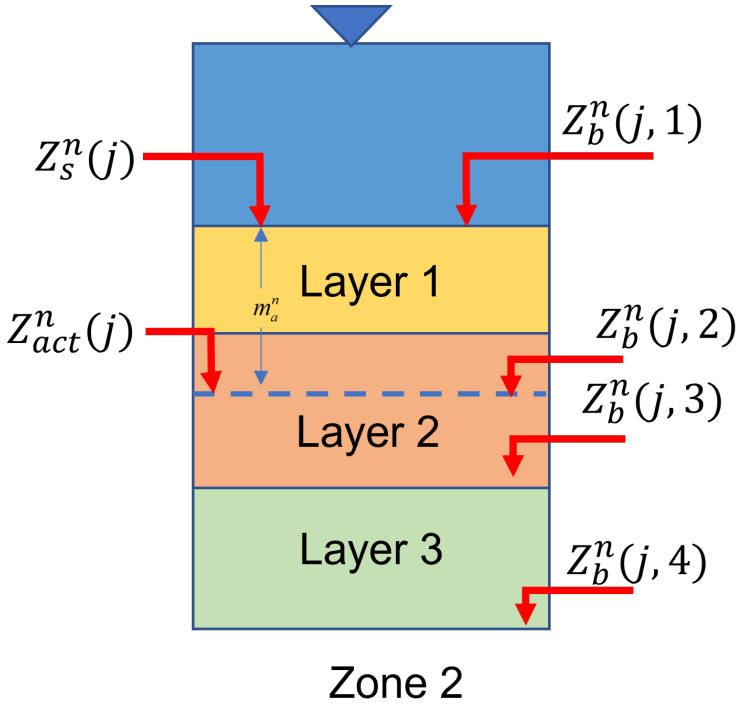

(b)

Figure 5.9 Layers Elevations considering active layer a) active layer thickness smaller than layer 1 b) Active layer thickness is greater than layer 1

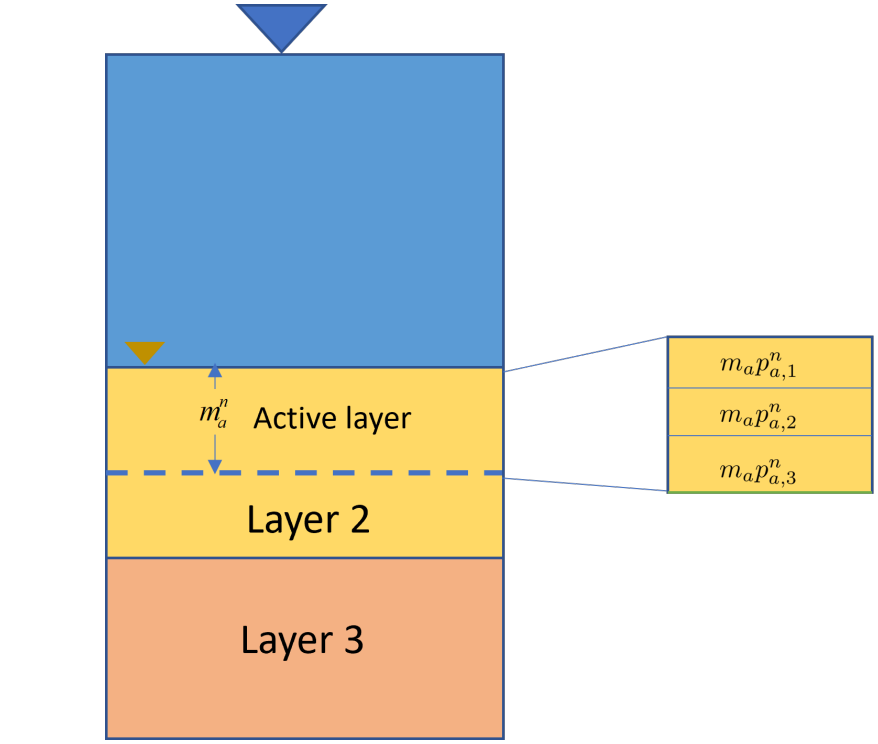

(a)

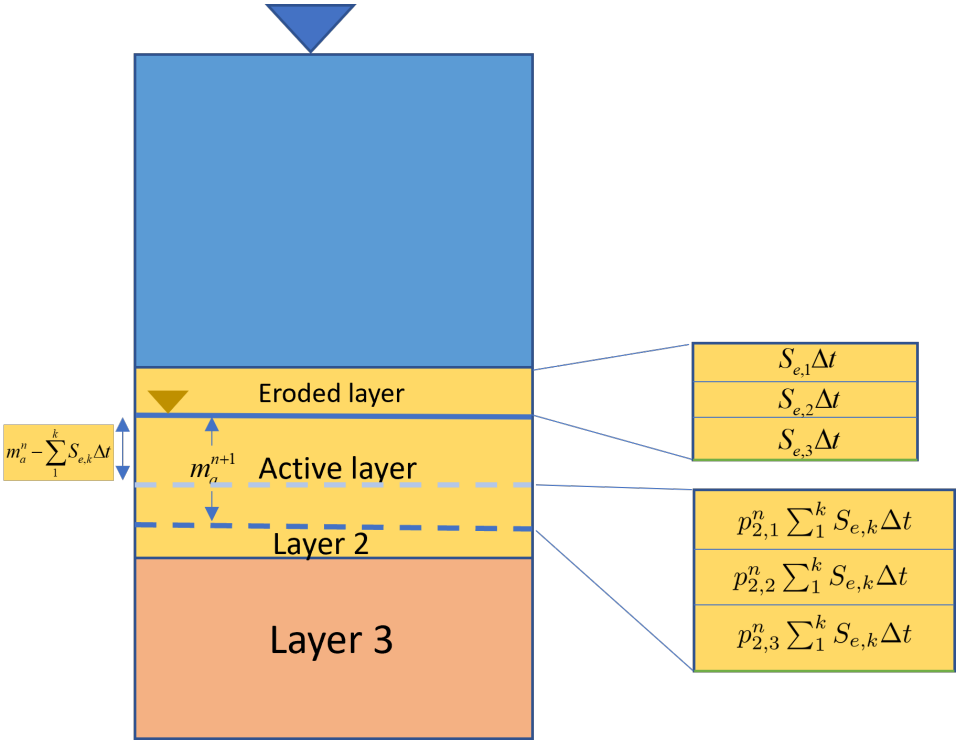

(b)

Figure 5.10 Active layer mass conservation for erosion at time step a)n and b)n+1

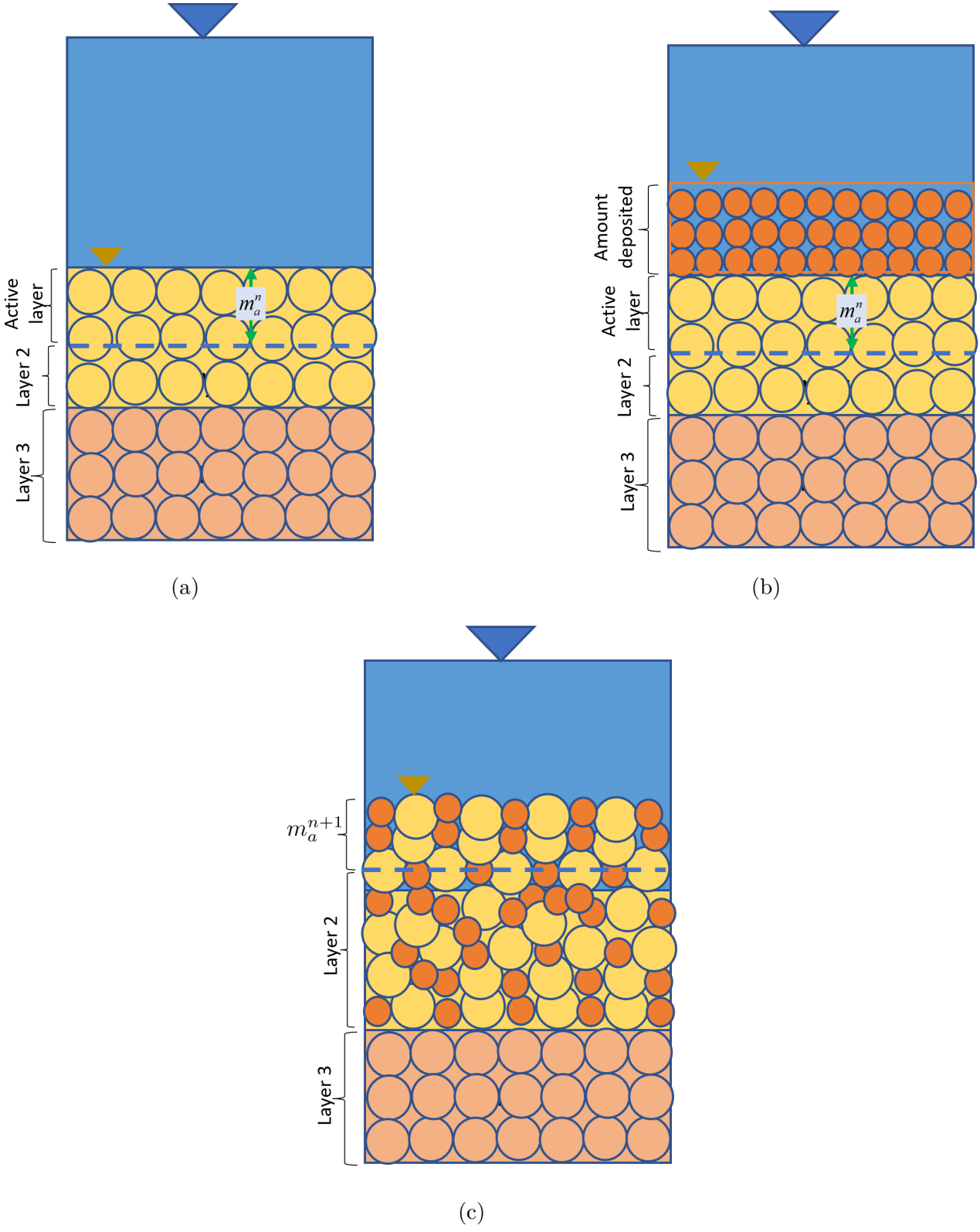

Figure 5.11 Active layer mass conservation for deposition at time step n (a) and n+1 for (b) and (c)

5.2.5 Algorithm from cell center to node

A collocated finite volume scheme discretizes the depth-averaged concentration equation by storing the dependent variables—such as water depth, flow velocities, and changes in bed elevation—at the cell center. STR2D employs an unstructured triangular mesh featuring three nodes per computational cell as can be observed in Figure 5.13, which shows six computational cells.

The nodes composing the mesh store bed elevation information. To modify the node bed elevation information, a subroutine redistributes the amount of material computed for the cell center and transfers it to the surrounding nodes.

Several cells can surround a node. Each cell has an ID. One array contains the IDs of the cells surrounding a node, while another array holds the number of cells that encircle a node. Next, the total material deposited or eroded for each cell surrounding a node is calculated, followed by averaging the material around each node. When the elevation of the node is obtained for the next time step, the elevation of the center cell is recalculated as the average of the elevations of the three surrounding nodes. Figure 5.12 shows the steps performed by the subroutine.

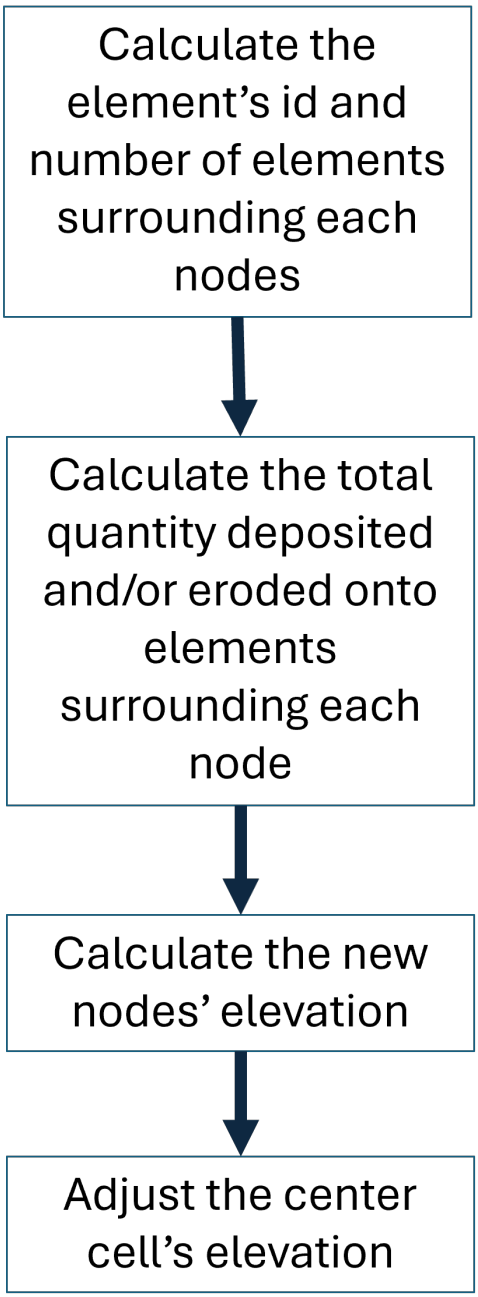

Figure 5.12 Bed evolution Computation Flowchart

The nodes that create the walls remain unchanged. The code distinguishes between real nodes and virtual nodes. The virtual nodes constitute the external fixed walls unless specified otherwise.

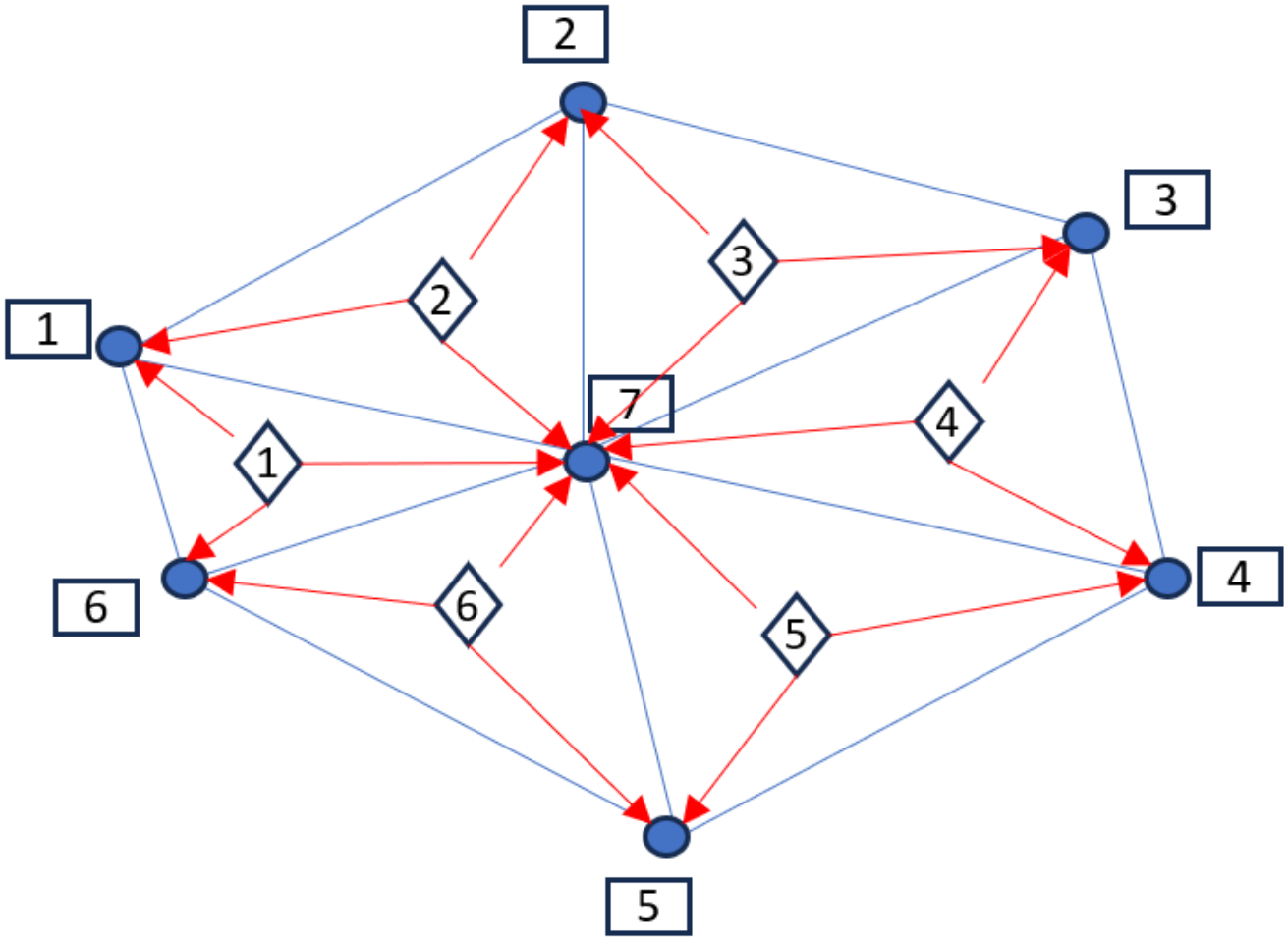

Figure 5.13 Sediment material is transferred from center cell to node

A real node can receive sediment material from the surrounding elements. For instance, in Figure 5.13, an amount of ΔZ is deposited to element 1; the same amount will be distributed to nodes 1, 6, and 7. Thus, the nodes receive an amount of ΔZ. Node 7 receives sediment material from elements 2, 3, 4, 5, and 6. Hence, cumulative sediment material is computed. In addition, the user can decide to divide the cumulative ΔZ received from the surrounding elements by a constant value to use as a calibration parameter, or the number of elements is used by default.

5.2.6 Equilibrium at inlet

As explained in Section 2.1.5, the equilibrium state is an ideal condition achieved when the concentration of solid transport corresponds to the concentration at capacity. STR2D is able to model this case by setting the inlet concentration as being at capacity. In other words, the model computes the sediment-water capacity and inject the corresponding concentration.

5.3 Sediment transport mode, f

The logarithmic matching method consists on handling complicated nonlinear by deriving two asymptotes and merging them into a single composite solution [68]. This method has been applied in various field such as open-channel flows, coastal hydrodynamics, and sediment transport. This method allows to have continuity in the derivative and to avoid unstable numerical oscillations [69].

The sediment transport mode parameter, f, describes the type of sediment mode of transport: bed load, suspended load, or mixed-load. It represents the ratio of suspended portion to the total sediment concentration for a single size class [40]; hence, if f is equal to one, then it is transported as pure suspended load, if it is equal to zero than it is transported as pure bed load, and if it is in between, it is a mixed of both transport modes. The suspension parameter Z influences the sediment transport mode parameter f. Greimann has derived a correlation between the two variables, made of two equations as in Equation 2.45 with a discontinuity in the derivative at $Z = 1$.

In this thesis, a new correlation is developed to consider a smooth transition, a spatial and a temporal lags as the bed load transition to suspended load and vice versa.

In the logarithmic matching method, Equation 2.45 are first transformed into two distinctly asymptotes presented in Equation 5.23 and Equation 5.24. The slopes K_1 and K_2 and the constants C_1 and C_2 of the asymptotes equations are derived from Equation 2.45 [68]:

$$Y_1 = K_1 * ln(x) + C_1 \tag{5.23}$$

$$Y_2 = K_2 * ln(x) + C_2 \tag{5.24}$$

After $C_1 = 0$, $C_2 = 0.92$, $K_1 = 0$, and $K_2 = -1$ are derived, it is possible to obtain x_0 which corresponds to the inflection point between the two logarithmic equations as shown in

Equation 5.25.

$$x_0 = \exp\left(\frac{C_1 - C_2}{K_2 - K_1}\right) \tag{5.25}$$

The parameter $x_0 = 2.5$ is obtained from Equation 5.25.

Guo presents two alternative methods to obtain the single composite solution: Model I shown in Equation 5.26 and Model II shown in Equation 5.27.

$$y_1 = K_1 \ln x + \frac{K_2 - K_1}{\beta} \ln\left\{1 + \left(\frac{x}{x_0}\right)^{\beta}\right\} + C_1 \tag{5.26}$$

$$y_2 = K_2 \ln x + \frac{K_1 - K_2}{\beta} \ln\left\{1 - \exp\left[-\left(\frac{x}{x_0}\right)^{\beta}\right]\right\} + C_2 \tag{5.27}$$

Figure 5.14 shows the application of logarithmic matching method after calibrating the parameter β. Model I was calibrated with a $\beta = 1.87$ for a residual of 0.035. Whereas, Model II was calibrated with a $\beta = 1$ for a residual of 11.6. Model I provided a slightly better result because it had more flexibility to calibrate β than Model II.

However, it is found that the original logarithmic matching method was not able to produce a satisfying single composite solution using Model I or Model II.

Figure 5.15 shows the two asymptotes and the single composite solution obtained through Model I and Model II. Both equations are not able to follow the asymptotes.

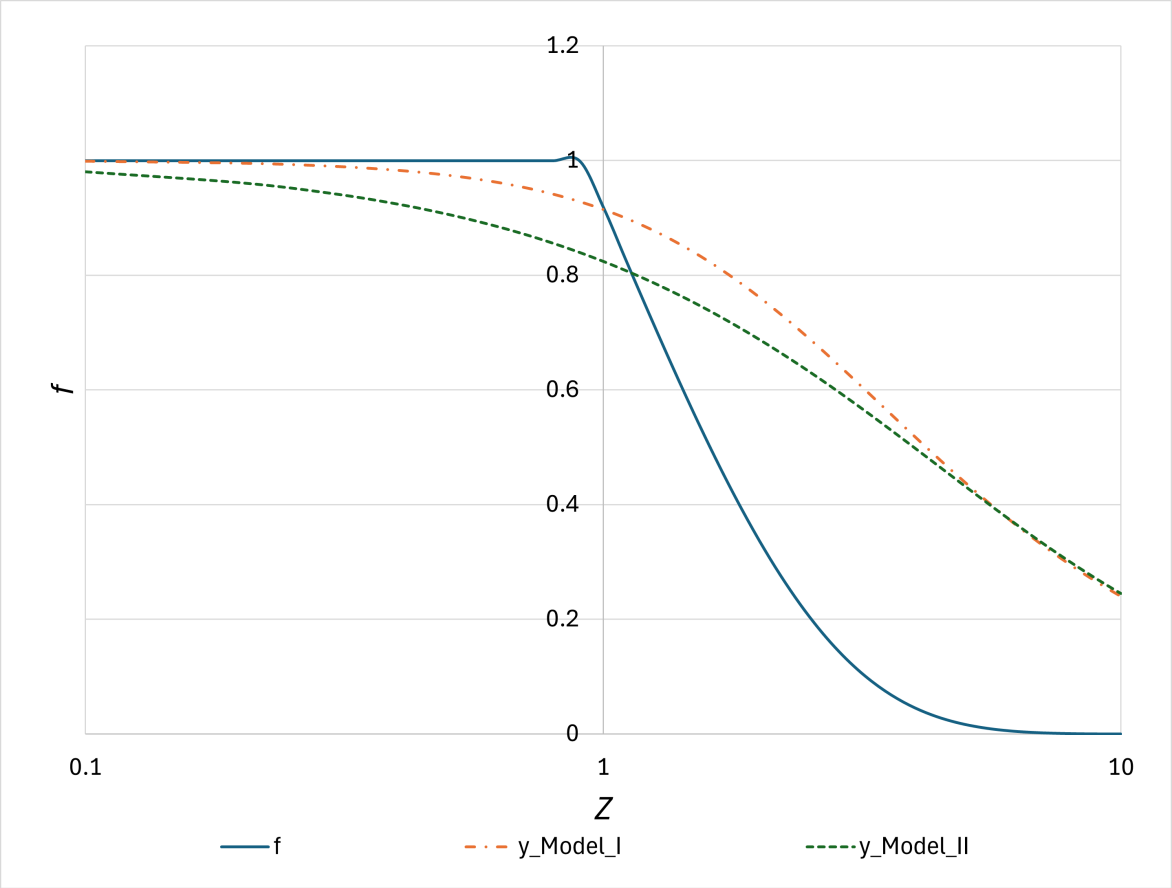

Figure 5.14 Log matching applied to the case

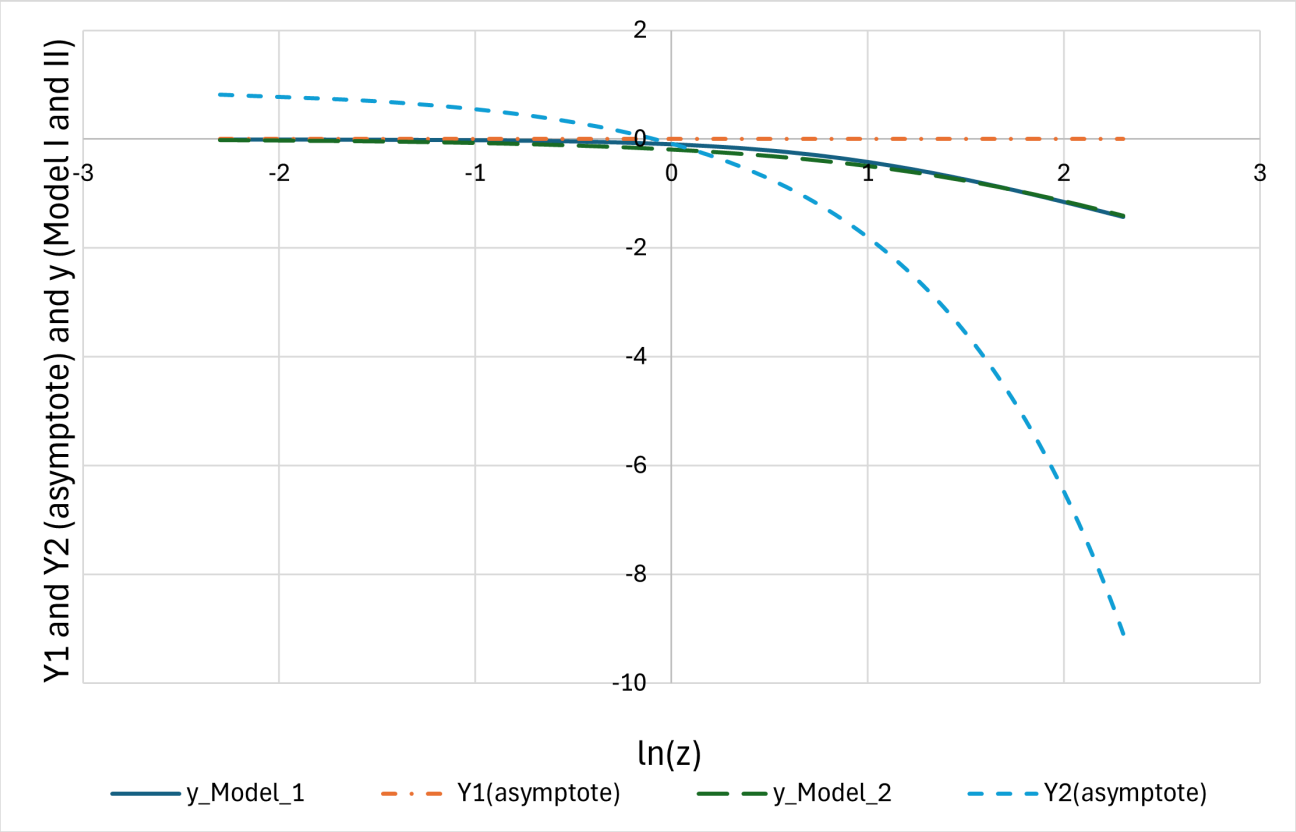

Figure 5.15 Log matching applied to the case in logarithmic scale

The logarithmic matching method is modified using Model I. Three additional parameters, $Param_1$, $Param_2$, and $Param_3$, are inserted in Equation 5.26. Instead of using β as an exponent, x_0 is used. Equation 5.28 is a modified version of the logarithmic matching method using Model I and provides a squared residual of 0.0175.

$$y = K_1 * \ln Z + \frac{K_2 - K_1}{\beta} * Param_3 * \ln\left(1 + \left(\frac{Z * Param_1}{x_0}\right)^{x_0 * Param_2}\right) + C_1 \qquad (5.28)$$

where x_0, $beta$, $Param_1$, $Param_2$, and $Param_3$ are the calibration parameters. The values of the calibration parameters are $x_0 = 1.7$, $beta = 0.7$, $Param_1 = 1.3$, $Param_2 = 4.0$, and $Param_3 = 0.3$.

Figure 5.16 shows that the new developed single composite solution follows well the sediment transport mode equation.

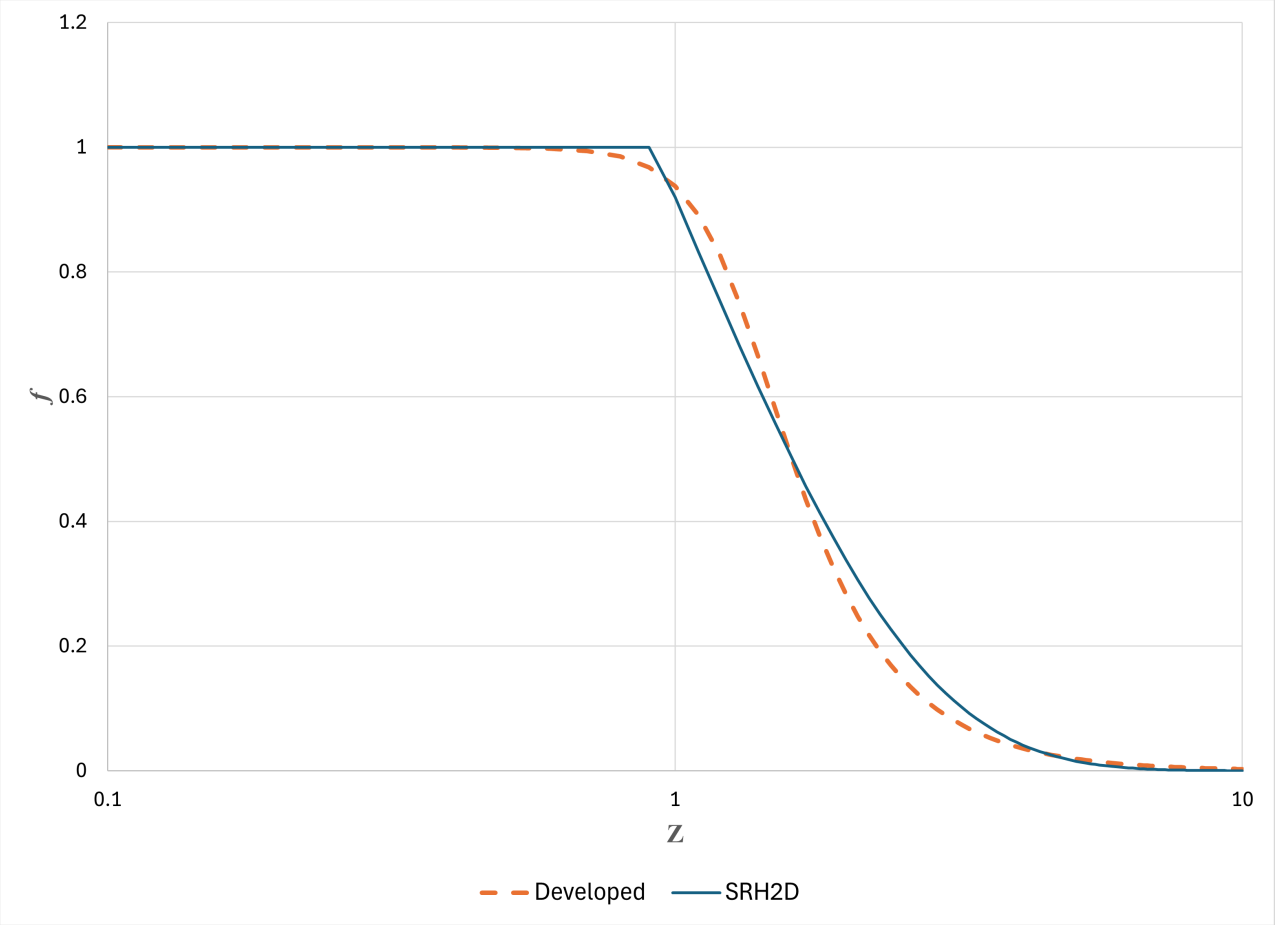

Figure 5.16 Modified Log matching applied

Figure 5.17 shows that the new developed single composite solution follows well the asymp-

totes.

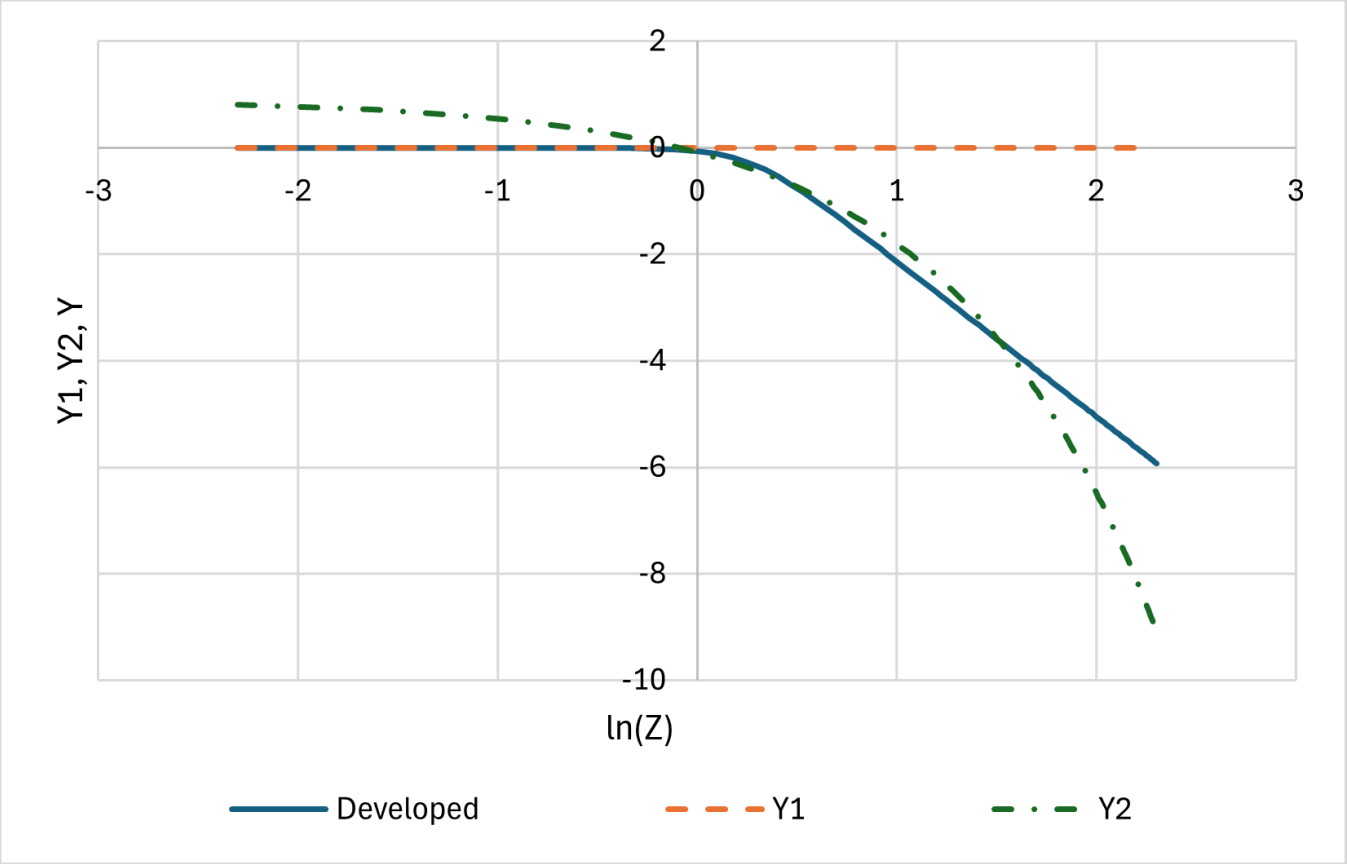

Figure 5.17 Modified Log matching applied in logarithmic scale

CHAPTER 6 RESULTS AND DISCUSSION

STR2D is first numerically verified with SRH2D, which allows comparison of the sediment-governing equations. After the verification process, a validation stage is followed.

6.1 Experimental benchmarks

6.1.1 Rectangular Channel

In a study performed at ETH University, Günter conducted ten experiments in a straight rectangular channel with nonuniform sediments. The third experiment performed by Günter is used as a numerical verification benchmark. The channel is 40 meters long and 1 meter wide, with vertical smooth walls and an initial slope of 0.25% with a mobile bed. The boundary conditions included a constant inflow rate of 0.056 m^3/s with no sediment concentration at the inlet and a constant water depth of 0.09 m at the outlet. A manning coefficient of 0.0182 $s/m^{\frac{1}{3}}$ is used. Figure 6.1 presents the initial and final experimental composition. The final experimental slope is 0.233%. Günter described that initially, the outlet eroded more rapidly than any other part of the channel, resulting in a steeper slope than the original bed slope. This steepening continues until it is constrained by the constant water depth at the outlet. Subsequently, the bed undergoes a rotation until it reaches a constant slope, which Günter refers to as a limit state [70].

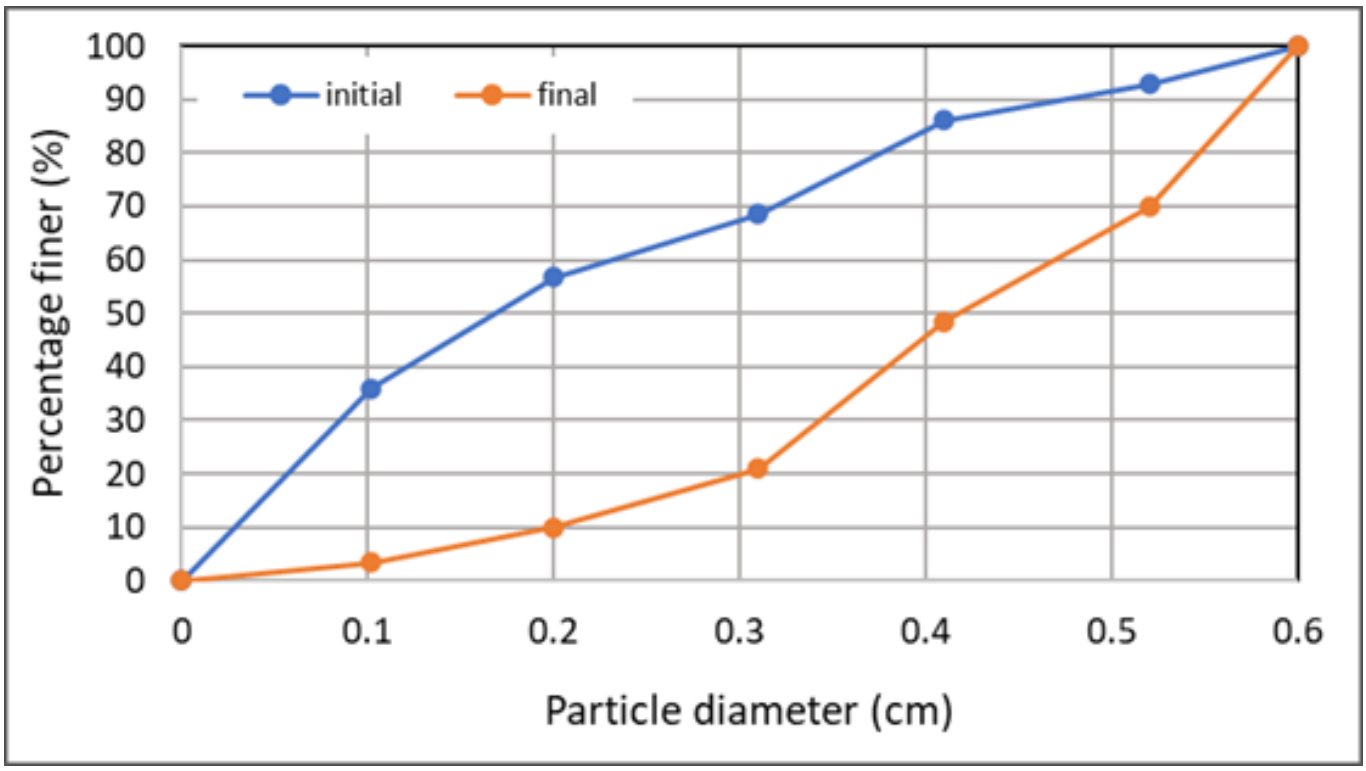

Figure 6.1 Initial and final bed composition of the river's bed

6.2 Verification process

During the verification stage, one sediment class is used to simplify the simulation and facilitate the detection of any numerical issues. This process assesses STR2D's capability to model behavior comparable to that of SRH2D in both nonequilibrium and equilibrium states.

6.2.1 Rectangular Channel

The verification process uses a sediment diameters ranging from 1.02 mm to 2.0 mm with a porosity of 0.339 and a specific gravity of 2.65. The modified Meyer-Peter Muller is selected as the empirical sediment transport equation to compute the sediment-water capacity when the equilibrium state is reached with a dimensionless critical shear stress of 0.047. The thickness of the active layer is set at $14.0 \star d_{50}$. A time step of 0.01 sec is employed, and an unstructured triangular mesh with a size of 0.1 m is used to represent the bathymetry.

Nonequilibrium inlet condition case

When the steady state is reached, the difference in the water surface elevation of the two models are compared in Figure 6.2. In this case, no sediment concentration is injected at the inlet in the channel.

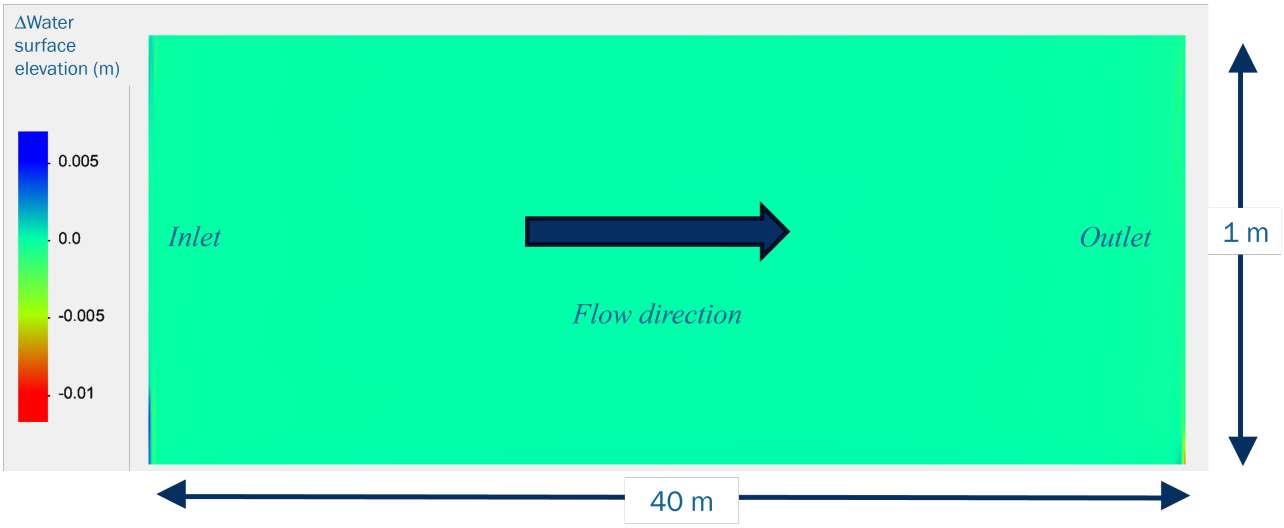

Figure 6.2 Difference of water surface elevation in meter between SRH2D and STR2D

For the first scenario, Figure 6.2 shows the maximum difference of water elevation between SRH2D and STR2D is of around 0.25 cm. A greater discrepancy is observed at the inlet and outlet near the walls. The difference is greater at the inlet near walls because both models consider them differently. SRH2D considers all the inlet cells even near wall to participate by letting the flow entering the channel. Whereas, STR2D does not consider the inlet cells near wall to let the flow in; hence, this explain the discrepancies observed in the results.

Then, the sediment transport module is activated. The difference of bed surface elevation for a simulation time of 30 min and 60 min are compared in Figure 6.3 and in Figure 6.5 respectively. Additionally, Figure 6.3 and Figure 6.5 illustrate the changes in bed elevation across the entire channel. It is evident that the most significant discrepancies occur at the inlet and outlet of the channel, particularly near the walls. The difference between the two models is measured at of a maximum difference of 3 cm and a mean difference of 0.3 cm after 30 minutes and of a maximum difference of 5 cm and of a mean difference of 0.5 cm after 60 minutes, respectively. These differences are considered acceptable.

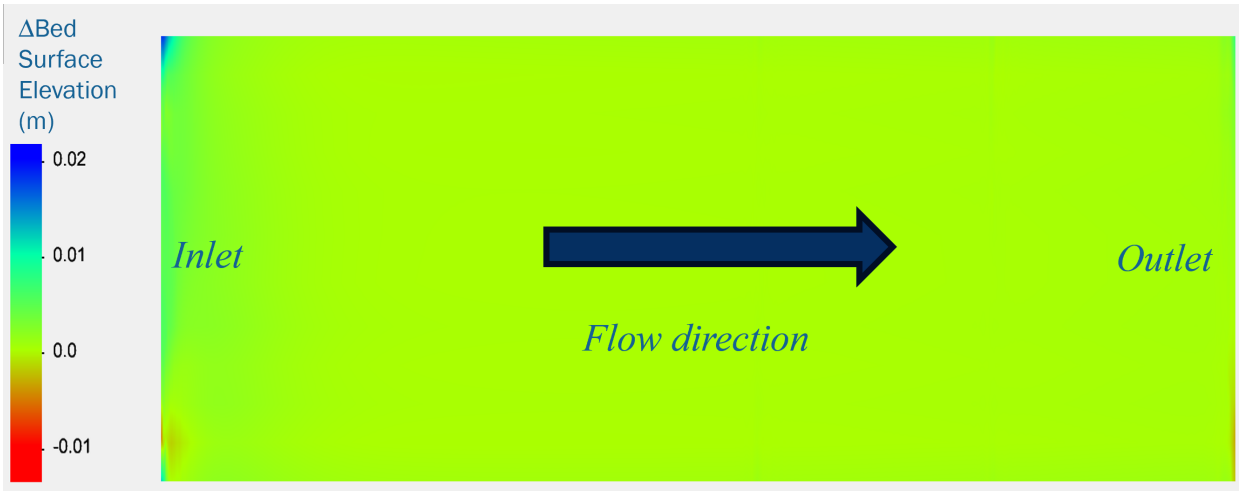

Figure 6.3 Comparison of bed evolution between SRH2D and STR2D in meters for a simulation time of 30 min

Figure 6.4 and Figure 6.5 compare the bed evolution along the longitudinal channel for a simulation time of 30 min and 60 min respectively. The STR2D model successfully captures the significant erosion occurring at the inlet, similar to the SRH2D model. The strong erosion happening at the inlet occurs because the water flowing in the channel does not carry any sediments, producing a flow with low sediment density. The water flow carries less than its maximum capacity. Hence, the flow would want to reach an equilibrium state by carrying more sediments, producing high erosion at the inlet.

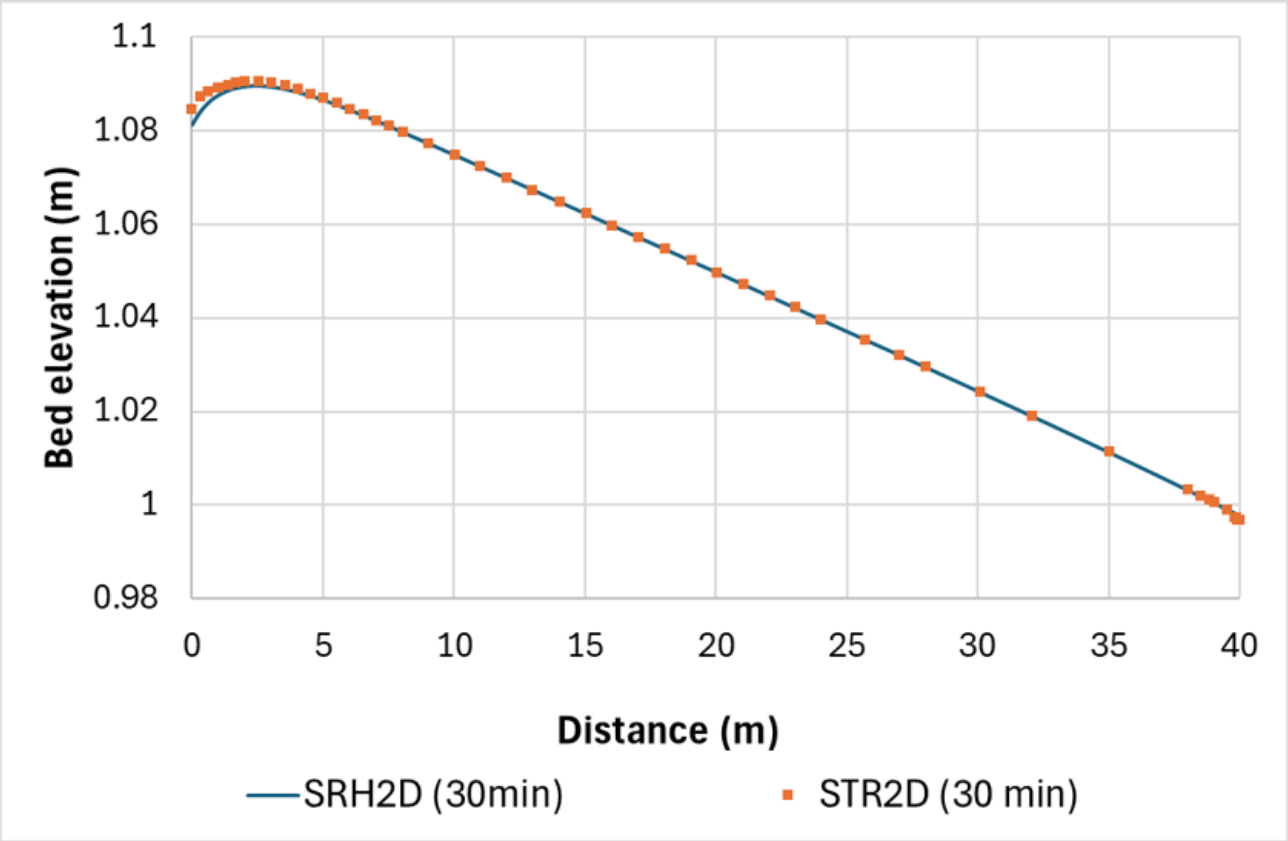

Figure 6.4 Longitudinal bed evolution for 30 min

It is observed that, at a simulation duration of 60 minutes in Figure 6.6, the difference between the two models has increased. The discrepancies at the inlet corner of the channel have also increased as observed in Figure 6.5 and may influence the bed surface elevation near the inlet.

Figure 6.7a and Figure 6.7b show the correlation of the bed evolution across the channel between STR2D and SRH2D.

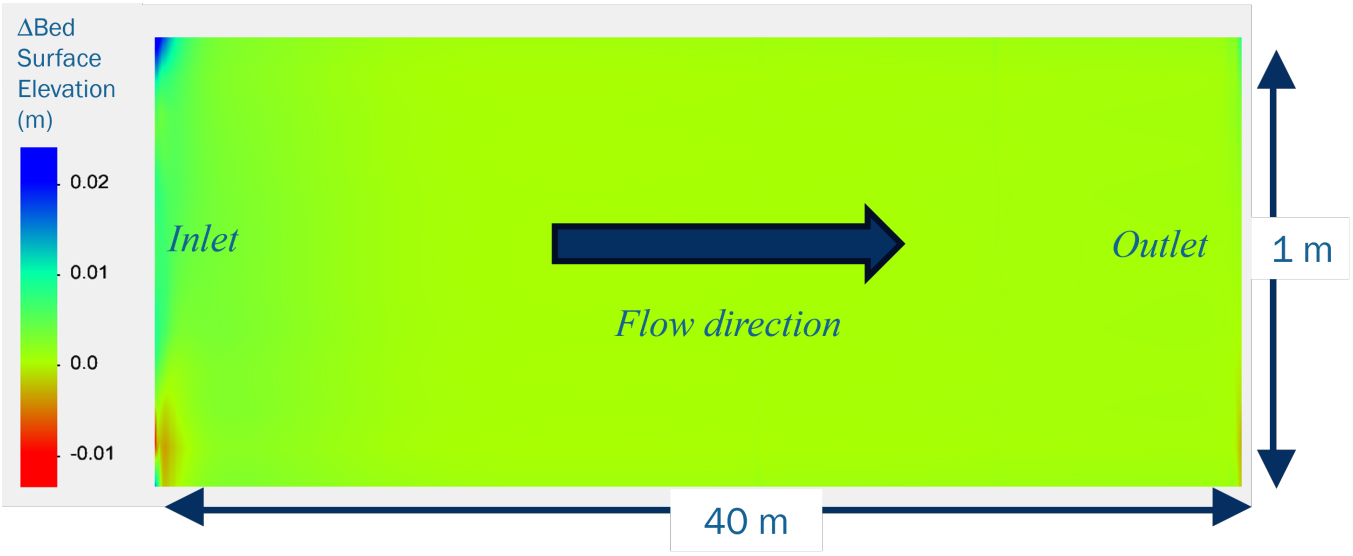

Figure 6.5 Comparison of bed evolution between SRH2D and STR2D in meters for a simulation of time of 60 min

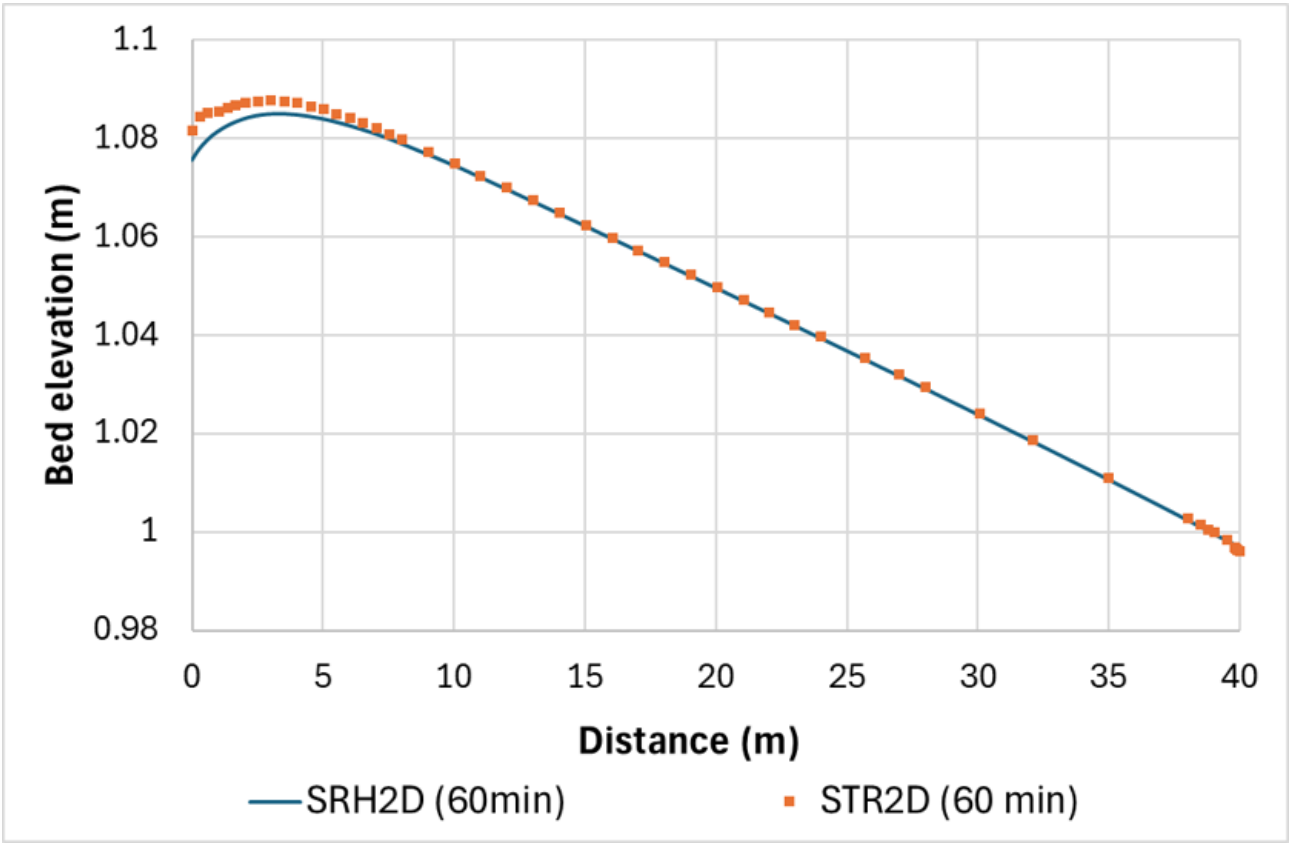

Figure 6.6 Longitudinal bed evolution for 60min

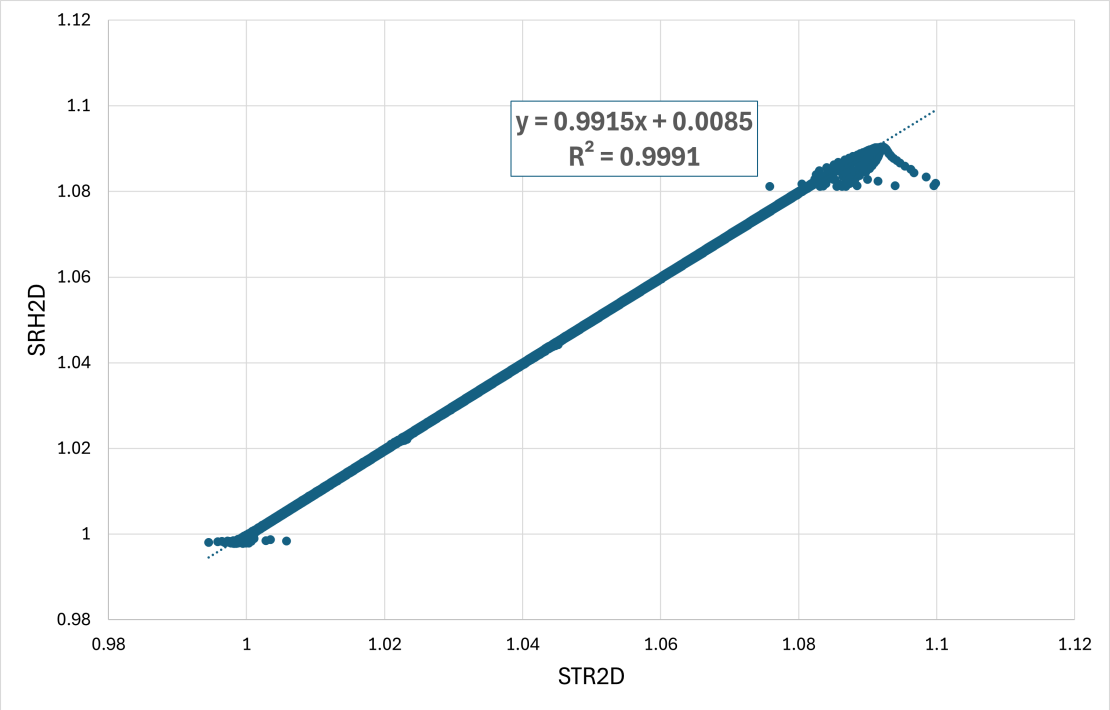

(a)

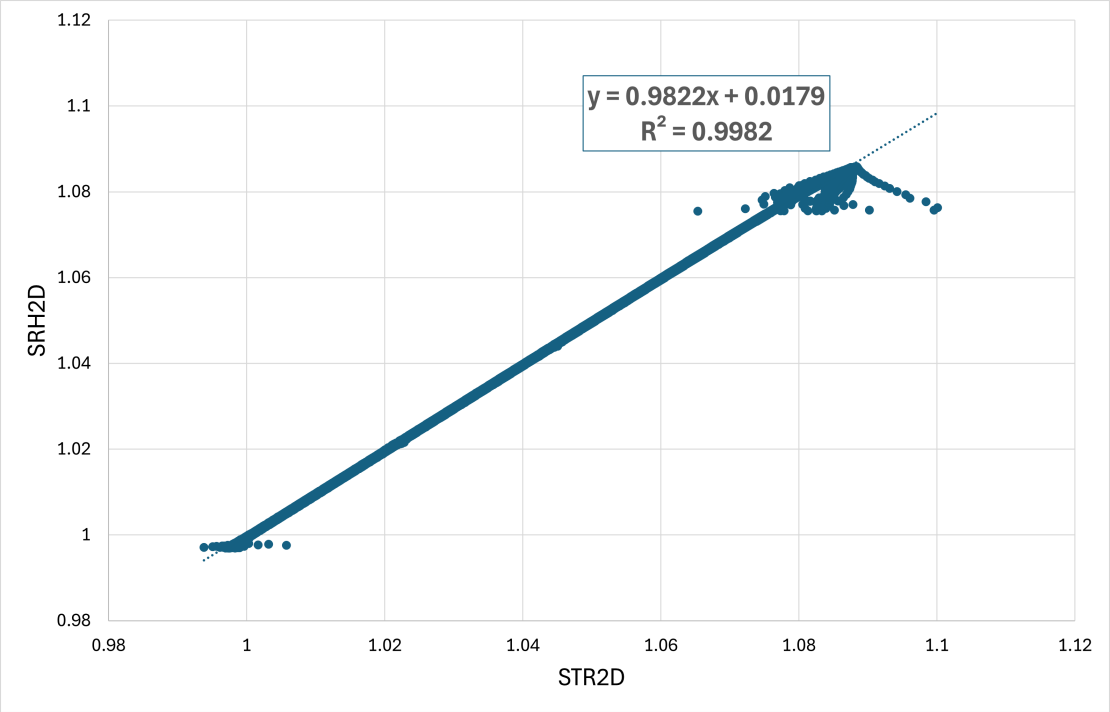

(b)

Figure 6.7 Correlation of Bed Surface Elevation between models for a simulation time of a)30 min and b) 60 min

In addition, the concentration traveling across the channel is also compared as shown in Figure 6.8a and Figure 6.8b display the sediment concentrations in parts per million (ppm) computed by the SRH2D and STR2D models, respectively. Both models exhibit similar behavior; however, the sediment concentration calculated by STR2D at the outlet is a bit higher than the sediment concentration computed by SRH2D. Further investigation is necessary to understand this discrepancy at the outlet.

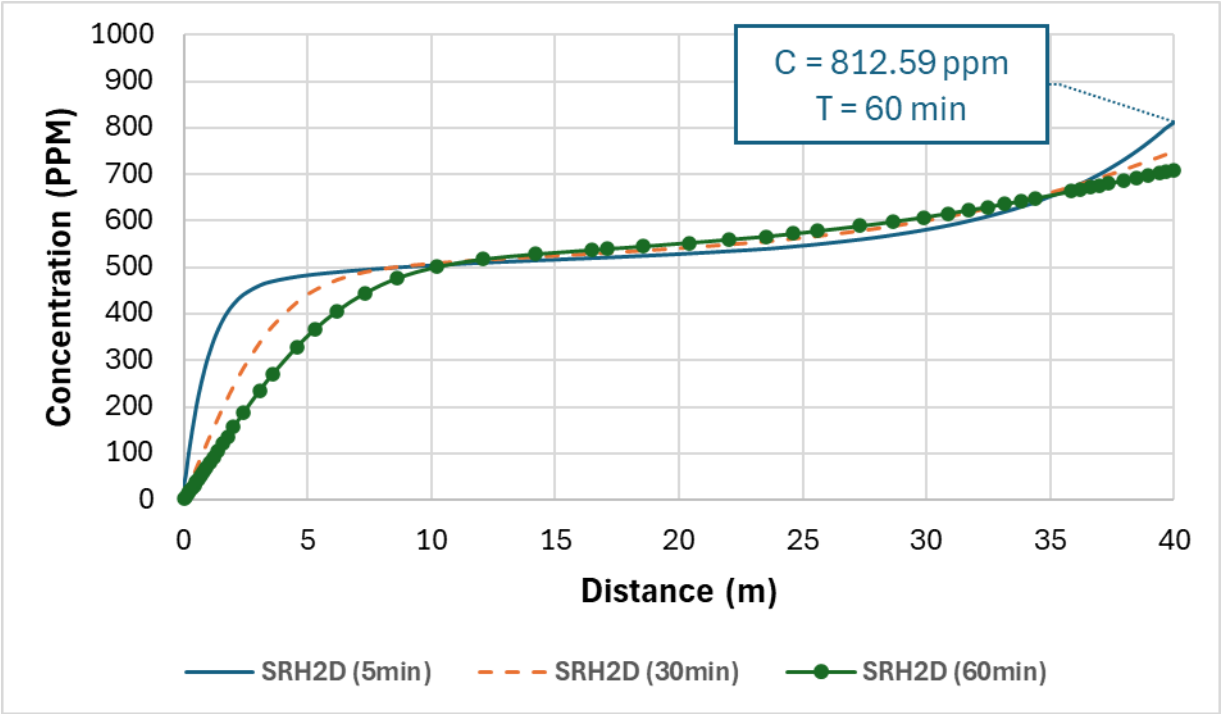

(a)

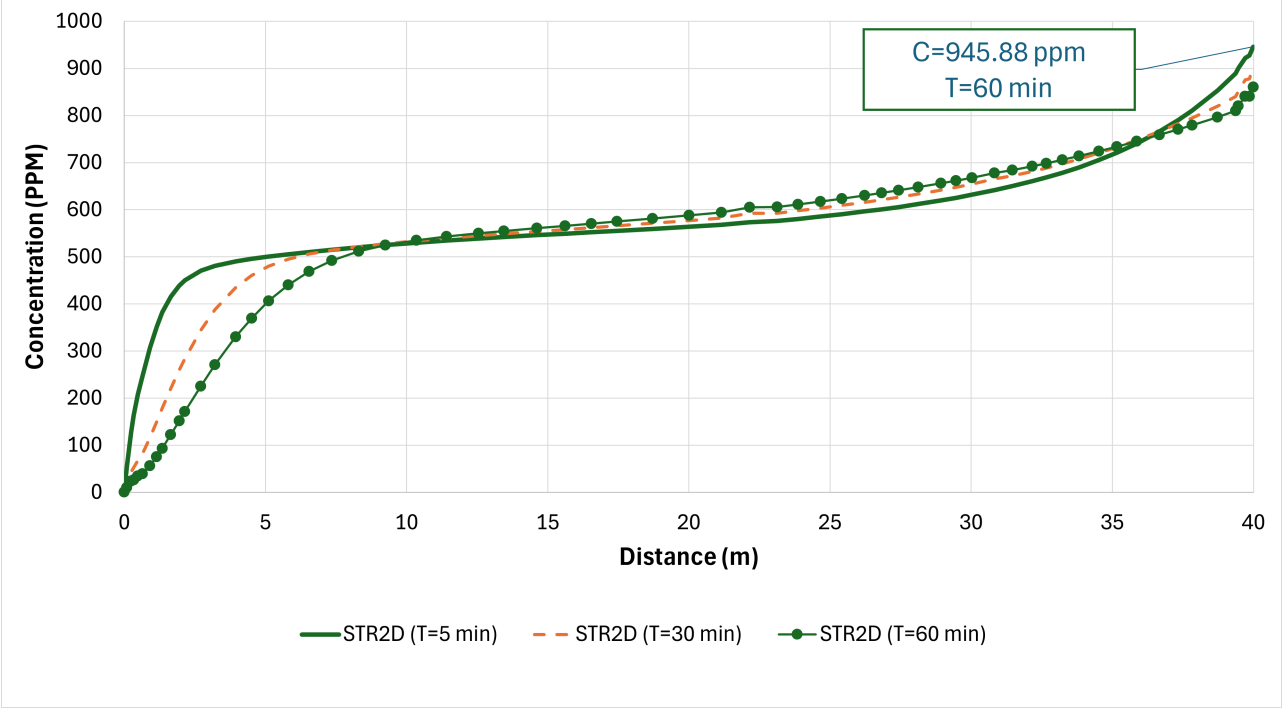

(b)

Figure 6.8 Longitudinal sediment concentration of a) STR2D and b) SRH2D

STR2D can capture the intensive erosion happening at the inlet as SRH2D and model the concentration traveling in the channel. The small discrepancies observed in the results are due to the difference in how both models handle the inlet and outlet conditions, because throughout the channel, the difference between the two models is quite negligible. The verification of this simple numerical benchmark case allows to detect if the model is able to replicate the numerical solution. And if so, to extend to a validation process.

Equilibrium state inlet condition

The second scenario considers an inlet sediment concentration at an equilibrium state. The longitudinal bed surface elevation for a simulation time of 30 min and 60 min are presented in Figure 6.9a and Figure 6.9b, which compares STR2D and SRH2D.

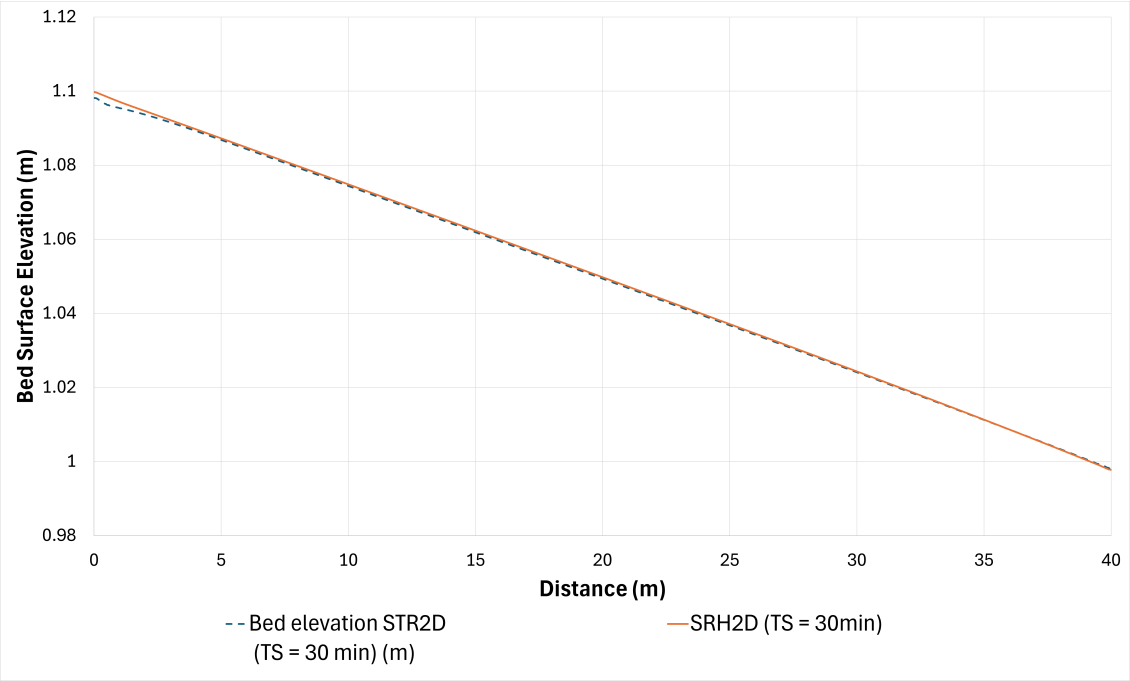

(a)

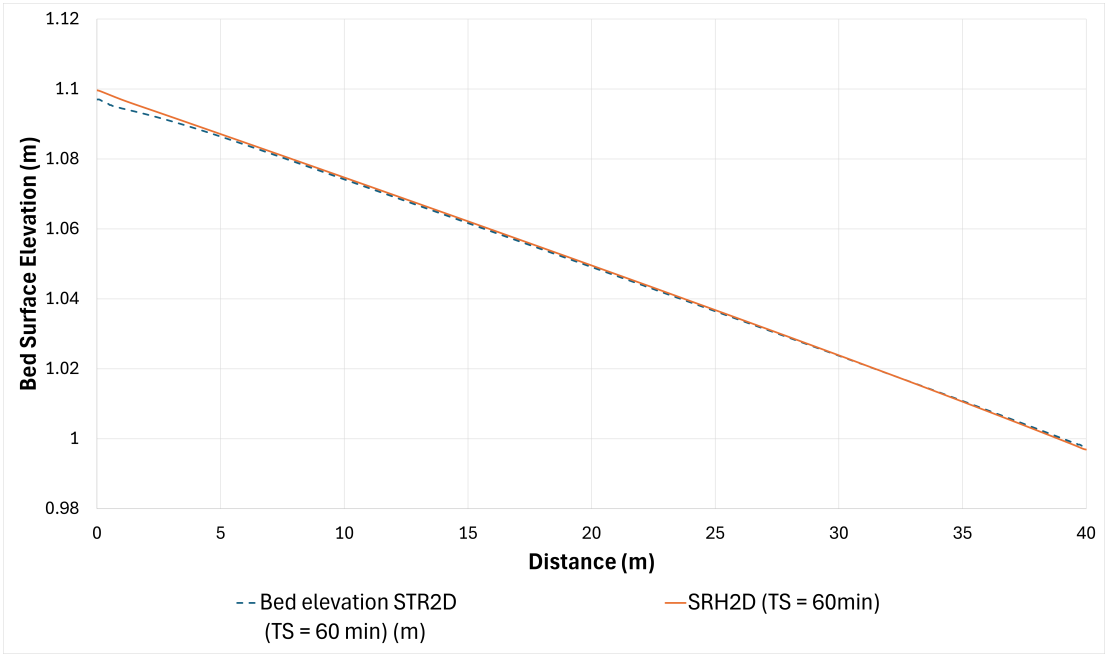

(b)

Figure 6.9 Bed Surface Elevation for simulation time of a) 30 min b) 60 min

Figure 6.10a and Figure 6.10b show the difference of bed surface elevation for a simulation time of 30 min and 60 min across the domain. The most significant discrepancy is observed at the inlet for both simulation times. The difference of bed surface elevation between the models is of maximum 0.52 cm and a mean difference of 0.032 cm for the 30-minute simulation and a maximum difference of 0.58 cm and a mean difference of 0.06 cm for the 60-minute simulation. The change in bed evolution has increased of about 0.06 cm. The parameter β_k was set to 0.25 for STR2D, which aligns with the concentration calculated by SRH2D. This parameter was found to significantly impact the computed sediment concentration, and the concentration predicted by STR2D closely follows the trend established by SRH2D.

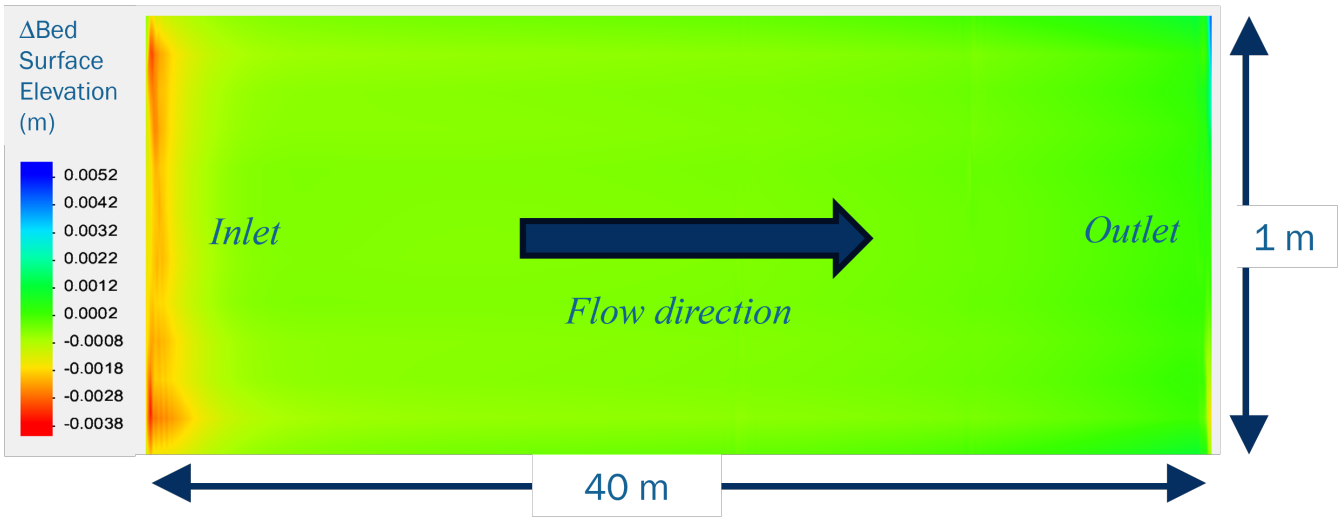

(a)

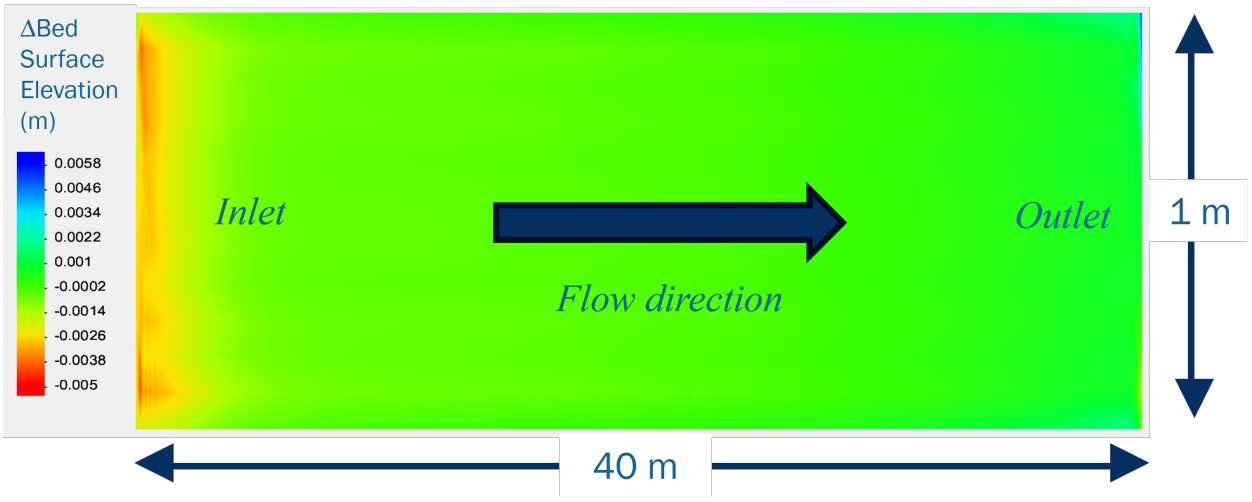

(b)

Figure 6.10 Difference of Bed Surface Elevation for simulation time of a) 30 min b) 60 min

It is observed that the most significant differences in concentration occur near the inlet and outlet, as shown in Figure 6.11a and Figure 6.11b. This discrepancy does not increase as the simulation time progresses. Figure 6.12a and Figure 6.12b illustrate the concentration profile along the channel.

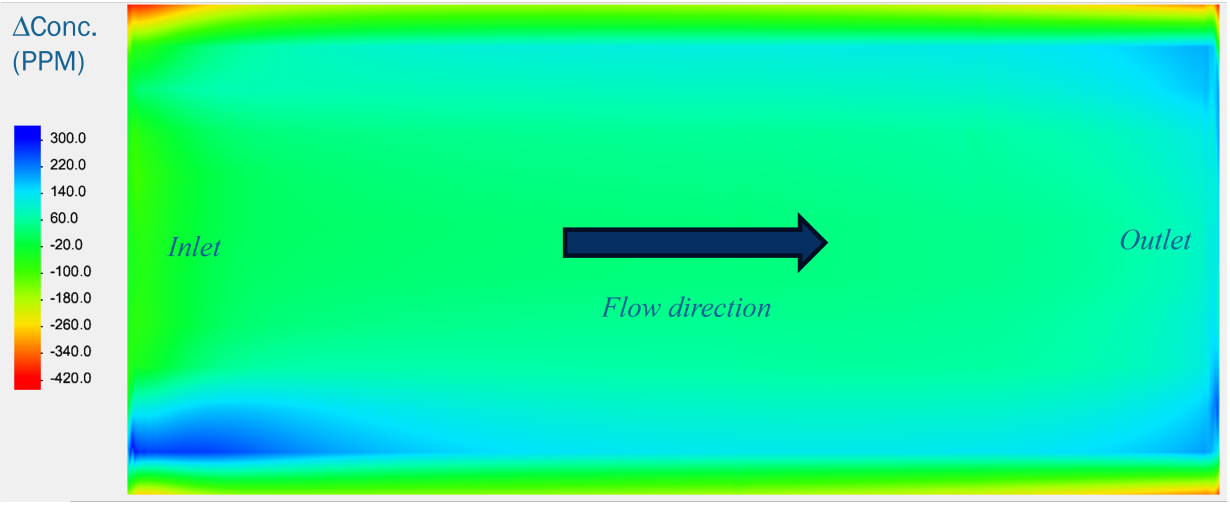

(a)

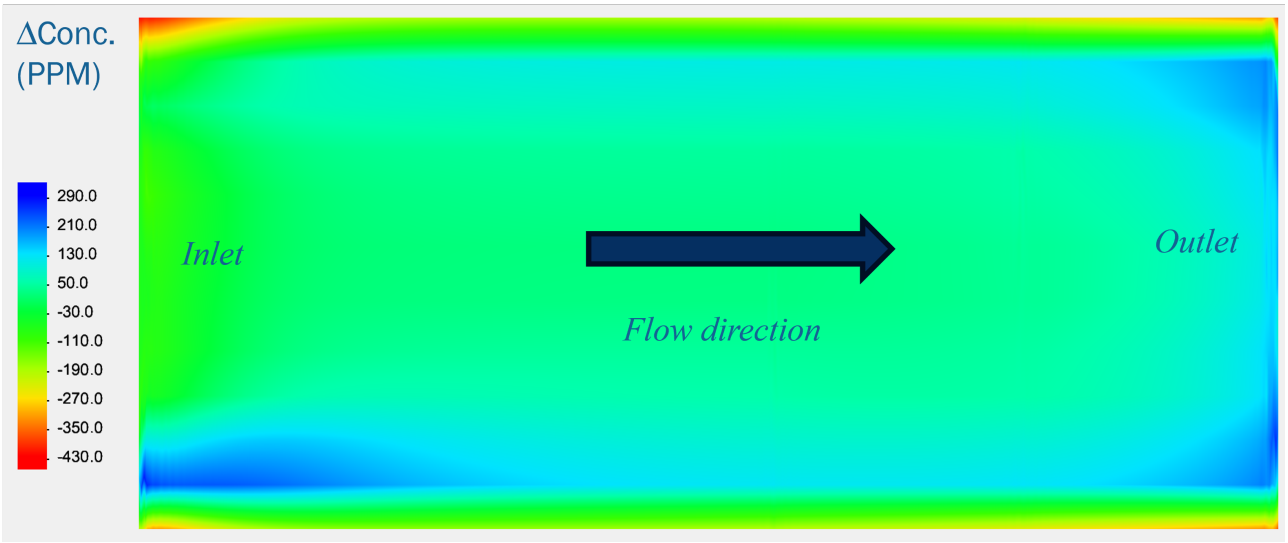

(b)

Figure 6.11 Difference of concentration in ppm for simulation time of a) 30 min b) 60 min

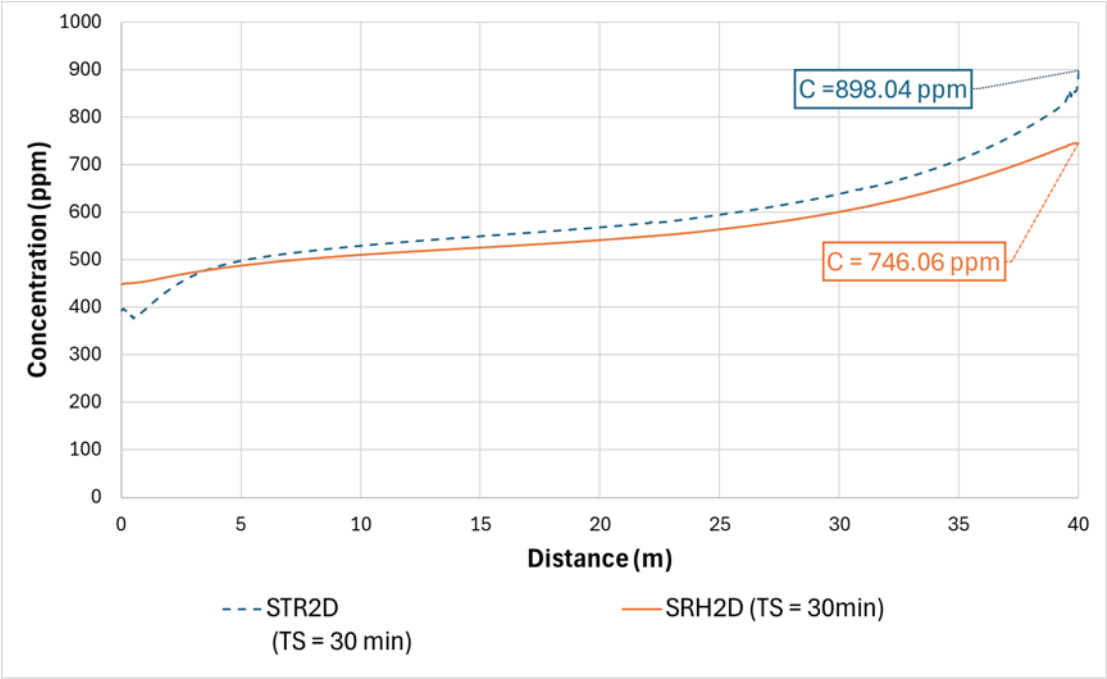

(a)

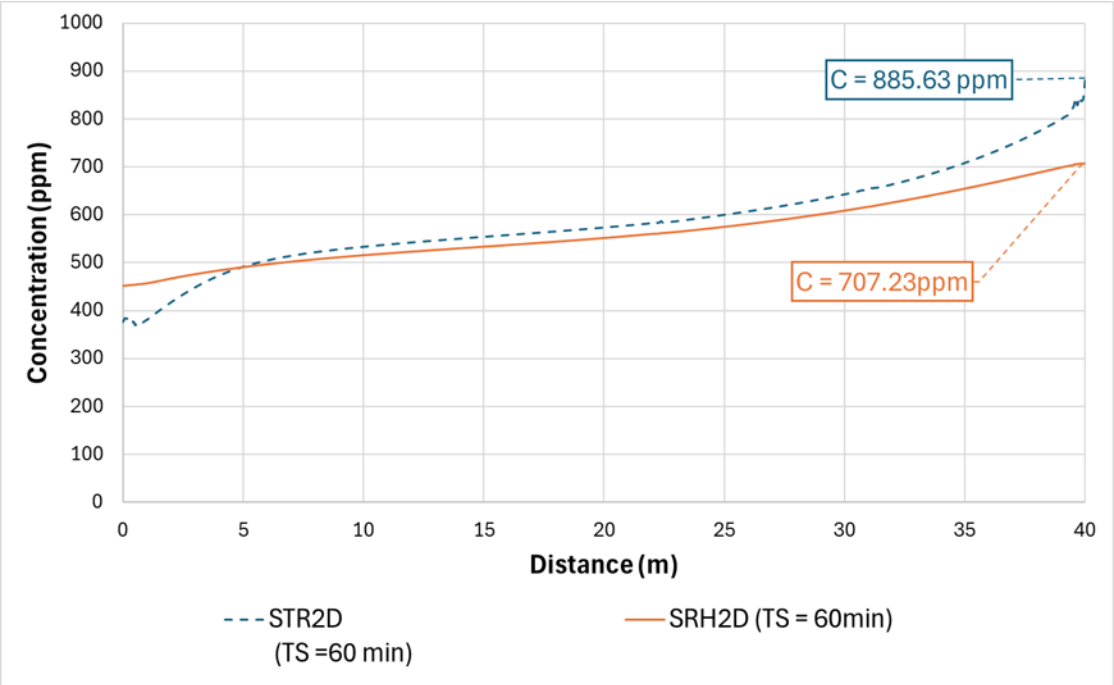

(b)

Figure 6.12 Concentration in ppm for simulation time of a) 30 min b) 60 min

6.3 Validation process

6.3.1 Rectangular Channel

Five sediment classes are presented in Table 6.1. They represent the bed composition using different types of sediment diameter, from coarse sand to fine gravel. Each sediment class represents an interval of sediment diameter with an upper and lower limit. A representative diameter of each class, the geometric diameter, is computed based on these limits forming the sediment class as explained in Section 5.2.3.

Table 6.1 Upper and lower sediment diameter for sediment class

Sediment class (k)	Upper sediment class (cm)	Lower sediment class (cm)
1	0.102	0.2
2	0.2	0.31
3	0.31	0.41
4	0.41	0.52
5	0.52	0.6

Figure 6.13 shows the composition at initial and final experiment performed by Günter for the five sediment class. The composition is represented by the non-cumulative sediment gradation which is a ratio of the presence of the material with respect to the total material of the five classes.

The blue bars indicate the initial condition, while the orange bars show the final composition. This allows for an easy assessment of changes in bed composition. Notably, the first sediment class, which consists of the smallest particles, has experienced erosion of more than half of its initial amount. Four calibration parameters are investigated to assess their influence on the bed composition: the inlet condition, the hiding-exposure effect, the adaptation length, and the active layer's thickness.

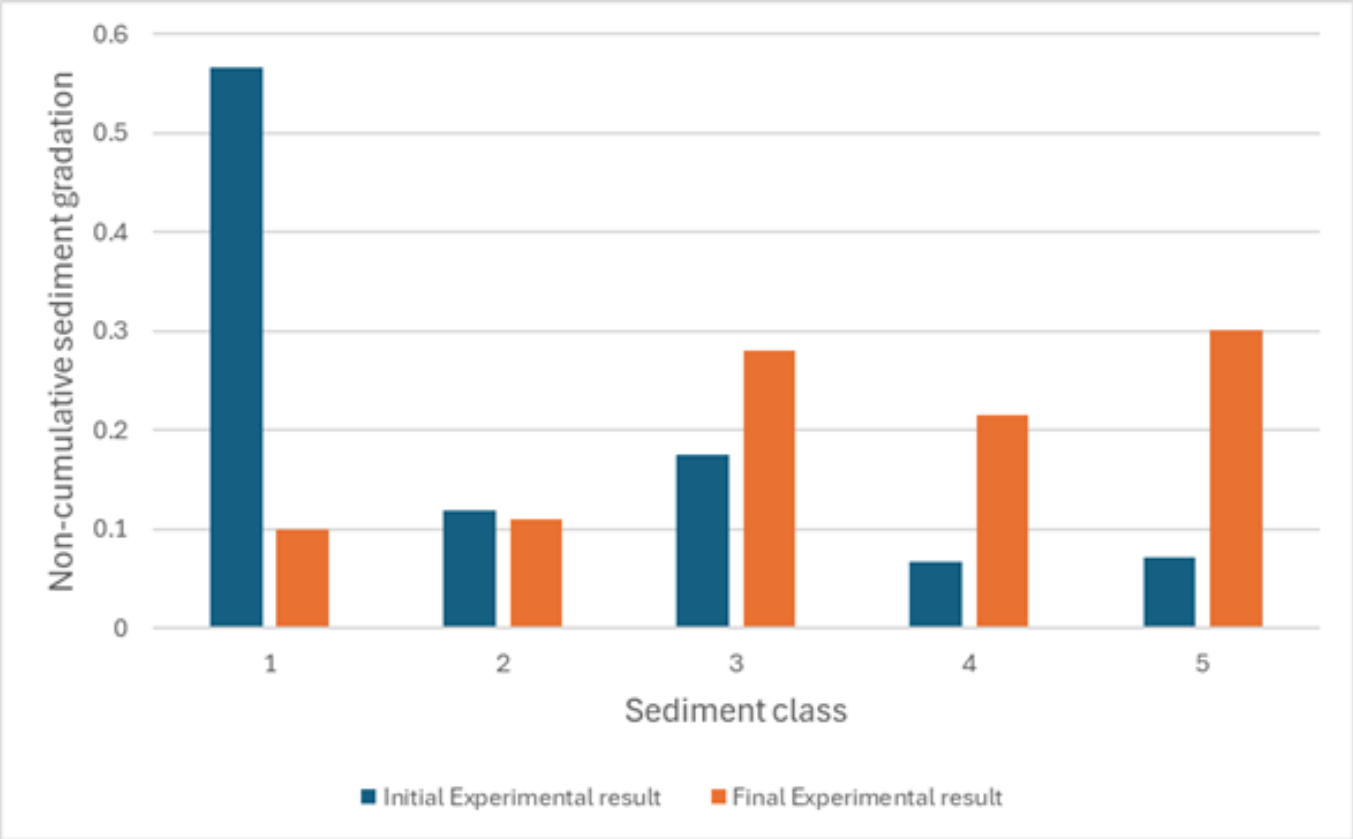

Figure 6.13 Non-cumulative experimental sediment gradation at initial and final state

Figure 6.14 presents the experimental benchmark showing the location of three monitor points that will be used to asses the bed composition during the simulation. SRH2D can only use monitor points to collect bed composition information. Meanwhile, obtaining the bed composition information from STR2D for the whole domain is possible. A five-hour simulation time was chosen because tended to reach a composition stability as shown in Figure 6.15.

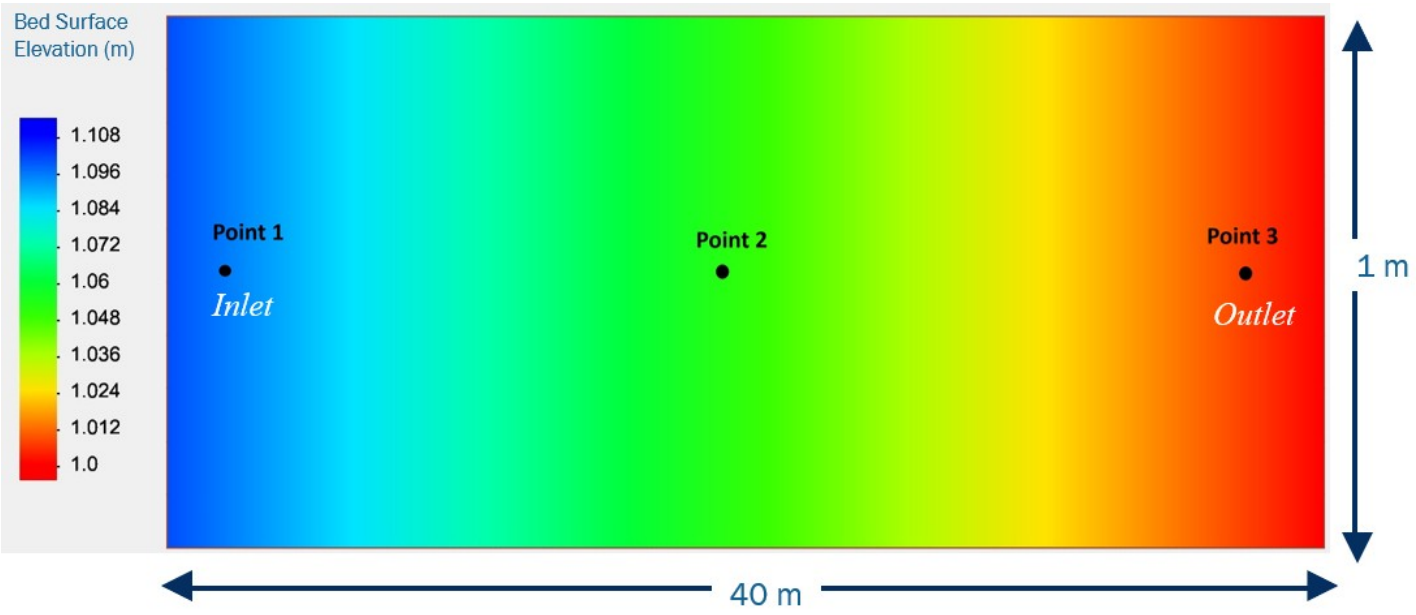

Figure 6.14 Location of monitor points along the channel

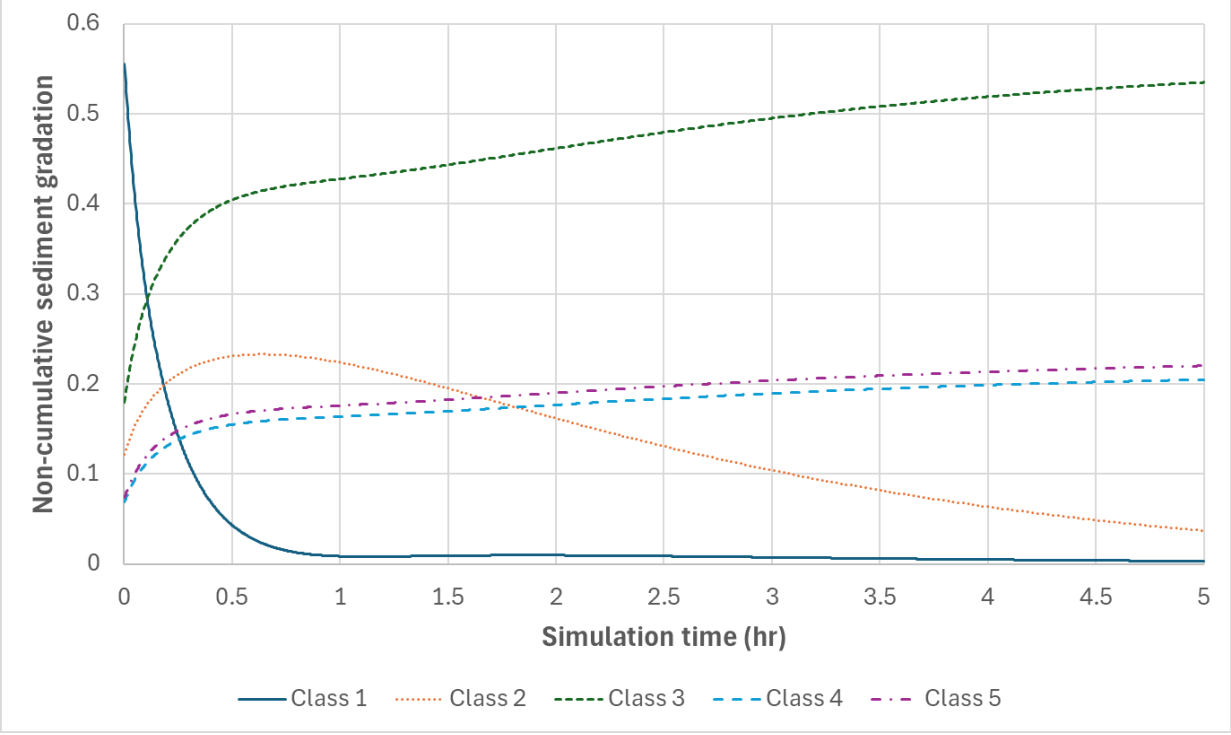

Figure 6.15 Non-cumulative sediment gradation at point 1 for a simulation time of 5 hours for SRH2D

A histogram is used to assess the impact of the calibration parameter on the bed composition. The bars represent different compositions of the five sediment classes, with the orange bar located at point 1, the dark green bar at point 2, and the blue bar at point 3, as shown in Figure 6.14. The continuous line in the histogram represent the experimental result which will be used as a guideline because the experiment has taken the bed composition of the whole domain.

A somewhat uniform erosion across the channel was observed overall by Günter [70], which shows a different behavior from what was observed in the first scenario of the verification case (no sediment injected at the inlet), where more significant erosion occurred at the inlet than compared to other parts of the channel. Hence, initially, the inlet condition is imposed at an equilibrium state. This boundary condition considers the water flow at its maximum capacity, reducing erosion at the inlet. However, the final simulated slope was steeper than the final experimental slope, and the bed's composition did not vary much over time as the experimental results. This can be explained by the fact that the water capacity is already at its limit and erodes mildly, and with little deposition. However, the simulated bed composition did not match the final experimental bed composition; hence, the inlet condition had to be changed to a non-equilibrium state.

Figure 6.16 shows the effect of hiding-exposure effect on the bed composition. A hiding-exposure effect is a calibration parameter that can be used when dealing with nonuniform sediments. The effect of the hiding-exposure effect on the erosion process is analyzed in order to calibrate this parameter. Figure 6.16 shows the results of four simulations in which hiding-exposure effect of 0.9 (a), 0.5 (b), 0.1 (c), and 0.0 (d) were used to analyze its effect on erosion. They are compared with the experimental result represented as a continuous line. The five sediment classes presented in Table 6.1 are presented in the abscissa. The ordinate presents the non-cumulative sediment gradation, which is the amount of the sediment class as a fraction to the total sediment volume (also known as the volume of fraction). Each sediment class has three bars representing the amount of sediment class at points 1 (in orange), 2 (in green), and 3 (in blue). These points correspond to the points defined in Figure 6.14. At each of these points, the non-cumulative sediment gradation of all of the five sediments classes adds up to 1. The curve represents the experimental final gradation curve which was obtained by through a sieve analyse [29]. The smallest particles (class 1) are found to be the most affected by the hiding-exposure effect. As the hiding-exposure effect decreases, their non-cumulative sediment gradation decreases as well. In other words, as the hiding-exposure effect decreases, there is more erosion of smaller particles (class 1), especially at the upstream end of the channel (point 1). The opposite is observed for larger particles (classes 4 and 5). As the hiding-exposure effect decreases, the non-cumulative sediment gradation increases for

sediment classes 4 and 5. Thus, as the hiding-exposure effect decreases, there is less erosion for larger particles. When there is no hiding-exposure effect, the results obtained by STR2D align more closely with the experimental results. Therefore, future analysis will not consider the hiding-exposure effect.

(a) Hiding-exposure effect of 0.9

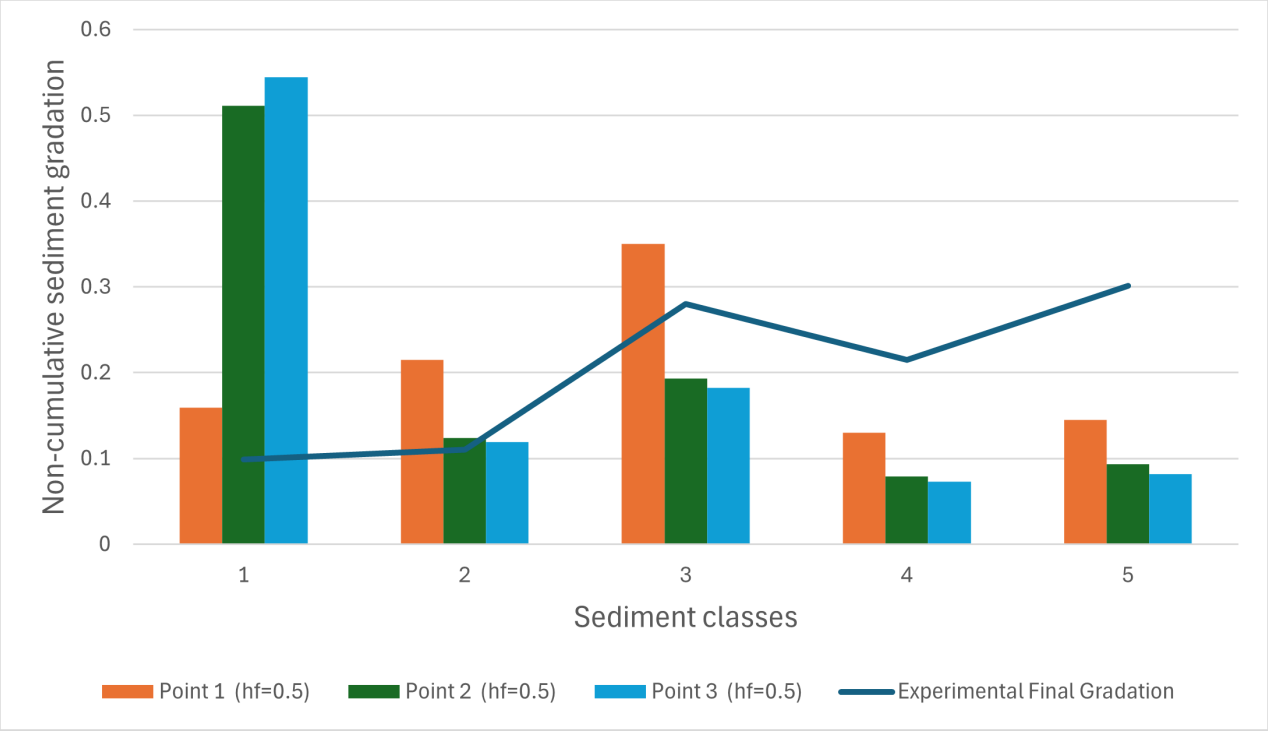

(b) Hiding-exposure effect of 0.5

Figure 6.16 Effect of hiding-exposure effect on the bed composition at point 1, point 2, and point 3 for a simulation of time 5 hours with a hiding-exposure effect of a) 0.9 b) 0.5 c) 0.1 d) 0.0

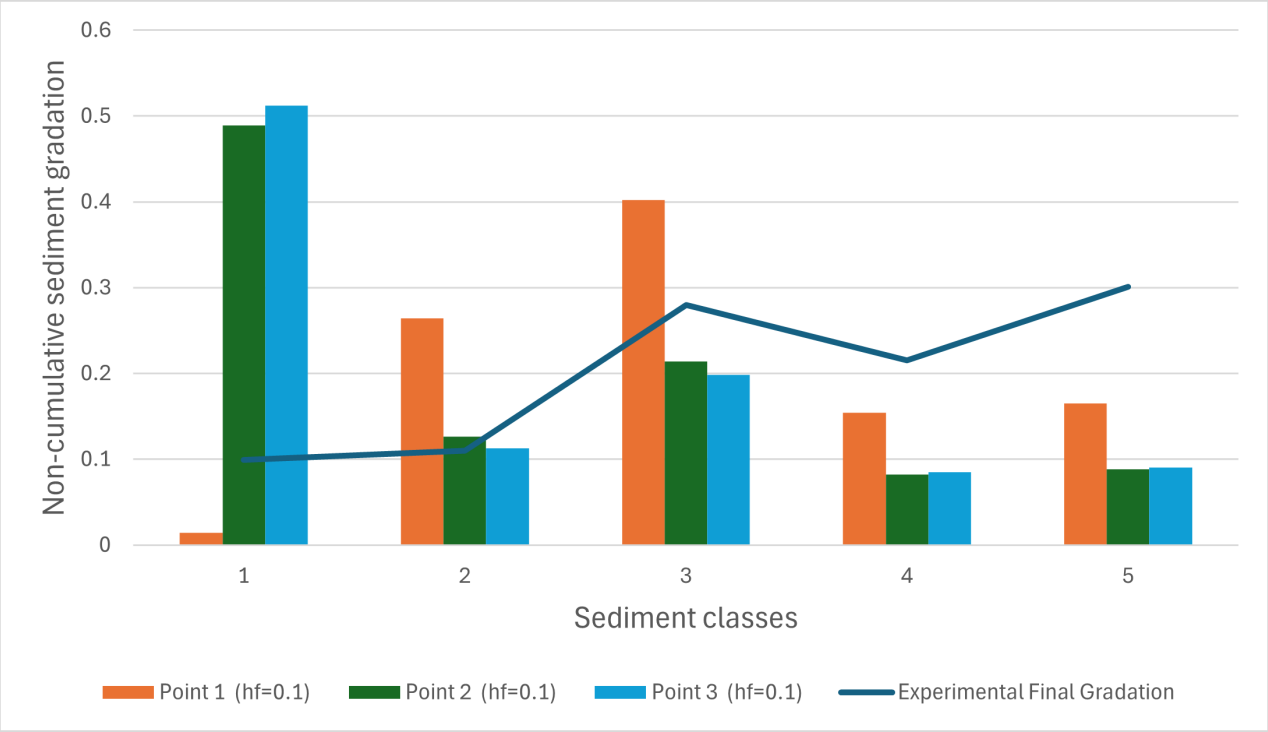

(c) Hiding-exposure effect of 0.1

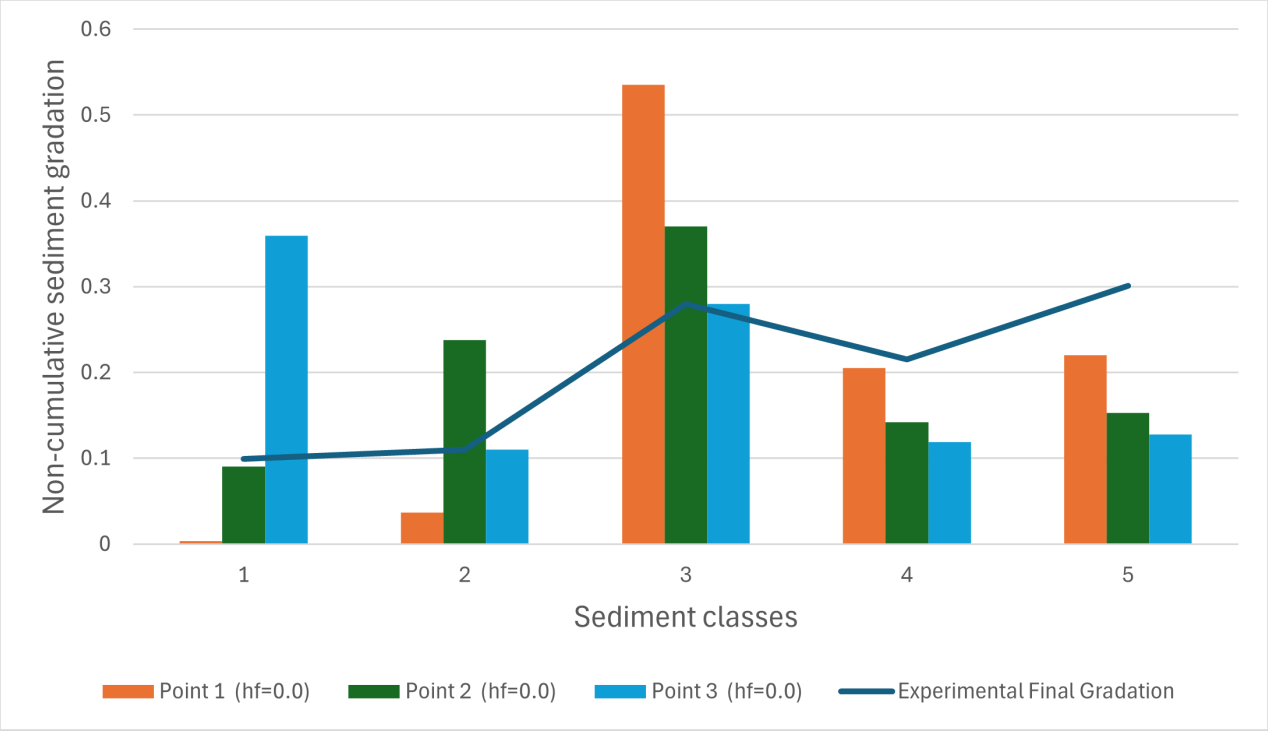

(d) No Hiding-exposure effect

Figure 6.16 Effect of hiding-exposure effect on the bed composition at point 1, point 2, and point 3 for a simulation of time 5 hours with a hiding-exposure effect of a) 0.9 b) 0.5 c) 0.1 d) 0.0 (continued)

Figure 6.17 shows the effect of the adaptation length on the bed composition which will be explained in the Discussion section. Furthermore, the effect of the bed load adaption length is also analyzed. Figure 6.17 shows the results of three simulations in which adaptation lengths of 0.1 m, 0.2 m, and 0.409 m where used. The bed composition was found to remain constant despite the variation in the adaptation length . Hence, an adaptation length of 0.409 m is chosen because it is greater than the mesh size [14].

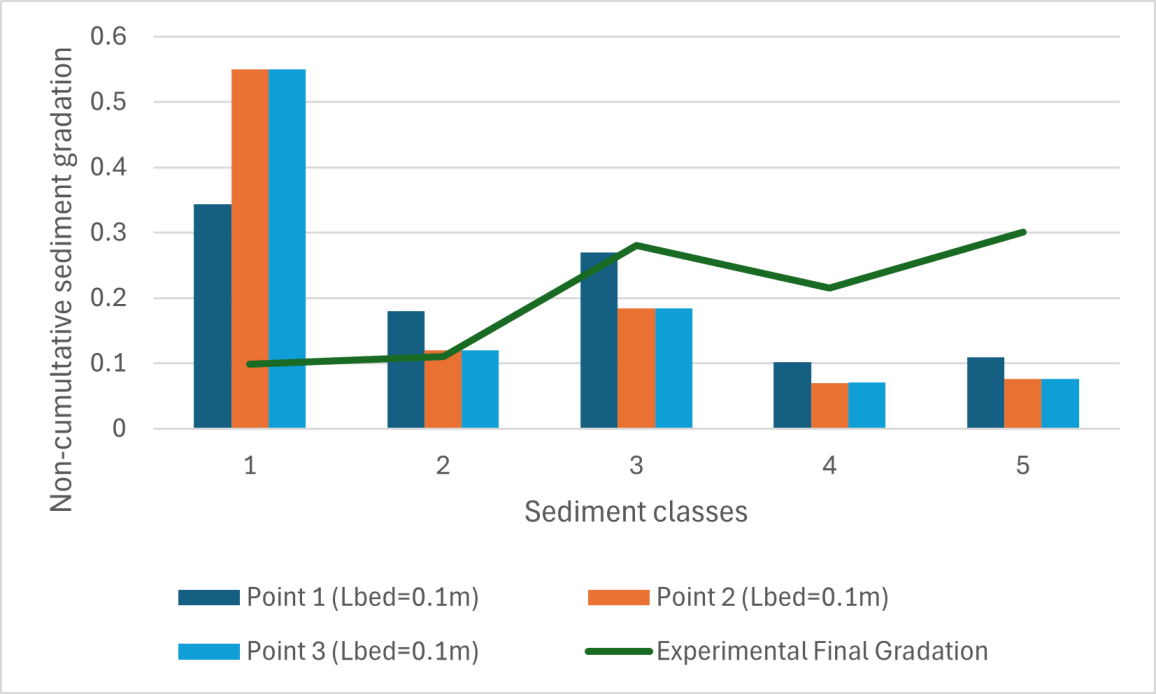

(a) Adaptation length of 0.1m

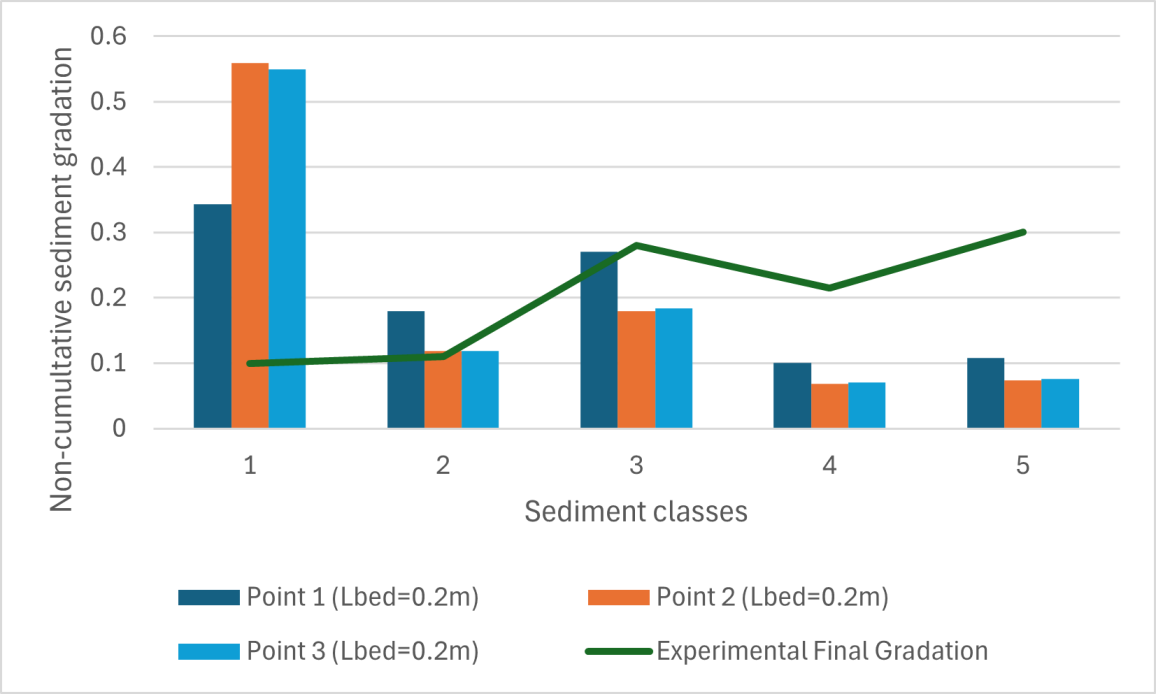

(b) Adaptation length of 0.2m

Figure 6.17 Comparing the effect of bed load adaptation length of 0.1 m, 0.2 m, and 0.409 m on the bed composition at a) point 1, b) point 2, and c) point 3 for a simulation time of 5 hours

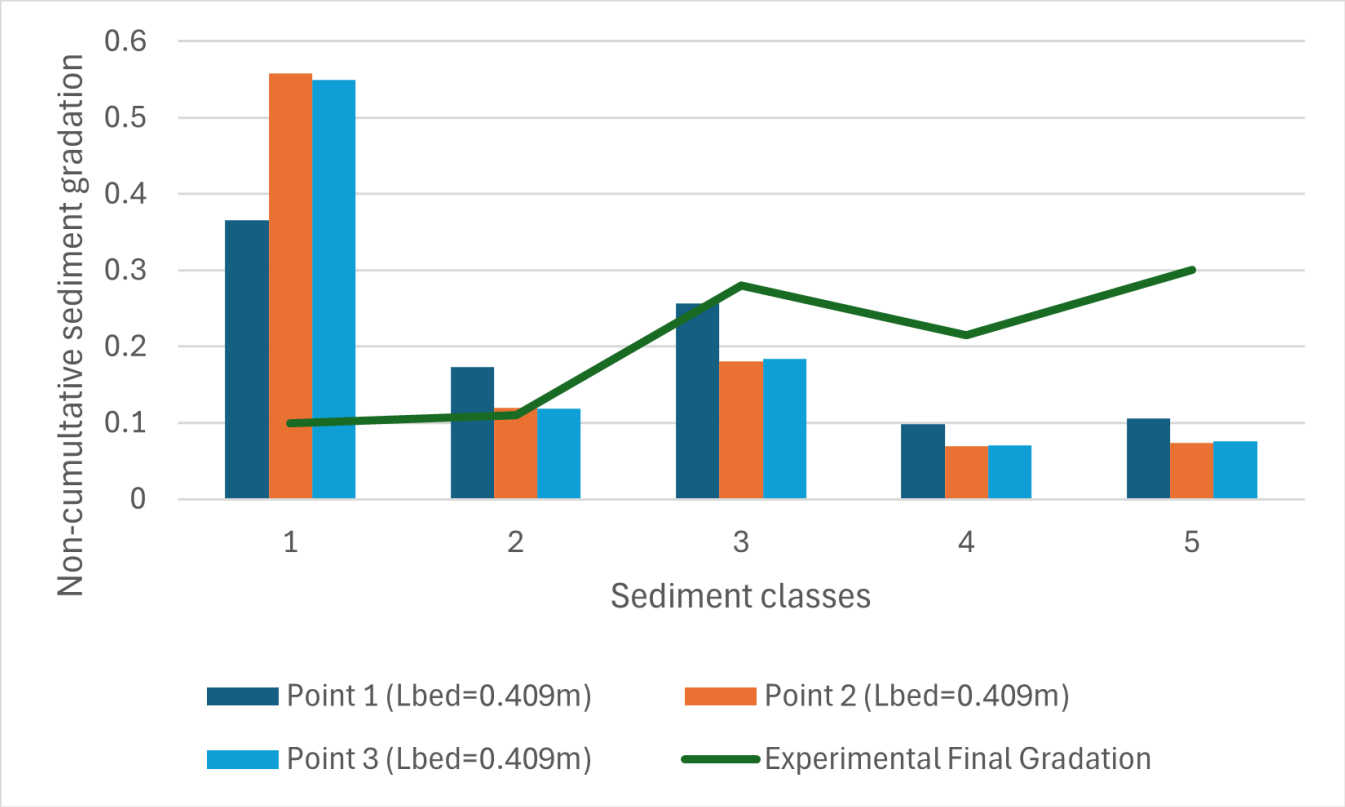

(c) Adaptation length of 0.409m

Figure 6.17 Comparing the effect of bed load adaptation length of 0.1 m, 0.2 m, and 0.409 m on the bed composition at a) point 1, b) point 2, and c) point 3 for a simulation time of 5 hours (continued)

Figure 6.18 shows the effect of the active layer thickness on the bed composition which will be explained in the next chapter. Another calibration parameter is the thickness of the active layer. Restricting the thickness of the active layer allows the control of the water capacity by not saturating it and by allowing more uniform erosion and deposition along the channel. Figure 6.18 shows the results of three simulations in which the active layer's thickness was set to $14.0 * \delta_a$ (a), $3.0 * \delta_a$ (b), and $1.0 * \delta_a$ (c). As seen from Figures 6.18 a, b, and c, as the active layer's thickness decreases, the non-cumulative sediment gradation also decreases for sediment class 1. Thus, as the active layer's thickness decreases, its capacity for erosion of small particles increases. The opposite is observed for larger particles. As the active layer's thickness decreases, the non-cumulative sediment gradation increases for sediment classes 3, 4, and 5. Thus, the active layer's ability to deposit larger particles increases as its thickness decreases. Decreasing the active layer's thickness further improves the composition's uniformity. A five-hour simulation time was chosen because, as shown in Figure 6.15, the bed composition tends to stabilize after that amount of time. As mentioned previously, the experimental result is used as guidance. It is observed that the first and second sediment classes experience more erosion at the inlet, which increases the presence of the other sediment classes at the inlet. The model is capable of simulating the high presence of the third sediment class.

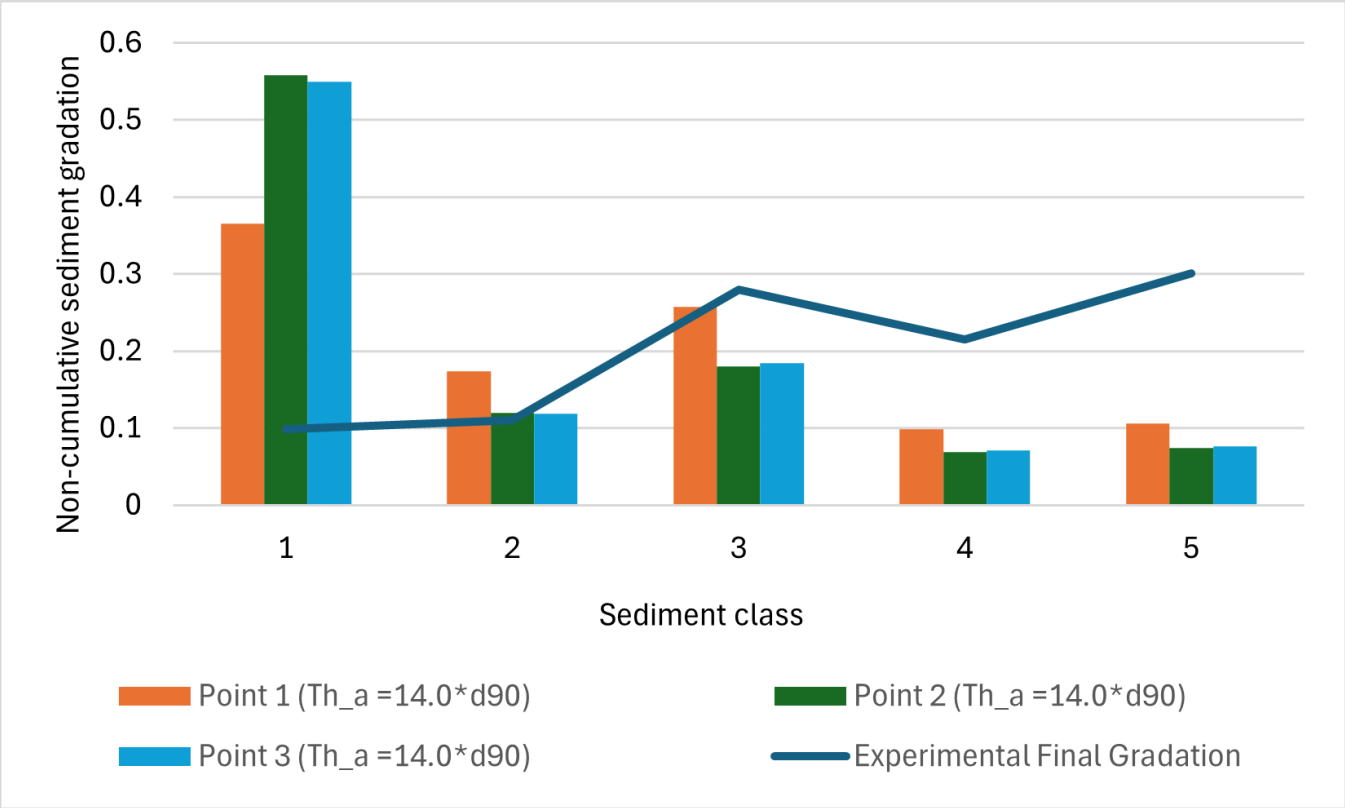

(a) Active layer thickness of $14.0 * d_{90}$

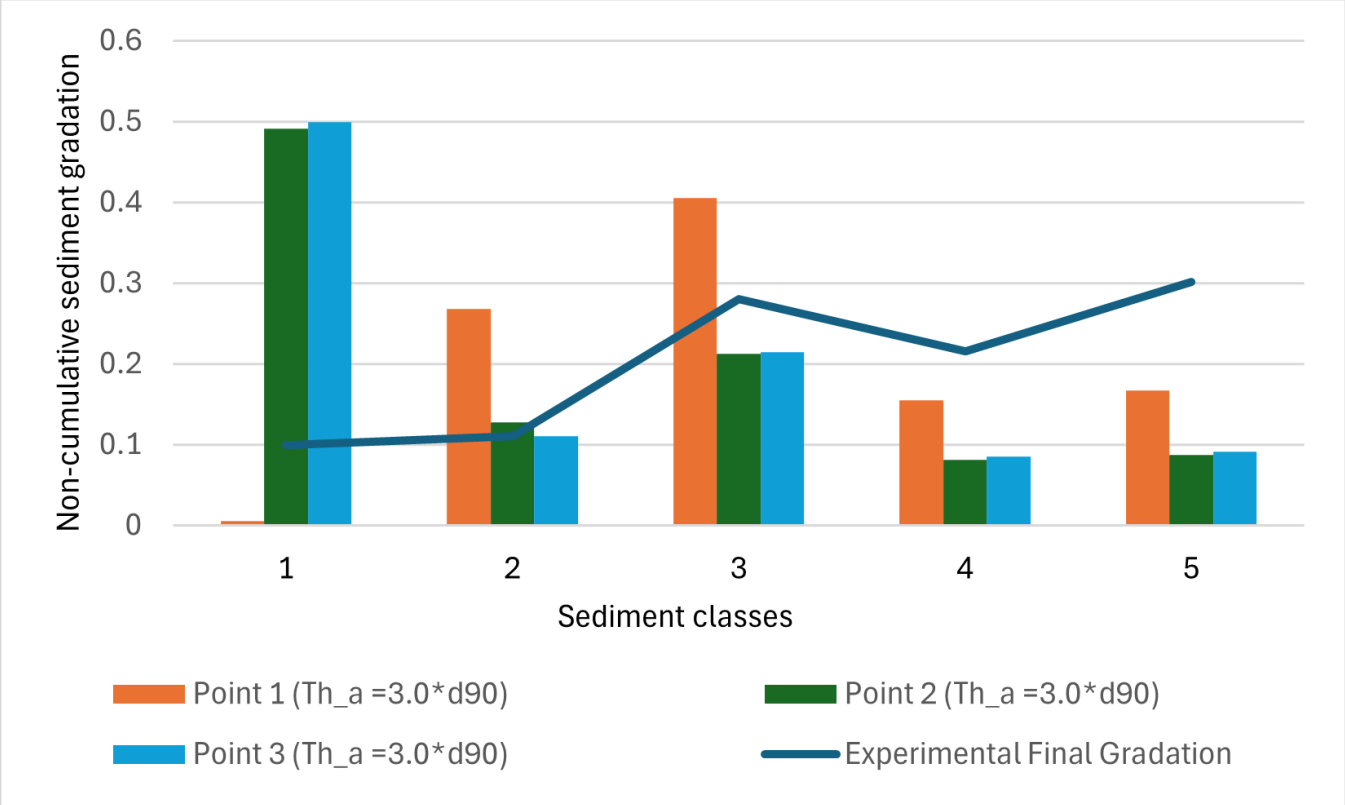

(b) Active layer thickness of $3.0 * d_{90}$

Figure 6.18 Comparing the effect of active thickness $14.0 * d_{90}$, $3.0 * d_{90}$, and $1.0 * d_{90}$ on the bed composition along the channel for a simulation time of 5 hours

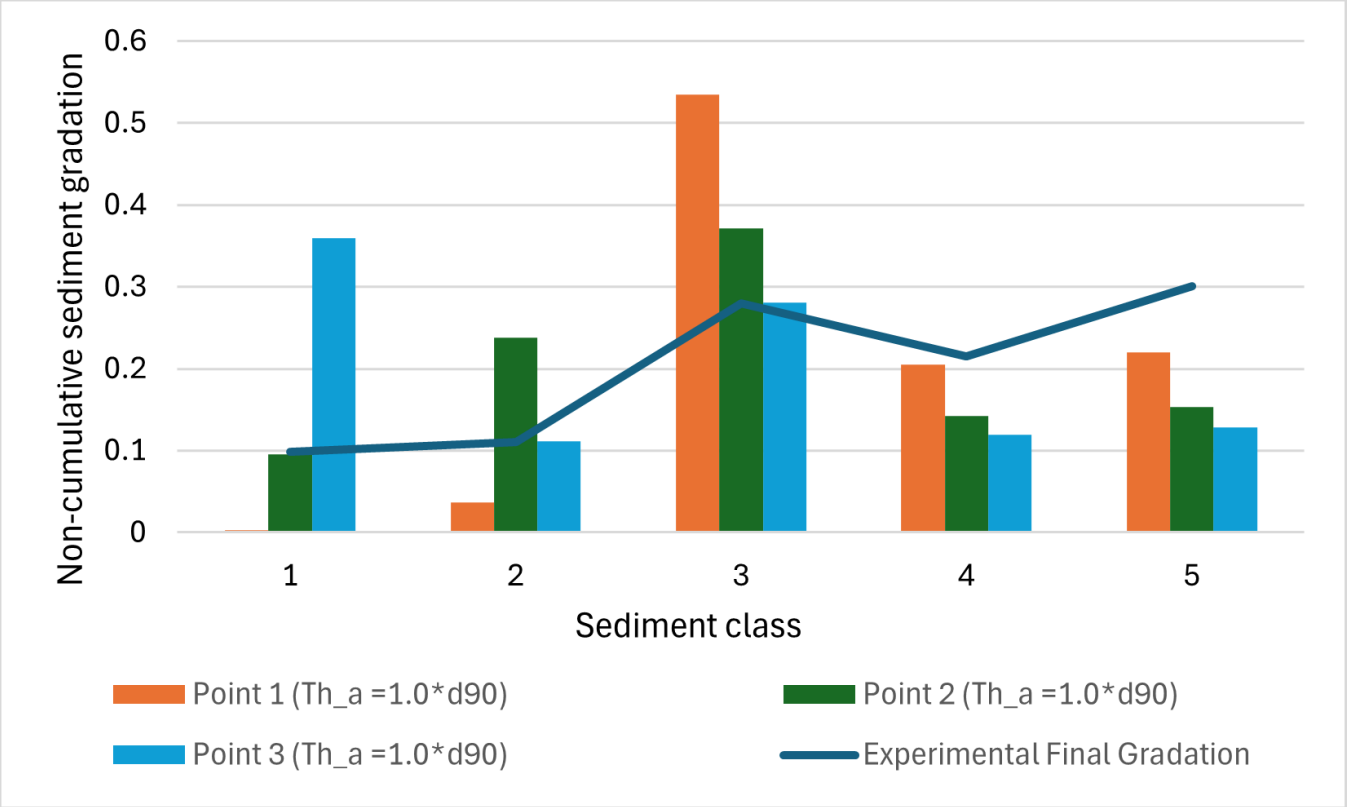

(c) Active layer thickness of $1.0 * d_{90}$

Figure 6.18 Comparing the effect of active thickness $14.0 * d_{90}$, $3.0 * d_{90}$, and $1.0 * d_{90}$ on the bed composition along the channel for a simulation time of 5 hours (continued)

Figure 6.19a shows the cumulative sediment gradation obtained from STR2D compared with the experimental results. The analysis is in detail in the next chapter. Figure 6.19b shows the non-cumulative sediment gradation along the channel. In addition, the final slope modeled by STR2D for a simulation time of 5 hours is 0.24%, which agrees with the final experimental slope of 0.233%. Figure 6.19a compares the cumulative sediment gradation obtained by Günter (1971), as a red-dashed line, and STR2D. The modeled bed composition follows the experimental result trend at the three locations of the channel. Nonetheless, except for sediment classes 1 and 2 at point 1, the cumulative sediment gradation obtained by the model tends to be overpredicted.

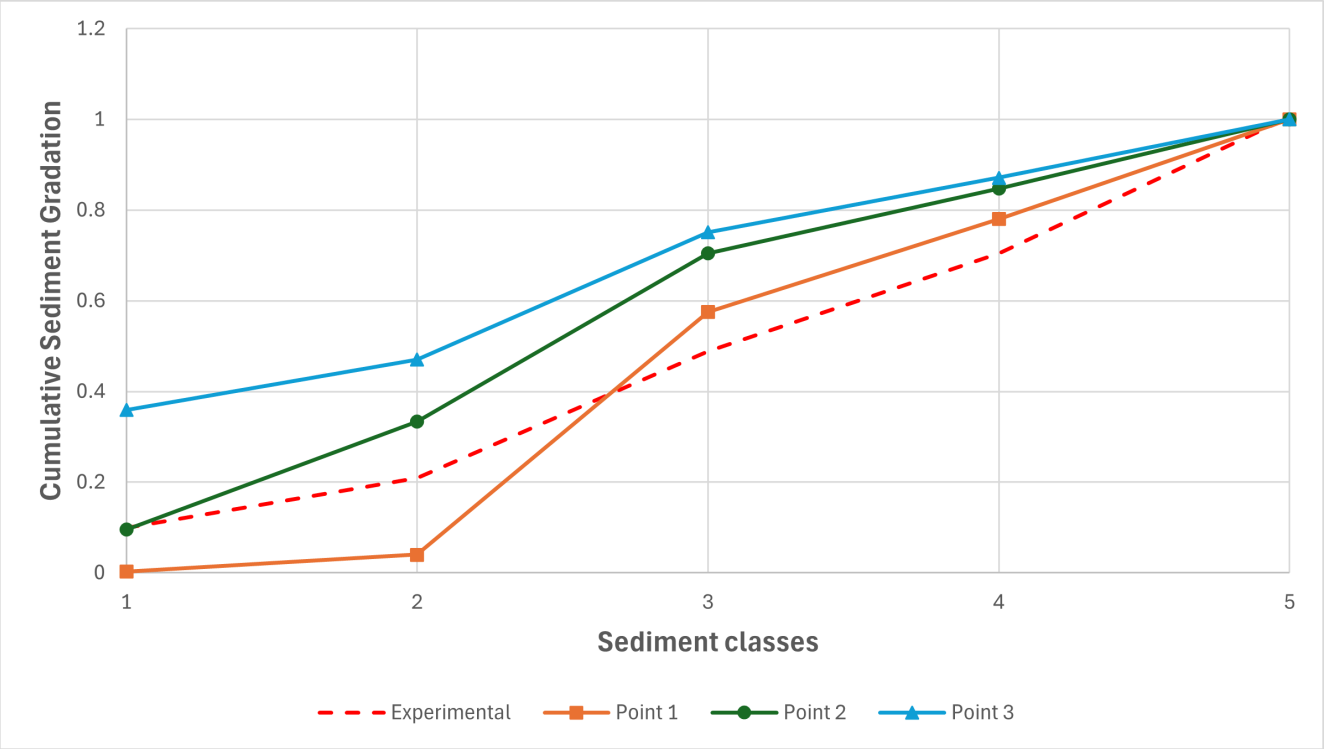

(a)

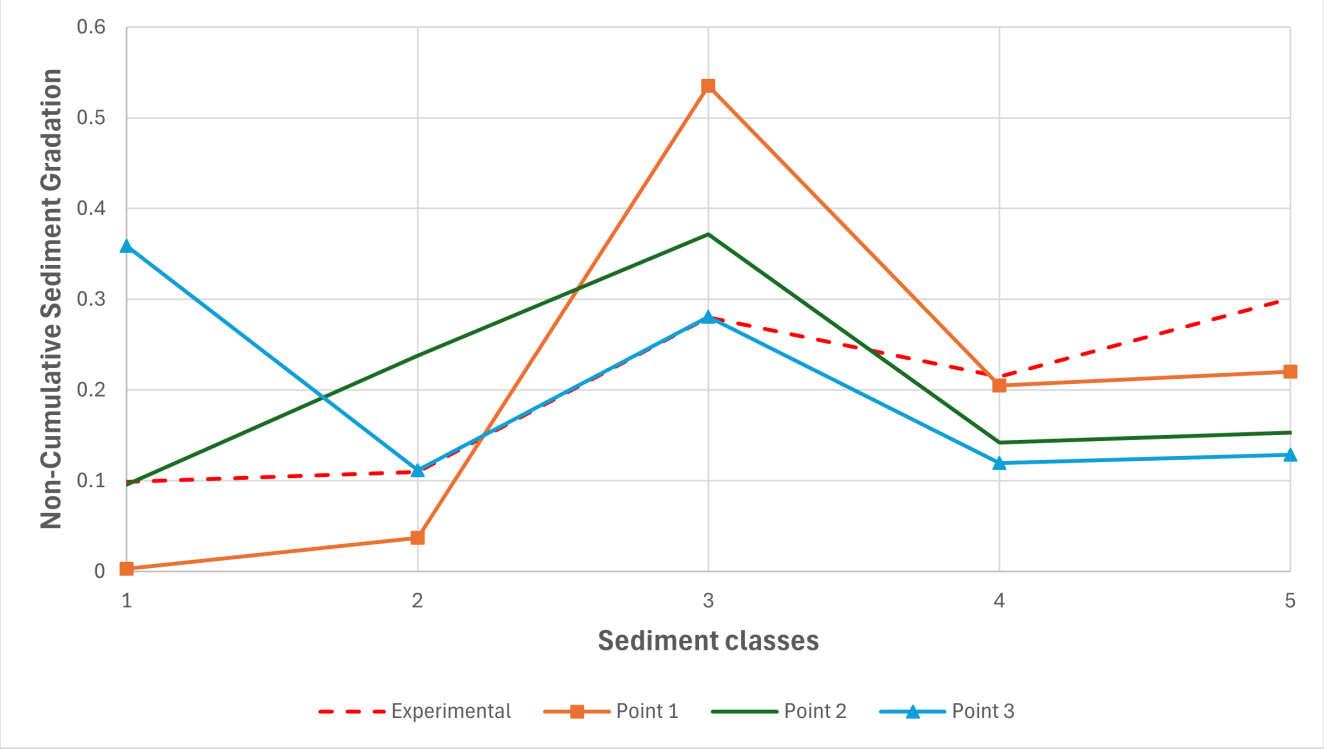

(b)

Figure 6.19 Comparing the a) cumulative sediment gradation and b) non-cumulative sediment gradation for adaptation length of 0.1*d90 for point 1, point 2, point 3, and the experimental result

Figure 6.20 compares the bed composition in non-cumulative gradation between SRH2D and STR2D for a simulation time of 4h30.

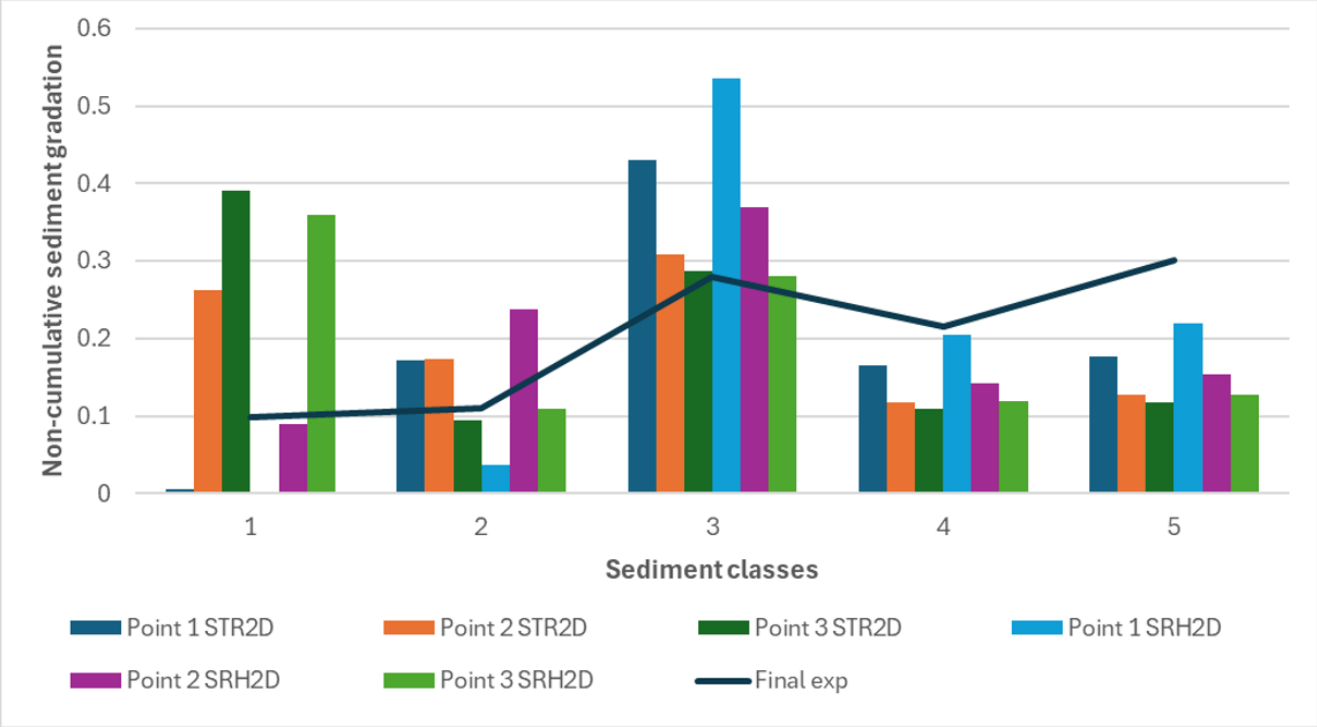

Figure 6.20 Comparison of the non-cumulative sediment gradation between SRH2D and STR2D at a simulation time of 4h30 hours

For both models, the non-cumulative sediment gradations of each of the five classes of Table 6.1 are plotted, as shown in Figure 6.20, at the three points defined in Figure 6.14. Thus, the results obtained by STR2D at points 1, 2, and 3 are shown in bars of navy blue, orange, and dark green, respectively. Similarly, the results obtained by SRH2D in points 1, 2, and 3 are presented in bars of blue, purple, and green, respectively. In both models, almost all sediments from the first sediment class are eroded at the inlet (point 1). For the first and second sediment classes, STR2D shows less fluctuation of the bed composition along the channel than SRH2D. The discrepancies between both models lessens as the sediment diameter increases. As the sediment diameter increases, both models tend to have similar results. Additionally, the overall trend observed in both models follows the experimental one. Furthermore, both models are capable of replicating the high presence of the third sediment class, as seen in the experimental results.

Figure 6.21 shows the bed change from SRH2D at initial time and at a simulation time of 5 hours. Figure 6.22 compares the final bed elevation of STR2D with SRH2D for a simulation

time of 4h30 with the experiment results.

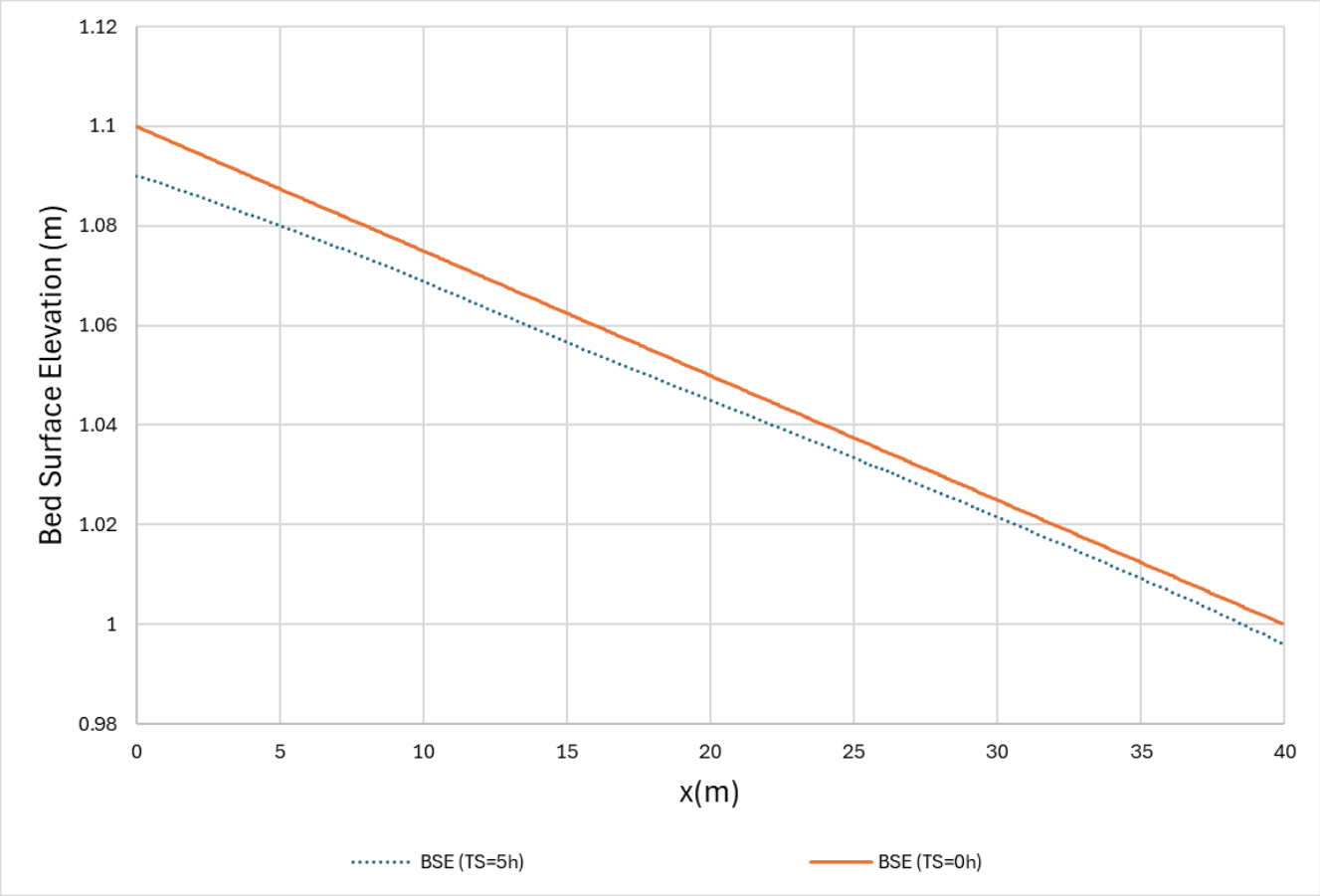

Figure 6.21 Bed surface elevation along the channel initial and at a simulation time of 5 hours for SRH2D

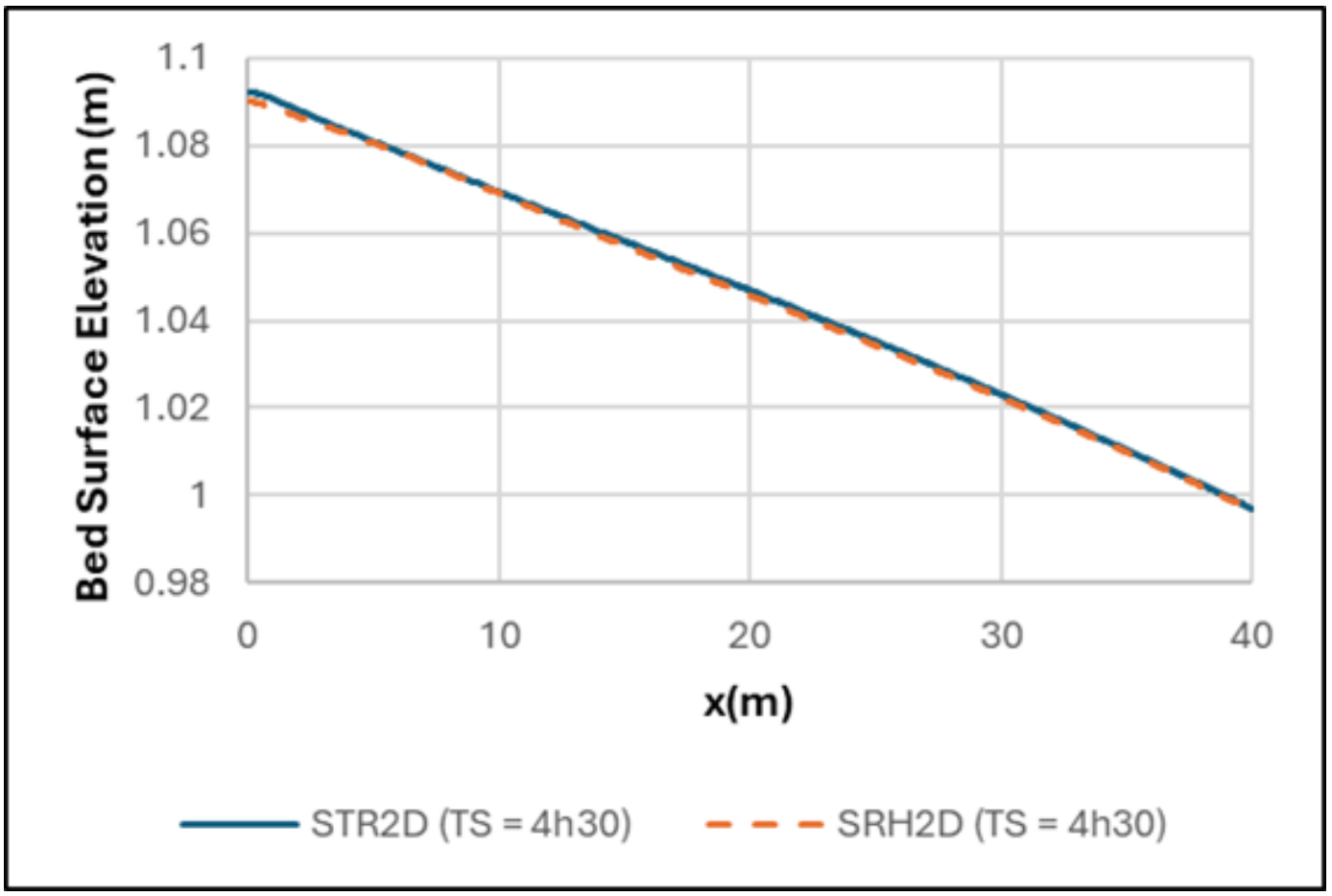

Figure 6.22 Comparison of the final bed elevation between SRH2D and STR2D at a simulation time of 4h30 hours

As seen in Figure 6.23a and Figure 6.23b, the difference between the bed elevation of SRH2D and STR2D and the water surface elevation for a simulation time of 4h30.

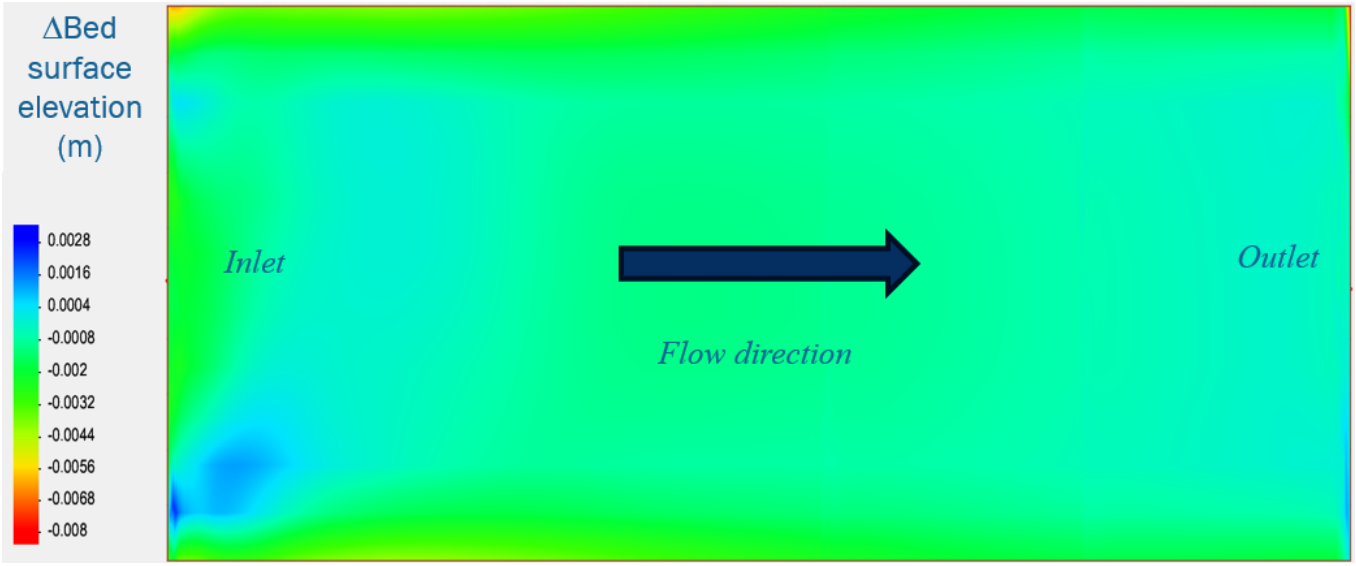

(a)

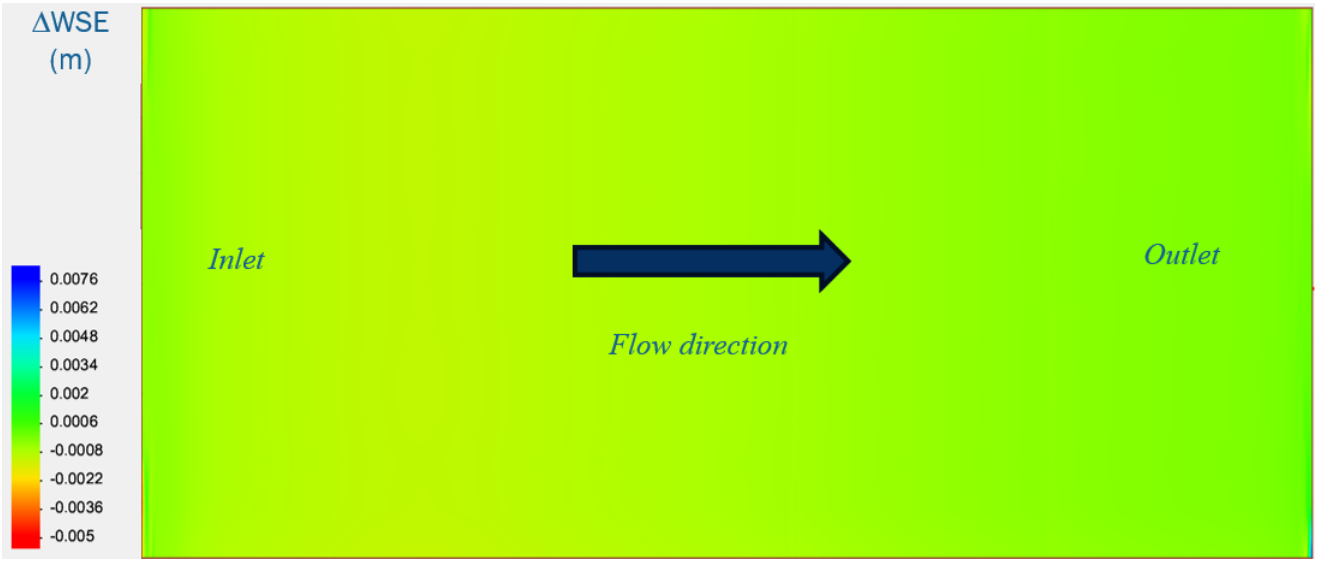

(b)

Figure 6.23 Comparison between SRH2D and STR2D at a simulation time of 4h30 a) final bed surface elevation b) water surface elevation

CHAPTER 7 GENERAL DISCUSSION

A numerical tool is quite handy, since it allows for easy testing of different conditions without incurring additional monetary costs. This does not downplay the importance of laboratory experiments, but instead highlights the versatility that a numerical tool can provide to complement laboratory work. Sediment transport is a complex phenomenon that demands a deeper understanding due to its significant impact on the populations living near rivers, ecosystems, and infrastructures. The primary aim of this research is to develop a tool that will allow for further investigation into sediment transport.

A 2d hydro-sedimentary, STR2D (Sediment Transport in Rivers in 2D), based on the joint method which uses the sediment transport parameter, f, is developed at École Polytechnique de Montréal. This research is the continuation of a previous work that developed a 2D hydrodynamic model, SF-Fluent, using a collocated finite volume scheme and solved using an iterative process, the SIMPLE algorithm. It solves the governing equations of two-dimensional hydro-sediment transport in a decoupled manner.

The first step taken was to develop a subroutine that permitted SF-Fluent to read the mesh format with imposed boundary conditions by SMS. Next, another subroutine was developed to allow the results produced by the model to be read by SMS, enabling visualization and analysis in SMS.

Next, the sediment transport module is developed. It solves the depth-averaged sediment concentration, represented by an advection-diffusion equation with a SIMPLE algorithm. The depth-averaged sediment concentration equation considers the secondary flow effect, the sediment velocity being different from the water flow, with the use of the ratio of sediment velocity, the sediment transport mode parameter that allows to shift between pure suspended load, mixed load, and pure bed load.

STR2D was implemented in TELEMAC to test its stability. When STR2D produced satisfying results, it was implemented into the hydrodynamic module developed at École Polytechnique de Montréal (SF-Fluent).

The sediment transport mode parameter developed by Greimann consists of two equations, one linear and the other exponential. It possesses a discontinuity in the derivative at about $Z = 1$. This parameter is in the diffusive partial difference term. Hence, to avoid unstable oscillations, an enhanced sediment transport mode parameter is developed using the logarithmic matching method. However, it is demonstrated that the logarithmic matching method

must be modified to obtain a satisfactory single composite solution.

The model was verified numerically using a commercial software called SRH2D, as it employs the same approach to model sediment transport as STR2D. The verification process allowed to determine whether STR2D can simulate bed evolution similarly to SRH2D under both nonequilibrium and equilibrium states at the inlet condition. A time step of 0.01 seconds and an unstructured triangular mesh of 0.1m are used.

In the validation, four parameters are calibrated manually to assess their influence on the bed composition and to validate the model: the inlet condition, the hiding-exposure effect, the adaptation length, and the active layer's thickness.

It is observed that the greatest difference in the results from the models occurs near the inlet and the outlet. This discrepancy can be explained by how the models consider the inlet cells near the walls.

Riverine parameters are included in the sediment transport module, STR2D. Among all the riverine parameters, the active layer had the most significant impact on water flow capacity and bed composition. It also limited the intense erosion occurring at the inlet, allowing it to match the final experimental slope. The final slope of the experimental bed was recorded at 0.24%, while SRH2D and STR2D simulated a final slope of 0.233%. These results indicate a favorable assessment of employing STR2D to address engineering challenges. Since STR2D is not yet optimized and parallelized, the computational time for a simulation time of about five hours was one month, while SRH2D required about half a day.

CHAPTER 8 CONCLUSION AND PERSPECTIVE

Sediment transport is a complex phenomenon influenced by various factors. Additionally, using mathematical models can enhance our understanding of this process. Because sediment transport in rivers is inherently complex, models designed for alluvial rivers rely on assumptions and unknown variables. This research aims to reduce these unknowns and provide a numerical tool that will help improve our understanding of sediment transport.

8.1 Summary of Works

A sediment transport module has been implemented into an existing hydrodynamic module. The sediment transport model operates in a decoupled manner, meaning that the hydrodynamic module is solved first. The sediment transport module receives the essential information needed to function properly.

The joint method is used to model sediment transport. This method uses a one advection-diffusion equation. A parameter f, the sediment transport mode parameter, developed by Greimann, allows the shift from suspended to bed load and vice versa, reducing the number of assumptions. Hence, the joint method is numerically lighter according to the literature. The sediment transport module simulates the processes of erosion and deposition. It evaluates the sediment-water capacity to determine whether a particular sediment class should be eroded or deposited, which in turn affects the bed elevation. The amount of material that is either eroded or deposited is recorded at the center of each cell. A subroutine then redistributes this material to the surrounding nodes. Validation of the model indicated that the patterns of erosion and deposition aligned with the trends observed in both SRH2D and experimental results for non-uniform sediments.

Additionally, the concept of active layer has been implemented in the model at the bed's uppermost layer. The active layer limits the erosion and manages the bed composition when newly material is deposited. As a matter of fact, the active layer's mass remains constant throughout the simulation. The validation process highlights the significance of using the active layer, as it is found to be the parameter that most greatly influenced the results. This thesis aims to provide a tool for understanding sediment transport in rivers that primarily exhibit a non-equilibrium state. While rivers strive to reach equilibrium, this process takes time, and even after attaining equilibrium, they often do not remain in that state for long.

To account for the time required to attain equilibrium, an adaptation length parameter is

implemented in the model. Furthermore, rivers primarily consist of nonuniform sediment, which is why a hiding-exposure effect has been introduced to account for the influence of larger particles on sediment transport. This thesis utilizes an experimental benchmark conducted at ETH to verify and validate a sediment transport model, developed at École Polytechnique de Montréal, which employs a joint method for both noncohesive uniform and nonuniform sediment. The STR2D model demonstrates a strong correlation with the bed evolution results obtained from the SRH2D model and experimental results, providing positive feedback on the effectiveness of STR2D in addressing engineering challenges.

8.2 Limitations

The tool described in this thesis is a decoupled model suitable for cases where the Froude number is less than one. The sediment transport mode parameter, f, is derived from an empirical equation based on experimental data. To enhance its applicability for river contexts, further investigation into the joint method is necessary.

8.3 Future Research

A tool is provided to model sediment transport and enhance its understanding using an approach developed by Greimann. The model has been verified and validated, but the model needs first to be optimized before being applied to real-case scenarios. Many features on sediment transport can be incorporated, such as implementing cohesive sediments, considering bank migration, adding newly developed sediment transport equations and adaptation length, extending the application of sediment transport mode parameter f , and solving the governing equations in a couple manner. In addition, STR2D needs further investigation to be extended to rivers.

REFERENCES

[1] T. F. Mahdi, "Prévision par modélisation numérique de la zone de risque bordant un tronçon de rivière subissant une rupture de barrage," Thesis, 2003. [Online]. Available: https://publications.polymtl.ca/7263/

[2] B. Munson *et al.*, *Fundamentals of Fluid Mechanics*. Wiley, 2013.

[3] M. M. Larmaei, J. Behzadi, and T. Mahdi, "Grid-independent depth-averaged simulations with a collocated unstructured finite volume scheme," *International Journal for Numerical Methods in Fluids*, vol. 69, no. 1, pp. 88–109, 2012.

[4] N. Arora, A. Kumar, and S. Kumar Singal, "Technological advancement in measurements of suspended sediment and hydraulic turbine erosion," *Measurement*, vol. 190, p. 110700, 2022. [Online]. Available: https://www.sciencedirect.com/science/article/pii/S0263224122000057

[5] V. Romanenko and G. Lujanienė, "Short review of plutonium applications for the sediment transport studies," *Journal of Environmental Radioactivity*, vol. 257, p. 107066, 2023. [Online]. Available: https://www.sciencedirect.com/science/article/pii/S0265931X22002570

[6] J. Zhang *et al.*, "Optimisation of reservoir operation mode to improve sediment transport capacity of silt-laden rivers," *Journal of Hydrology*, vol. 594, p. 125951, 2021. [Online]. Available: https://www.sciencedirect.com/science/article/pii/S0022169420314128

[7] Z. Sirabahenda, "Modélisation numérique du transport des sédiments en suspension dans une rivière en aménagement: Cas de la rivière-aux-sables au québec," Thesis, 2012. [Online]. Available: https://publications.polymtl.ca/886/

[8] G. M. Kondolf *et al.*, "Sustainable sediment management in reservoirs and regulated rivers: Experiences from five continents," vol. 2, no. 5, pp. 256–280, 2014. [Online]. Available: https://agupubs.onlinelibrary.wiley.com/doi/abs/10.1002/2013EF000184

[9] "Recommandations canadiennes pour la qualité des eaux: protection de la vie aquatique - matières particulaires totales," Conseil canadien des ministres de l'environnement, Report, 2002.

[10] G. P. Williams and G. W. M., "Downstream effects on dams on alluvial rivers," US Government Printing Office, Report, 1984.

[11] K. A. Bigham, T. D. Keane, and T. L. Moore, "Effect of flow regulation on streambank erosion: A perspective downstream of a flood control dam, kansas, usa," *River Research and Applications*, vol. 40, no. 1, pp. 14–28, 2024.

[12] A. Foucher *et al.*, "Quantification of bank erosion in a drained agricultural lowland catchment," vol. 31, no. 6, pp. 1424–1437, 2017. [Online]. Available: https://onlinelibrary.wiley.com/doi/abs/10.1002/hyp.11117

[13] V. Peychev and M. Stancheva, "Changes of sediment balance at the bulgarian black sea coastal zone influenced by anthropogenic impacts," in *Proceedings of the Bulgarian Academy of Sciences*, vol. 62, no. 2, pp. 277–285.

[14] W. Wu, *Computational River Dynamics*. London: CRC Press, 2007.

[15] ——, "Depth-averaged two-dimensional numerical modeling of unsteady flow and nonuniform sediment transport in open channels," *Journal of Hydraulic Engineering*, vol. 130, no. 10, pp. 1013–1024, 2004. [Online]. Available: https://ascelibrary.org/doi/abs/10.1061/%28ASCE%290733-9429%282004%29130%3A10%281013%29

[16] W. H. Graf and M. S. Altinakar, *Hydraulique fluviale: écoulement et phénomènes de transport dans les canaux à géométrie simple*, 2nd ed. Lausanne, [Suisse]: Presses polytechniques et universitaires romandes, 2000, vol. v. 16.

[17] M. Spasojevic and F. M. Holly, "2-d bed evolution in natural watercourses—new simulation approach," *Journal of Waterway, Port, Coastal, and Ocean Engineering*, vol. 116, no. 4, pp. 425–443, 1990. [Online]. Available: https://ascelibrary.org/doi/abs/10.1061/%28ASCE%290733-950X%281990%29116%3A4%28425%29

[18] Y. Audouin *et al.*, "Gaia user manual," TELEMAC-MASCARET, Report, March 2022.

[19] "D-morphology, 1d/2d/3d user manual," Deltares, Report, 2025.

[20] D. Vetsch *et al.*, "Basement-basic simulation environment for computation of environmental flow and natural hazard simulation: Basement reference manual," Report, 2015. [Online]. Available: http://www.basement.ethz.ch/download/documentation.html

[21] C. Swartenbroekx, Y. Zech, and S. Soares-Frazão, "Two-dimensional two-layer shallow water model for dam break flows with significant bed load transport," *International Journal for Numerical Methods in Fluids*, vol. 73, no. 5, pp. 477–508.

[22] A. Armanini and G. Di Silvio, "A one-dimensional model for the transport of a sediment mixture in non-equilibrium conditions," *Journal of Hydraulic Research*, vol. 26, no. 3, pp. 275–292, 1988. [Online]. Available: https://doi.org/10.1080/00221688809499212

[23] C. T. Yang and J. Ahn, "User's manual for gstars4," Colorado State University, Report, 2011.

[24] L. Yong G. and D. Gaeuman, "User's manual: Sediment transport and mobile-bed modeling with srh-2d," U.S. Department of the Interior Bureau of Reclamation Technical Service Center, Denver, Colorado, Tech. Rep., 2019.

[25] E. Lane *et al.*, "Report of the subcommittee on sediment terminology," *American Geophysical Union*, vol. 28, no. 6, pp. 936–938, 1947. [Online]. Available: https://agupubs.onlinelibrary.wiley.com/doi/abs/10.1029/TR028i006p00936

[26] H. Breusers, "Lecture notes on sediment transport 1," Delt Hydraulics, Report, 1988.

[27] "Some fundamentals on particle size analysis," U.S. Interagency Committee on Water Resources, Sucommittee on Sedimentation, Report no. 12, 1957.

[28] W. W. Rubey, "Setting velocities of gravel, sand, and silt particles," *American Journal of Science*, vol. vo. 25, pp. 325–338, 1933.

[29] C. T. Yang, *Sediment transport: theory and practice.* Malabar, Florida: Krieger Pub, 2003.

[30] S. Komura and B. R. Colby, "Discussion of "sediment transportation mechanics: Introduction and properties of sediment, progress report by the task committee on preparation of sedimentation manual of the committee on sedimentation of the hydraulics division"," *Journal of the Hydraulics Division*, vol. 89, no. 1, pp. 263–268, 1963. [Online]. Available: https://ascelibrary.org/doi/abs/10.1061/JYCEAJ.0000837

[31] W. Wu and S. S. Y. Wang, "Formulas for sediment porosity and settling velocity," *Journal of Hydraulic Engineering.*

[32] R. J. Garde and K. G. Raju, *Mechanics of Sediment Transportation and Alluvial Stream Problems.* India: Wiley Eastern Limited, 1985.

[33] W. Wu, D. A. Vieira, and W. Sam S. Y, "One-dimensional numerical model for nonuniform sediment transport under unsteady flows in channel networks," *Journal of Hydraulic Engineering*, vol. 130, no. 9, 2004.

[34] J. P. Bennett and C. F. Nordin, "Simulation of sediment transport and armouring," *Hydrological Sciences Bulletin*, vol. 22, no. 4, pp. 555–569, 1977. [Online]. Available: https://doi.org/10.1080/02626667709491760

[35] Z. Cao *et al.*, "Shallow water hydro-sediment-morphodynamic equations for fluvial processes," *Journal of Hydraulic Engineering*, vol. 143, no. 5, p. 02517001, 2017.

[36] M. Wong and G. Parker, "Reanalysis and correction of bed-load relation of meyer-peter and muller using their own database," *Journal of Hydraulic Engineering*, vol. 132, no. 11, pp. 1159–1168, 2006. [Online]. Available: https://ascelibrary.org/doi/10.1061/%28ASCE%290733-9429%282006%29132%3A11%281159%29

[37] H. Q. Huang, "Reformulation of the bed load equation of meyer-peter and müller in light of the linearity theory for alluvial channel flow," *Water Resour. Res.*, vol. 46, no. 9, 2010. [Online]. Available: https://agupubs.onlinelibrary.wiley.com/doi/abs/10.1029/2009WR008974

[38] C. J. McCarron *et al.*, "The hiding-exposure effect revisited: A method to calculate the mobility of bimodal sediment mixtures," *Marine Geology*, vol. 410, pp. 22–31, 2019. [Online]. Available: https://www.sciencedirect.com/science/article/pii/S0025322718302226

[39] D. Wang and P. Tassi, "Secondary flow corrections into the telemac-mascaret modelling system," in *Proceedings of the 21st TELEMAC-MASCARET User Conference 2014*, Grenoble–France, 15th-17th October 2014, pp. 225–233. [Online]. Available: https://henry.baw.de/server/api/core/bitstreams/00530e4d-cbdc-4367-adc4-dc74ac5756d8/content

[40] B. Greimann, Y. Lai, and J. Huang, "Two-dimensional total sediment load model equations," *Journal of Hydraulic Engineering*, vol. 134, no. 8, pp. 1142–1146, 2008. [Online]. Available: https://ascelibrary.org/doi/abs/10.1061/%28ASCE%290733-9429%282008%29134%3A8%281142%29

[41] C. Hu and Y. Hui, "Bed-load transport: I: Mechanical characteristics," *Journal of Hydraulic Engineering*, vol. 122, no. 5, pp. 245–254, 1996.

[42] J. R. D. Francis, "Experiments on the motion of solitary grains along the bed of a water-stream," *Proceedings of the Royal Society of London, Series A, Mathematical and Physical Sciences*, vol. 332, no. 1591, pp. 443–471, 1973.

[43] C. Lai, *Numerical Modeling of Unsteady Open-Channel Flow*. Elsevier, 1986, vol. 14, pp. 161–333. [Online]. Available: https://www.sciencedirect.com/science/article/pii/B9780120218141500082

[44] X. Chen, "Coupling an unstructured grid three-dimensional model with a laterally averaged two-dimensional model for shallow water hydrodynamics and transport processes," *International Journal for Numerical Methods in Fluids*, vol. 93, no. 5, pp. 1468–1489, 2021. [Online]. Available: https://onlinelibrary.wiley.com/doi/abs/10.1002/fld.4938

[45] G. K. Demeke, D. H. Asfaw, and Y. S. Shiferaw, "3d hydrodynamic modelling enhances the design of tendaho dam spillway, ethiopia," *Water*, vol. 11, no. 1, p. 82, 2019. [Online]. Available: https://www.mdpi.com/2073-4441/11/1/82

[46] Y. Yang *et al.*, "Numerical investigation of flow and scour around complex bridge piers in wind–wave–current conditions," *Journal of Marine Science and Engineering*, vol. 12, no. 1, p. 23, 2024. [Online]. Available: https://www.mdpi.com/2077-1312/12/1/23

[47] B. H. Johnson *et al.*, "Validation of three-dimensional hydrodynamic model of chesapeake bay," *Journal of Hydraulic Engineering*, vol. 119, no. 1, pp. 2–20, 1993. [Online]. Available: https://ascelibrary.org/doi/abs/10.1061/%28ASCE%290733-9429%281993%29119%3A1%282%29

[48] Y. Fan *et al.*, "A coupled 1d-2d hydrodynamic model for urban flood inundation," *Advances in Meteorology*, vol. 2017, no. 1, p. 2819308, 2017. [Online]. Available: https://onlinelibrary.wiley.com/doi/abs/10.1155/2017/2819308

[49] R. Nogherotto *et al.*, "A combined hydrological and hydraulic modelling approach for the flood hazard mapping of the po river basin," *Journal of Flood Risk Management*, vol. 15, no. 1, p. e12755, 2022. [Online]. Available: https://onlinelibrary.wiley.com/doi/abs/10.1111/jfr3.12755

[50] B. S. Caruso, B. Newman, and T. Econopouly, "Hydrodynamic modeling improves green river reconnection with floodplain wetlands for endangered fish species recovery," *Journal of the American Water Resources Association*, vol. 55, no. 3, pp. 622–640, 2019. [Online]. Available: https://onlinelibrary.wiley.com/doi/abs/10.1111/1752-1688.12727

[51] G. Brunner, G. Savant, and R. E. Heath, "Modeler application guidance for steady versus unsteady, and 1d versus 2d versus 3d hydraulic modeling," US Army Corps

of Engineers, Report, 2020. [Online]. Available: https://www.hec.usace.army.mil/publications/TrainingDocuments/TD-41.pdf

[52] M. Iqbal *et al.*, "Hydrus-1d simulation of soil water dynamics for sweet corn under tropical rainfed condition," *Applied Sciences*, vol. 10, no. 4, p. 1219, 2020. [Online]. Available: https://www.mdpi.com/2076-3417/10/4/1219

[53] "Mike 21 & mike 3 flow model fm sand transport module scientific documentation," DHI, Report. [Online]. Available: https://manuals.mikepoweredbydhi.help/latest/Coast_and_Sea/MIKE_FM_ST_Scientific_Doc.pdf

[54] "Hec-ras 2d sediment transport reference manual," US Army Corps of Engineers, Report, 2025. [Online]. Available: https://www.hec.usace.army.mil/confluence/rasdocs/d2sd/ras2dsedtr/latest/model-description/sediment-transport/total-load

[55] L. Yong G., "Theory and user manual for srh-w version 1.1," U.S. Department of the Interior, Report, November 2006. [Online]. Available: https://www.usbr.gov/tsc/techreferences/computer%20software/models/srh2d/downloads/SRH-W%20v1.1%20User%20Manual%20June2007.pdf

[56] Y. G. Lai, L. J. Weber, and V. C. Patel, "Nonhydrostatic three-dimensional model for hydraulic flow simulation. i: Formulation and verification," vol. 129, no. 3, pp. 196–205.

[57] Y. G. Lai, "Two-dimensional depth-averaged flow modeling with an unstructured hybrid mesh," *Journal of Hydraulic Engineering*, vol. 136, no. 1, pp. 12–23, 2010. [Online]. Available: https://ascelibrary.org/doi/abs/10.1061/%28ASCE%29HY.1943-7900.0000134

[58] R. Ata, "Telemac-2d new finite volume schemes for shallow water equations with source terms on 2d unstructured grids," in *Proceedings of the XIXth TELEMAC-MASCARET User Conference 2012*, St Hugh's College, Oxford. Oxfordshire: HR Wallingford, 18-19 october 2012, pp. 93–98. [Online]. Available: https://hdl.handle.net/20.500.11970/104290

[59] "Telemac-2d user manual v8p3," Report, 2021.

[60] S. V. Patankar, *Numerical heat transfer and fluid flow.* New York;Washington: CRC Press.

[61] M. Moradi Larmaei, "A deth-averaged numerical model for simulating heat and fluid flows in vegetated channels," thèse de doctorat, Dép. de génie civil, géologiques, et

des mines, École Polytechnique de Montréal, Montréal, QC, 2012. [Online]. Available: http://publications.polymtl.ca/932/

[62] M. Moradi Larmaei and T.-F. Mahdi, "Depth-averaged turbulent heat and fluid flow in a vegetated porous medium," *International Journal of Heat and Mass Transfer*, vol. 55, no. 4, pp. 848–863, 2012. [Online]. Available: https://www.sciencedirect.com/science/article/pii/S0017931011005928

[63] AQUAVEO, "Sms - surface-water modeling," 2025. [Online]. Available: https://aquaveo.com/software/sms/introduction

[64] N. N. Yanenko and M. Holt, *The Method of Fractional Steps: The Solution of Problems of Mathematical Physics in Several Variables*, 1st ed. Springer-Verlag Berlin Heidelberg, 1971.

[65] L. Yong G. and G. Blair P., "Predicting contraction scour with a two-dimensional depth-averaged model," *Journal of Hydraulic Research*, vol. 48, no. 3, pp. 383–387, 2010. [Online]. Available: https://doi.org/10.1080/00221686.2010.481846

[66] J. Guo, "Logarithmic matching and its applications in computational hydraulics and sediment transport," *Journal of Hydraulic Research*, vol. 40, no. 5, pp. 555–565, 2002. [Online]. Available: https://doi.org/10.1080/00221680209499900

[67] J. A. Cunge, F. M. Holly, and A. Verwey, *Practical aspects of computational river hydraulics*, 1980.

[68] A. Gunter, "Die kritische mittlere sohlenschubspannung bei geschiebemischungen unter berücksichtigung der deckschichtbildung und der turbulenzbedingten sohlenschubspannungsschwankungen," Thesis, 1971. [Online]. Available: https://ethz.ch/content/dam/ethz/special-interest/baug/vaw/vaw-dam/documents/das-institut/mitteilungen/1970-1979/003.pdf

APPENDIX A SEDIMENT TRANSPORT MODULE USER MANUAL

A.1 Input Variables

The code will read the text file containing the sediment parameters. It will obtain from that file the number of sediment classes, the sediment transport equation, the type of inlet condition, the water temperature, the adaptation length, the calibration parameters for the erosion and deposition, the active layer thickness, thickness of each layer, the upper and lower boundary of a class, the volume of fraction present in each layer of a class, the spatial distribution (uniform or not), the number of zones and the text file for the zonal distribution. When, all this information is gathered at the beginning, the code will check the type of spatial distribution. The code allows the user to use the zonal text file for uniform or non-uniform spatial distributions. Uniform spatial distribution considers the domain, in other words all the cells composing the domain, to have the same properties regarding the number of classed, the number of layers, the thickness of these layers, as well as having the same composition for the active layer. On the other hand, the non-uniform spatial distribution considers these properties to be independent from the other zones meaning that the domain itself can be discretized in many zones. This allows the user to consider different type of soils present in the domain.

The reference is the bedrock since the bed surface elevation is transformed sometimes with void and to no void and back to void. Hence, the physical reference used is the bedrock elevation remains constant unlike the other bed surface elevations.

APPENDIX B SMS USER MANUAL

The home code, SF-Fluent, developed at École Polytechnique de Montréal, was able to read the SMS mesh format before implementing the sediment transport module. SF-Fluent initially was able to read the mesh of the format .fneut. The following section introduces the mesh format used and generated by SMS, as well as the initial .fneut mesh format read by SF-Fluent. Additionally, this section outlines how SMS can be used to impose boundary conditions and describes a subroutine developed and implemented in SF-Fluent to read the SMS mesh format and the associated boundary conditions.

B.1 Domain Discretization

SMS can produce both quad-split (structured) and unstructured meshes. It depends how the geometry, also referred to as the domain, is discretized. The following sections present how to generate both types of meshes with SMS.

B.1.1 Projection

Before starting a new project in SMS, it is important to verify the *Projection* is set to meters under the *Display* tab in the *Toolbar* tab. In the *Toolbar* tab, then under the *Elements* tab, then select the option *Triangulate*.

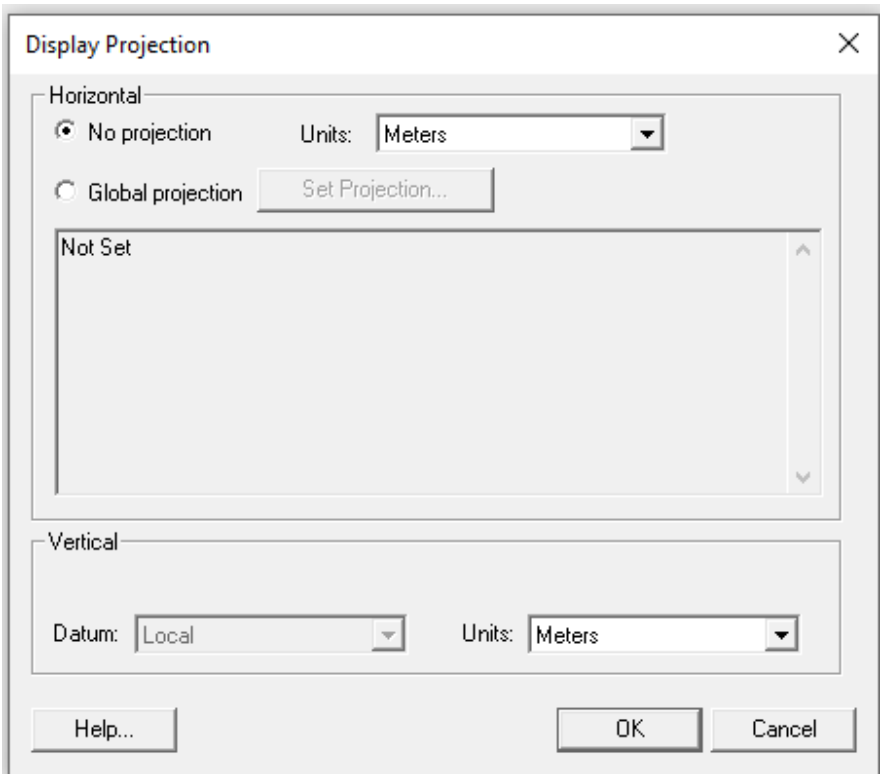

Figure B.1 Display Projection

B.1.2 Structured mesh

A small code, Interpolation_sides.f95, written in FORTRAN by the author, was created to produce points within the domain and at the boundaries to create a quad-split mesh as shown in Figure B.2. However, this code only applies to rectangular domains with a zero-sloped bed. Interpolation_sides.f95 generates a .2dm file that can be visualized in SMS in the Mesh Module.

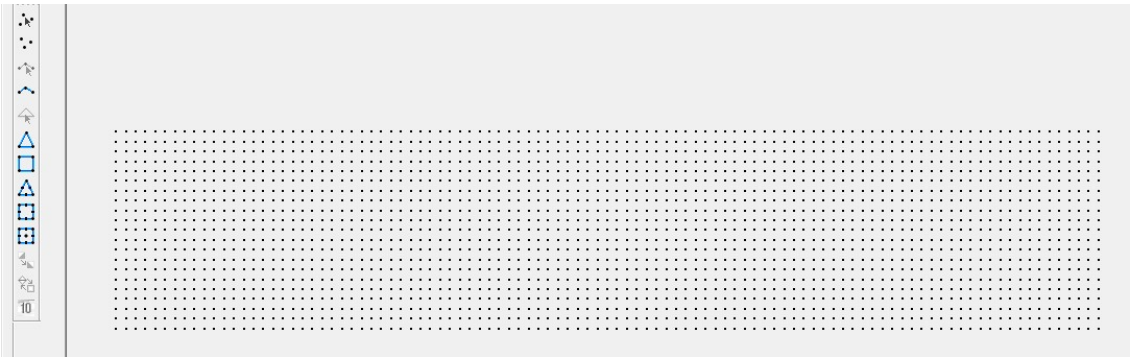

Figure B.2 Discretized domain

For other more complex geometries, it is possible to construct them directly on SMS which will be discussed in more detail in Section B.1.3.

B.1.3 Unstructured Mesh

When the user wants to produce an unstructured mesh, they will primarily use the *Scatter* and *Map Modules* to create the geometry, along with the *Mesh Module* to construct the unstructured mesh.

Simple Rectangular zero bed slope channel

For a simple rectangular channel with a zero-bed slope, 5 meters in longitudinal length and 1 meter in width, a code called Interpolation_sides_map_module2.f95 was created to produce a .map file. All the points of the geometry must be specified in the .map file after the label XY in the .map file. In addition, these nodes should follow the label ARCVERTICES with the number of vertices as shown in Figure B.3.

The user should only print the coordinates of the nodes that define the boundaries of the rectangular geometry to produce the unstructured mesh; otherwise, it will produce a structured mesh. The area is defined by the nodes (13.18, 82.08), (13.18,83.08), (18.18, 82.08), and (18.18, 83.08).

```
MAP VERSION 8
BEGCOV
COVFLDR "Mesh Generator02"
COVNAME "Mesh Generator02"
COVELEV 0.000000
COVID 26165
COVGUID 5d4a7d01-223d-4558-a777-09af50d55e4d
COVATTS VISIBLE 1
COVATTS ACTIVECOVERAGE Mesh Generator02
COVATTS PROPERTIES MESH_GENERATION
NODE
XY 13.1300001 82.0800018 0.0
ID 1
END
ARC
ID 2
ARCELEVATION 0.000000
NODES        1        1
ARCVERTICES 239
13.180000100000001 82.080001800000005 0.000000000000000
13.230000100000000 82.080001800000005 0.000000000000000
13.280000100000001 82.080001800000005 0.000000000000000
13.330000099999999 82.080001800000005 0.000000000000000
13.380000100000000 82.080001800000005 0.000000000000000
13.430000100000001 82.080001800000005 0.000000000000000
```

Figure B.3 File of the Outer Geometry in Map Module

Drag the .map file generated by the code into the *Project Explorer* to visualize in SMS. Make sure that the .map file have the type *Mesh Generator* as shown in Figure B.4.

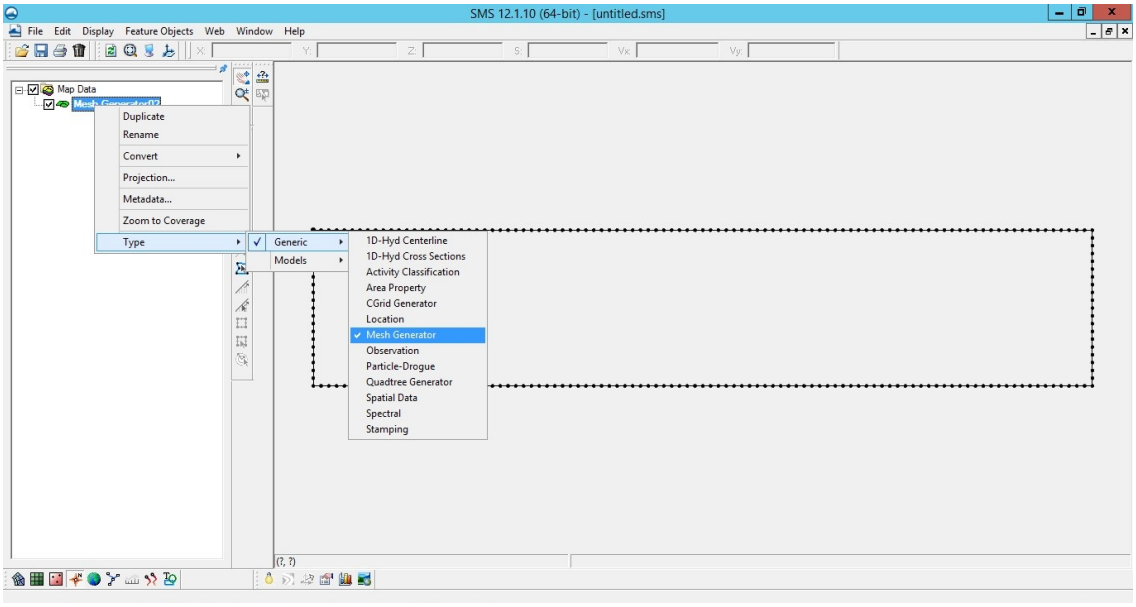

Figure B.4 Change the type of the Area Property

Then, select *Feature Object* in the toolbar and click on *Build Polygons*. Then, right click on the domain and select *Attributes*. Select *Paving* as a *Mesh Type*. Then, right click on the *Area Property* and select *Convert from Map to 2D Mesh*. A warning box as shown in Figure B.5 can appear.

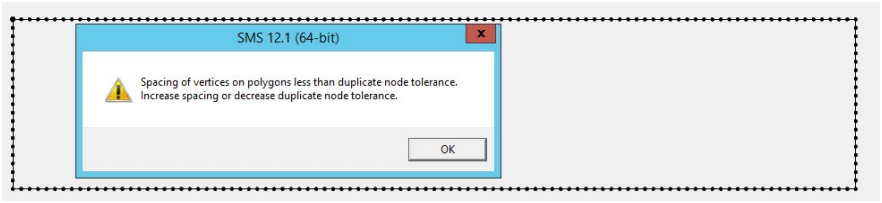

Figure B.5 Warning Box

This warning indicates the user needs to go to the *Mesh module* and go under *Node* in the *tool bar* and go to *options* and reduce the *Tolerance* as shown in Figure B.6.

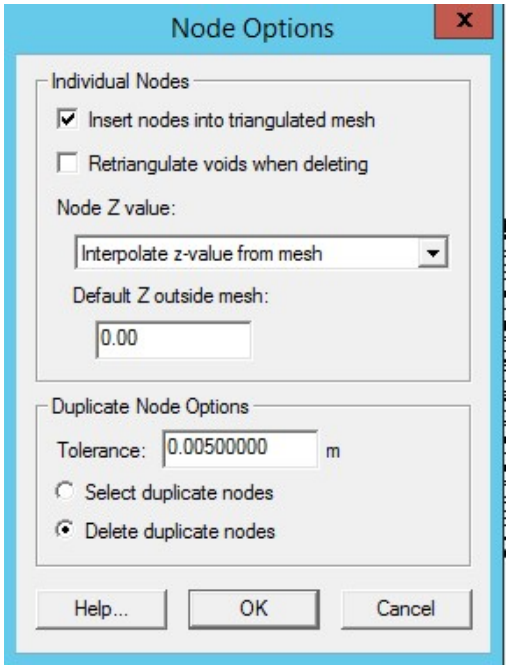

Figure B.6 Node Options

The resulting unstructured mesh is shown in Figure B.7.

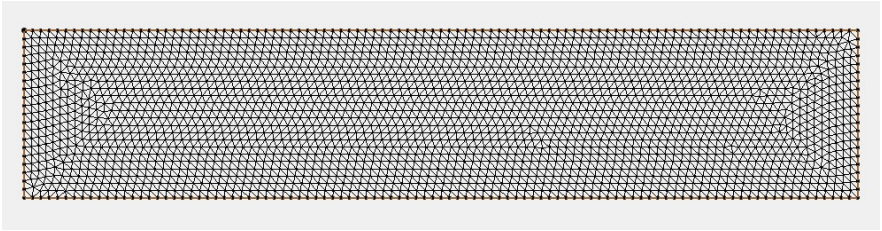

Figure B.7 Unstructured mesh

A trapezoidal shape channel

This subsection presents how to produce a geometry from scratch using SMS only without the need of creating a code since some geometries may be more complex than others. A simple trapezoidal channel with a bottom length of 2.0 m, a top length of 10.0 m, a side slope of 1.23, and a bed slope of 0.00001 as shown in Figure B.8.

Click on the *Scatter Module* and construct the base portion of the trapezoidal channel as shown in Figure B.9.

Then, convert the scatter file into a map file by right clicking on the scatter file and selecting

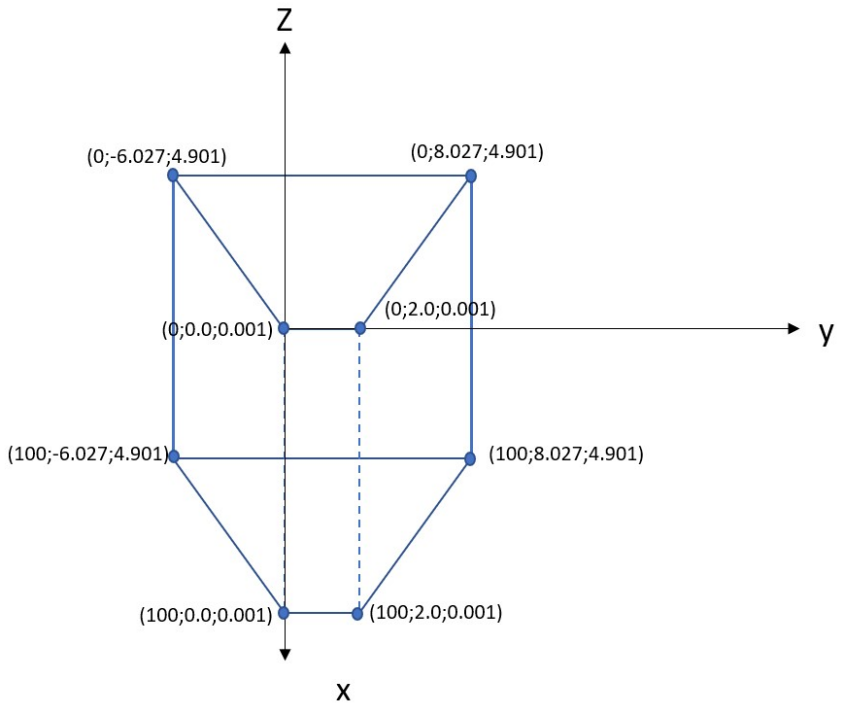

Figure B.8 Trapezoidal geometry

Figure B.9 Trapezoidal base in Scatter Module

Convert and *Scatter Boundary to Map* and select *Create new coverage*. This will create a new .map file. In the new map file, add the side channel of the trapezoidal and convert it to *Scatter* as shown in Figure B.10.

Figure B.10 Initial Geometry in the Map Module

Then, convert from *Map to Scatter* this time and check the appropriate options as shown in Figure B.11. This scatter file will be used later.

Then, coming back to the map file and right click on the arc and select *Split the Arc* in 1.0 m (or the size that you want the mesh to be constructed). It is important to remember that the type of the map file must be Mesh Generator. Then, build the geometry as a Polygon

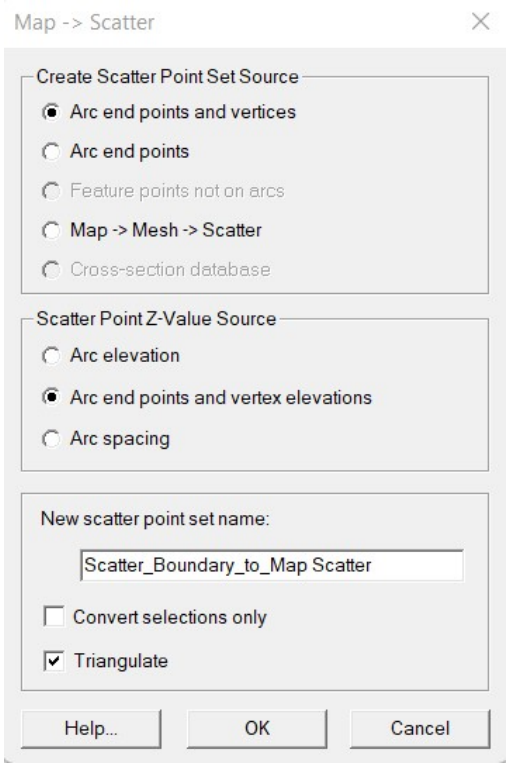

Figure B.11 Map to Scatter Box

which is located under the Feature Objects in the Menu Bar.

Figure B.12 Build Polygon

Then, right click on the map file and choose *Convert and Map* to *2D Mesh* and the mesh is generated but there is a last step to do.

Select the last scatter file generated, right click on it, select *Interpolate to*, and select the mesh to which the scatter file should be interpolated as shown in Figure B.14.

Lastly, it is possible to verify the *Mesh Quality* using *Plot Wizard* in SMS. On the toolbar, select Display and click on *Plot Wizard* and select *ARR Mesh Quality* as shown in Figure B.16.

It can be observed in Figure B.17 that all the mesh that are above the green curve are good.

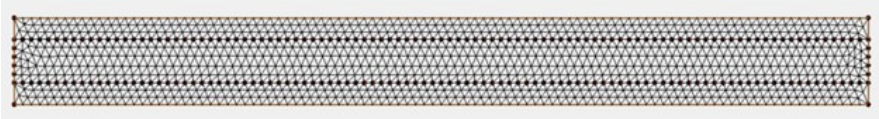

Figure B.13 Mesh Generated

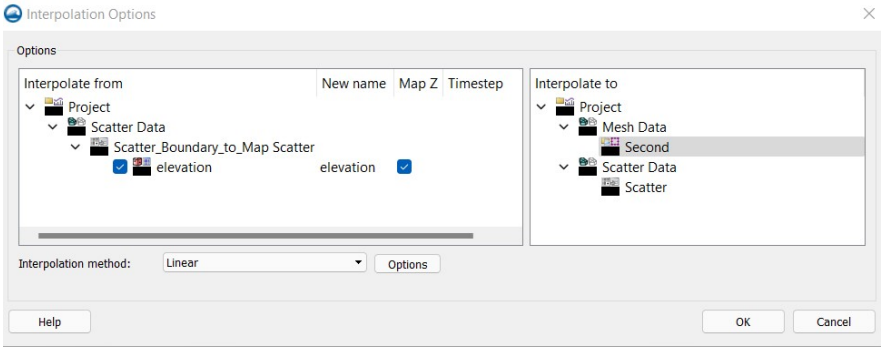

Figure B.14 Interpolation box

If they are below the red curve then it would mean the mesh to be of bad quality. In order to easily find which cells are of bad quality, the user can click on the point located below the red curve and SMS will highlight these cells.

The same process can be repeated if the user wants to have coarser or finer mesh, it depends of the Split length of the arc.

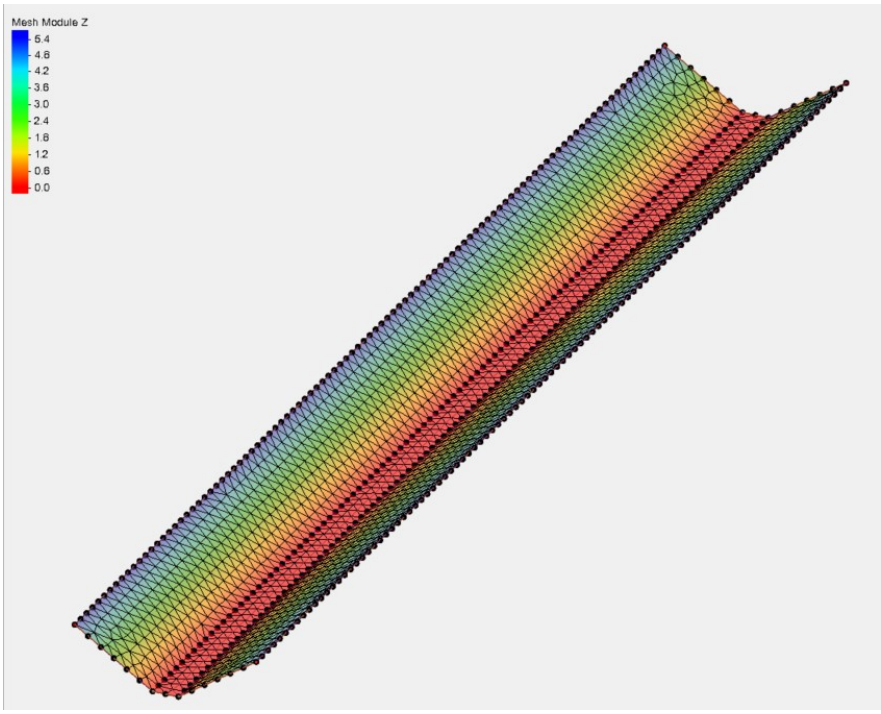

Figure B.15 Interpolation box

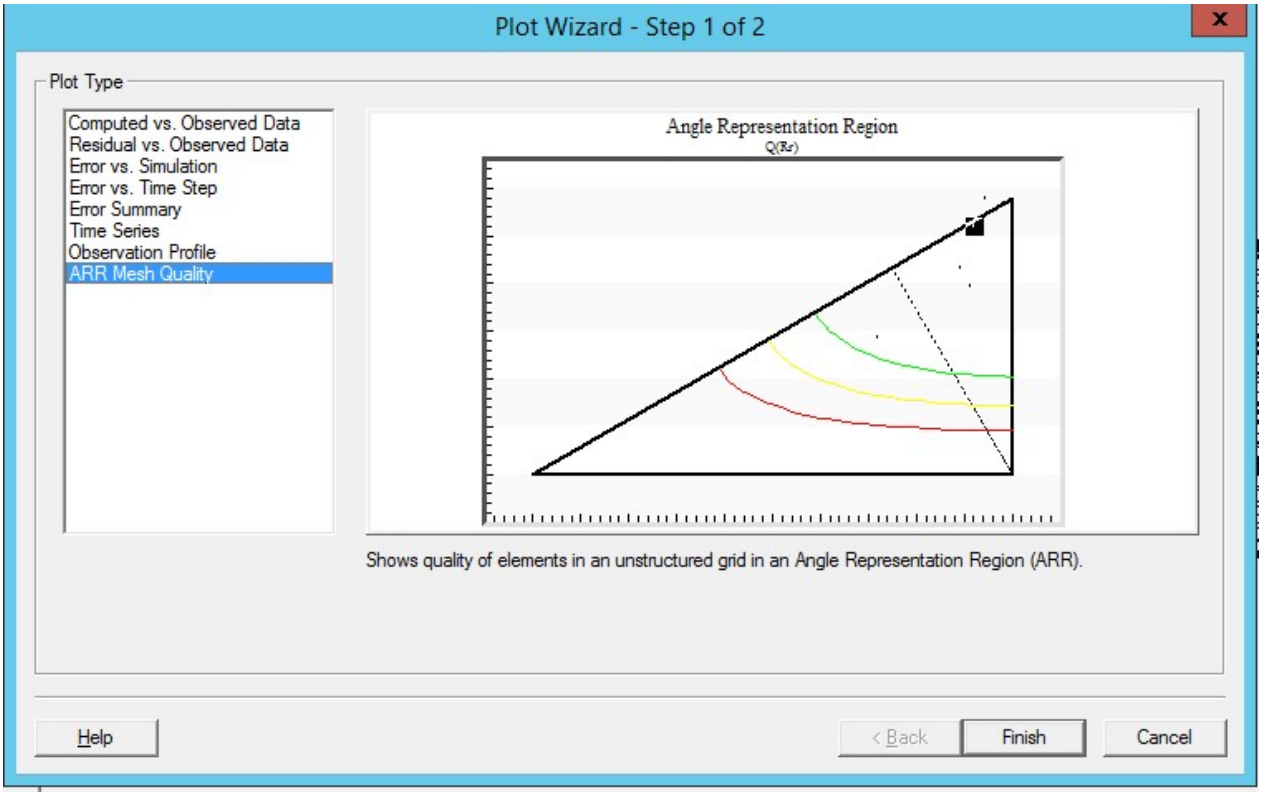

Figure B.16 Plot Wizard

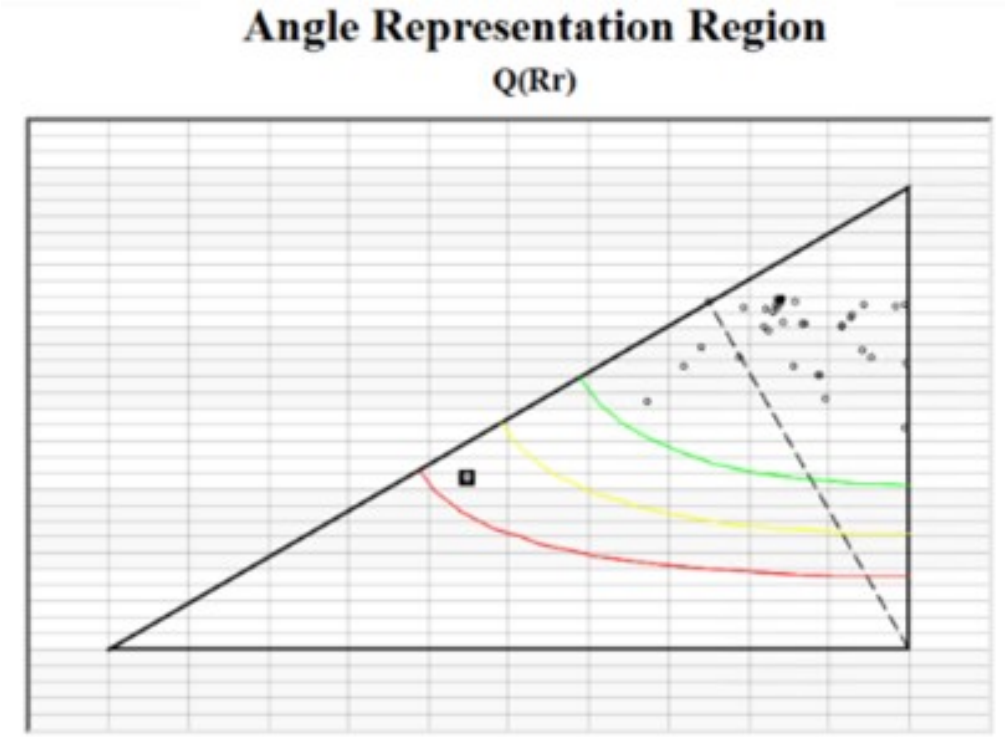

Figure B.17 Mesh Quality

2dm file

A .2dm file can be Saved As from SMS. However, to be used by STR2D, it still needs the boundary condition which will be discussed in the next section.

B.2 Boundary Conditions

It is important to make the difference between cells from the domain and cells from the boundaries. Cells from the domain needs three nodes because STR2D works only for triangular mesh. Whereas, the boundaries cells (inlet, outlet, walls, and section) needs two nodes. In the previous chapter, the cells of the domain are generated by SMS and can be viewed in the file .2dm. We will use the nodestring provided by SMS to delimit the boundaries. In STR2D, there is four types of boundaries: inlet, outlet, wall, and section. The inlet is the inlet boundary condition. The outlet is the outlet boundary condition. The walls are normally external boundaries. And the sections are boundaries where the results will be outputted. The SMS full version is used to describe the following steps.

STR2D gives the options of the following boundary conditions:

- (1) Fluid
- (2) Internal Fixed Wall
- (3) Velocity Inlet
- (4) Outlet
- (5) Moving Wall
- (6) External Fixed Wall
- (7) Pressure Outlet
- (8) ASCII Section

Fluid represents the elements composing the domain. In STR2D, there are two types of walls: internal and external. There is only one type of inlet boundary condition which is Velocity Inlet, and two types of outlet boundary conditions which are the Outlet and the Pressure Outlet.

A simple rectangular channel with zero bed slope will be used to illustrate how to impose the boundary conditions. In this example, only wall, section and pressure boundary conditions are used as shown in Figure B.18.

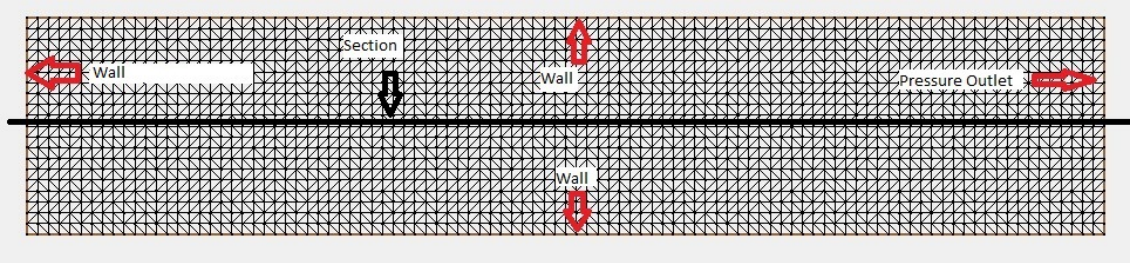

Figure B.18 Boundaries conditions

The following steps will show how to impose the boundary conditions in SMS full version. Click on the mesh file and select *Create nodestring*. In this example there will be five nodestrings that will be imposed which can be observed in Figure B.19 by squared shape located at the middle of each nodestring.

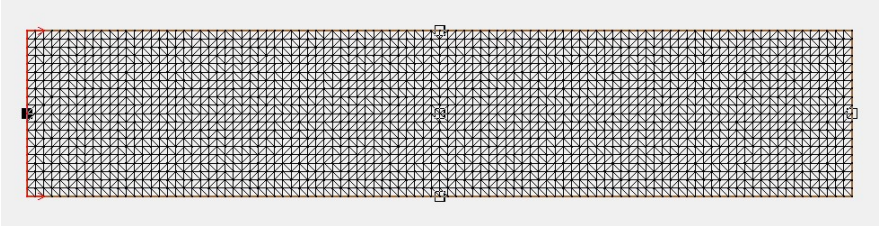

Figure B.19 Nodestrings

On the *tool bar*, under *Data* select *Switch Current Model* and click on *Generic Model*. Then, a tab named *Mesh* appears.

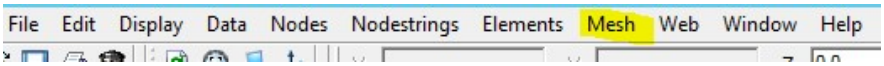

Figure B.20 Mesh Tab

Under the *Mesh* Tab, select *Define Model* and then select *Boundary Conditions*. A window called *Mesh Boundary Conditions* appears. Select the *Nodestring* tab. The name that will be written in the *Mesh Boundary Conditions* will be not of great importance. It is more a general term that can be written. Click on *Define* as shown in B.21.

Another window appears called *Definition Parameter* as shown in Figure B.22. The name that is written in this window is crucial. It is important to write the exact name as the boundary conditions listed above because these names are supported by STR2D. For the section boundary condition, it is important to check the *Legal on interior* box as shown in

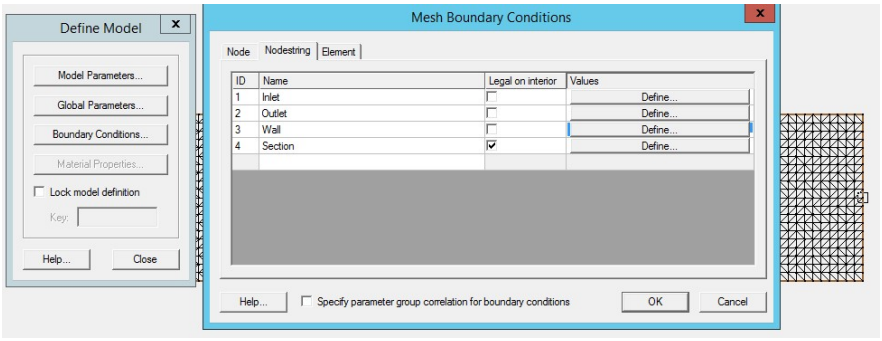

Figure B.21 Mesh Boundary Conditions Window

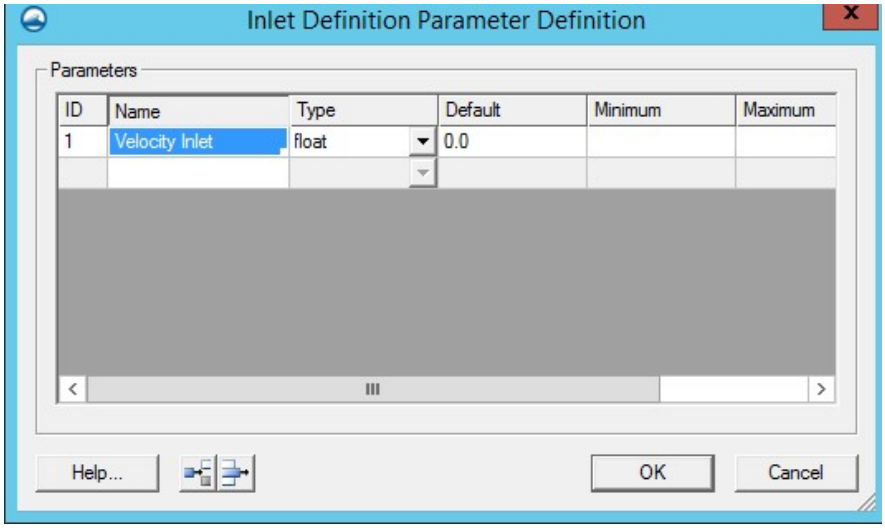

Figure B.22 Definition Parameter

Figure B.23 or else SMS will not allow the boundary condition to be inserted in the domain. Then, right click on the boundary condition and select *Assign Boundary Condition* and select the boundary condition. In this example, the left side is an *External Fixed Wall* condition, the right side is a *Pressure Outlet*, the top side is an *External Fixed Wall* and the bottom side is also an *External Fixed Wall*. Furthermore, a section boundary condition is transversally cutting the domain in which later be used to obtain results from that section.

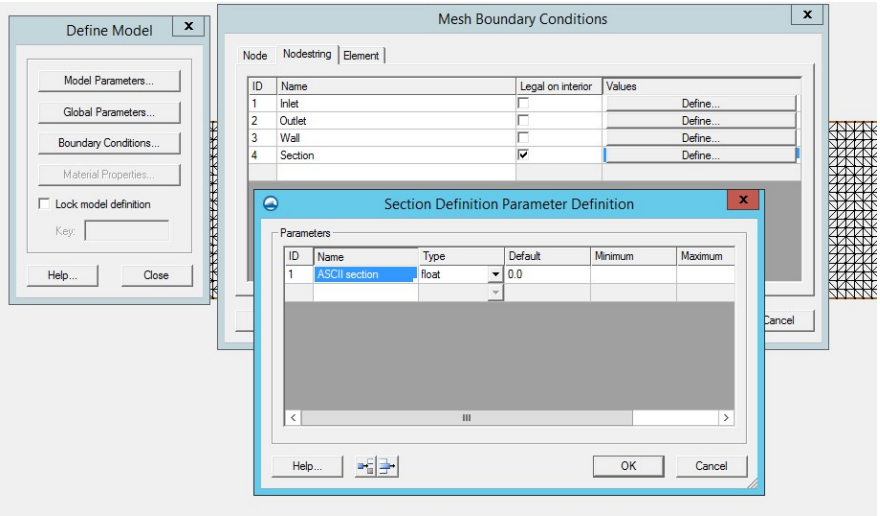

Figure B.23 Section boundary condition

B.2.1 Fdneut structure

The Fdneut file can be read originally by SF-Fluent. At first, the mesh file starts by presenting the nodal coordinates at the beginning. The fdneut file will also display the different types of groups, referred to as *entity names* in SF_Fluent code, each having their own id assigned to them.

The different entity names followed by their id are fluid (1), internal fixed wall (2), velocity inlet(3), outlet(4), moving wall(5), external fixed wall (6), pressure outlet (7), and ASCII section (8). As shown in Figure B.24, the head of the fdneut file provides the number of nodes, the number of elements, and the number of groups followed by the nodal coordinates which are the x, y and z coordinates of each nodes. The rest are not important information and are not used in the SF_Fluent program. Next, Figure B.25 shows the fluid group. The first element is made of the id nodes 61, 60 and 62. SF_Fluent only works with triangular elements which can be structured or unstructured mesh. The rest of the entity names are boundary conditions. The boundaries, such as the case of an external fixed wall as presented in Figure B.26, are made up of two nodes instead of three.

```
**FIDAP NEUTRAL FILE
TOMINAGA
VERSION   8.6

  NO. OF NODES   NO. ELEMENTS NO. ELT GROUPS          NDFCD          NDFVL
           441            920              7              2              2
  STEADY/TRANS     TURB. FLAG FREE SURF FLAG    COMPR. FLAG   RESULTS ONLY
             0              0              0              0              0
TEMPERATURE/SPECIES FLAGS
0 0 0 0 0 0 0 0 0 0 0 0 0 0 0 0
PRESSURE FLAGS - IDCTS, IPENY MPDF
        1         1         0
NODAL COORDINATES
        1    0.0000000000E+00    0.1000000000E+01    0.0000000000E+00
        2    0.5000000000E-01    0.1000000000E+01    0.0000000000E+00
        3    0.1000000000E+00    0.1000000000E+01    0.0000000000E+00
        4    0.1500000000E+00    0.1000000000E+01    0.0000000000E+00
```

Figure B.24 Section specification

```
 ELEMENT GROUPS
GROUP:        1 ELEMENTS:       800 NODES:            3 GEOMETRY:     2 TYPE:     2
ENTITY NAME:   1 FLUID
       1      61      60      62
       2      62      60      81
       3      81      59      82
       4      59      81      60
       5      82      59      58
```

Figure B.25 Fluid group

```
GROUP:        4 ELEMENTS:        20 NODES:            2 GEOMETRY:     0TYPE:   17
ENTITY NAME:    6External Fixed Wall
     841      61      62
     842      62      63
     843      63      64
     844      64      65
     845      65      66
     846      66      67
     847      67      68
```

Figure B.26 Boundary condition group

B.2.2 2dm file

The 2dm file is generated by first selecting the *Mesh file* under the *Mesh Module folder* located in the *Project Explorer*. Then, in order to save it, select on *File* in the *Menu Bar* and *save as* a .2dm file and save it in the location of your preference. The file .2dm contains the elements id 'E3T' as shown , the nodes id 'ND', and the nodestrings 'NS' id as shown in Figure B.27, Figure B.28, and Figure B.29.

```
MESH2D
MESHNAME "MESH"
NUM_MATERIALS_PER_ELEM 1
E3T 1 221 220 241 1
E3T 2 222 241 340 1
E3T 3 241 222 221 1
E3T 4 220 219 241 1
E3T 5 241 219 242 1
E3T 6 244 218 217 1
E3T 7 243 219 218 1
E3T 8 244 217 216 1
E3T 9 222 340 223 1
E3T 10 340 241 242 1
E3T 11 340 341 440 1
E3T 12 341 340 242 1
E3T 13 242 243 341 1
E3T 14 223 340 439 1
E3T 15 243 244 343 1
```

Figure B.27 Elements

The nodestrings compose the boundary conditions and the sections (which will be used to print the results from STR2D). Each line following NS can have a maximum of ten nodes. A negative value shows the end of the nodestring at the same time can represent the last nodes in the nodestring. For this tutorial, there are five nodestrings. The positive number following the negative value is the nodestring id. It is important to put the nodestring corresponding to the boundary condition of sections at the end of the file if SMS puts them somewhere else. If it is not placed at the end, then the SF-Fluent program will not run. Following the definitions of each element, node, and nodestring, the boundary condition definitions are listed as shown in Figure B.29. Then, it follows the boundary conditions description as shown in Figure B.30.

It can be observed from Figure B.29 following *BC*, are the boundary conditions specified in the *Mesh boundary condition window* as shown in Figure B.21. Next to BC_DEF corresponds to boundary condition id defined in the *Definition Parameter Window* as shown in Figure B.22.

```
E3T 3991 101 100 2121 1
E3T 3992 2121 99 2120 1
E3T 3993 2120 2021 2121 1
E3T 3994 2117 96 95 1
E3T 3995 2018 1919 2019 1
E3T 3996 2012 2111 2110 1
E3T 3997 1718 1719 1817 1
E3T 3998 1406 1405 1307 1
E3T 3999 1211 1309 1210 1
E3T 4000 1181 1280 1279 1
ND 1 0.00000000e+000 1.00000000e+000 0.00000000e+000
ND 2 5.00000000e-002 1.00000000e+000 0.00000000e+000
ND 3 1.00000000e-001 1.00000000e+000 0.00000000e+000
ND 4 1.50000000e-001 1.00000000e+000 0.00000000e+000
ND 5 2.00000000e-001 1.00000000e+000 0.00000000e+000
ND 6 2.50000000e-001 1.00000000e+000 0.00000000e+000
ND 7 3.00000000e-001 1.00000000e+000 0.00000000e+000
ND 8 3.50000000e-001 1.00000000e+000 0.00000000e+000
ND 9 4.00000000e-001 1.00000000e+000 0.00000000e+000
ND 10 4.50000000e-001 1.00000000e+000 0.00000000e+000
ND 11 5.00000000e-001 1.00000000e+000 0.00000000e+000
ND 12 5.50000000e-001 1.00000000e+000 0.00000000e+000
ND 13 6.00000000e-001 1.00000000e+000 0.00000000e+000
ND 14 6.50000000e-001 1.00000000e+000 0.00000000e+000
ND 15 7.00000000e-001 1.00000000e+000 0.00000000e+000
```

Figure B.28 Nodes

```
NS  221 222 223 224 225 226 227 228 229 230
NS  231 232 233 234 235 236 237 238 239 240
NS  -1 1
NS  1 2 3 4 5 6 7 8 9 10
NS  11 12 13 14 15 16 17 18 19 20
NS  21 22 23 24 25 26 27 28 29 30
NS  31 32 33 34 35 36 37 38 39 40
NS  41 42 43 44 45 46 47 48 49 50
NS  51 52 53 54 55 56 57 58 59 60
NS  61 62 63 64 65 66 67 68 69 70
NS  71 72 73 74 75 76 77 78 79 80
NS  81 82 83 84 85 86 87 88 89 90
NS  91 92 93 94 95 96 97 98 99 100
NS  -101 2
NS  121 120 119 118 117 116 115 114 113 112
NS  111 110 109 108 107 106 105 104 103 102
NS  -101 3
```

Figure B.29 Nodestrings list

The subroutine implemented in STR2D called mesh_transform.f95 will look for the keyword BC_DEF. The first value after BC_DEF corresponds to the boundary condition id. For instance, in Figure B.29, the Velocity Inlet id is 1), the Pressure Outlet id is 2), the ASCII section id is 3), and the External Fixed Wall id is 4).

A code was written by the author to convert SMS mesh to STR2D mesh. This code is called mesh_transform.f95 and will read the corresponding BC and BC_DEF ids.

Then, the code will look for BC_VAL which connects the boundary condition and the nodestring. BC_VAL is followed by N(node) or E(element) or S(nodestring), in this case we are working with nodestring which are denoted with S. Then, it is followed by nodestring id and then the corresponding boundary condition id. It is observed from Figure B.30, that the nodestring id 1, 2, and 4 are External Fixed Wall, the nodestring 3 corresponds to the

```
BC  1 "Inlet" 1 0 0 "(none)"
BC_DEF 1 1 "Velocity Inlet" 2 0.00000000e+000 -1.79769313e+308 1.79769313e+308
BC_DISP_OPTS 1 1 0 0 0 0 0 0 0
BC  1 "Outlet" 2 0 0 "(none)"
BC_DEF 2 1 "Pressure Outlet" 2 0.00000000e+000 -1.79769313e+308 1.79769313e+308
BC_DISP_OPTS 2 1 0 0 0 0 0 0 0
BC  1 "Section" 3 0 1 "(none)"
BC_DEF 3 1 "ASCII section" 2 0.00000000e+000 -1.79769313e+308 1.79769313e+308
BC_DISP_OPTS 3 1 0 0 0 0 0 0 0
BC  1 "Wall" 4 0 0 "(none)"
BC_DEF 4 1 "External Fixed Wall" 2 0.00000000e+000 -1.79769313e+308 1.79769313e+308
BC_DISP_OPTS 4 1 0 0 0 0 0 0 0
DISP_OPTS entity   2 0 0 0 1 0 0 0
DISP_OPTS inactive 2 0 0 0 1 0 1 0
DISP_OPTS multiple 2 0 0 0 1 0 1 0
BEFONT  2 1
MAT 1 "material 01"
MAT_MULTI 0
ENDPARAMDEF
BEG2DMBC
BC_VAL S 1 4 1 0.00000000e+000
BC_VAL S 2 4 1 0.00000000e+000
BC_VAL S 4 4 1 0.00000000e+000
BC_VAL S 3 2 1 0.00000000e+000
BC_VAL S 5 3 1 0.00000000e+000
END2DMBC
BEGCURVE Version: 1
ENDCURVE
```

Figure B.30 Boundary Condition Descriptor

Pressure Outlet and the nodestring 5 correspond to the ASCII section.

Note: it is important to check the order of the NS in Figure B.29. STR2D has a specific order to follow for the boundary condition as follow:

- (A) Fluid elements
- (B) Boundary surfaces e.g: Internal Fixed Wall, Velocity Inlet, Outlet, Moving Wall, External Fixed Wall, and Pressure Outlet
- (C) Section surfaces
- (D) Grid quality control surfaces (not in the code yet)

B.3 2dm to fdneut format

As mentioned in the previous section, the code that allows to transform the format from 2dm to fdneut is the code mesh_transform.f95. This code is already placed in the Mesh module in the subroutine mesh_sms_fdneut. The 2dm file does not provide the number of nodes, elements and group. This code uses dynamic array meaning that it will read the 2dm files and then generate vectors for the desired variables such as elements, nodes and group.

Automatically, the code considers that all elements starting with the label $E3T$ belongs to the fluid group. The code counts the number of elements from the fluid group using the COUNT_ELEM_FLUID. Furthermore, the code looks for label starting with ND and counts the number of nodes in the 2dm file using the COUNT_NODE variable.

In addition, the number of boundary condition is counted using the COUNT_BC variable. In fortran, the cursor stays at the end of the file after the reading is completed. A function REWIND is used to replace the cursor at the top of the code for a new reading of the file.

Once the code has found the fluid group, it will then find the other types of groups which are presented by the label NS. First, the code will count the number of nodestrings the 2dm file have using the variable COUNT_NS_TOT. NS_ID will store the nodestring id, which is the positive value following the negative value and COUNT_NODES_NS will store the number of nodes per nodestrings.

Now we know the number of nodes each nodestring has and the number of nodestrings. A matrix called ARRAY_NS(COUNT_NS_TOT,TOTNODES_NS) will store the nodes for each nodestrings. For example, in one nodestring (COUNT_NS_TOT =1) there may be 10 id nodes (ex:1,2,3,4,5,6,7,8,9,10).

Each nodestring in the 2dm file is placed in a horizontal and only ten nodes can be displayed per line. A nodestring ends always by a negative value. Since each nodestrings has there own nodestring id, the code will find to which boundary condition the nodestring belongs to and form a group in the fdneut file. Whereas in a fdneut file, the nodes are placed in two columns and they are separated in different groups.

Since the number of nodes for each nodestring is known, a vector called NS_ID_TEMP can be define to store the nodestring IDs following the label BC_VAL. In addition, a vector called BC_ID_TEMP is defined to store the boundary condition for each nodestring which is the value following the nodestring id's after the BC_VAL.

The BC_ID_ENTITY vector will store the boundary condition id following the label BC_DEF and the vector ENTITY_NAME will store the name of the boundary condition is important to write the name of the boundary condition in the *Definition Parameter Definition* in Figure B.6 exactly as the entity index which is used in the mesh_sms_fdneut.f95 code so that the code can recognize each of these entities. These vectors have the size of the number of boundary conditions that are declared. For example, for the dam-break tutorial, three boundary conditions each having different id numbers were declared: the External Fixed Wall, the Pressure Outlet, and the ASCII section. Thus, the vectors BC_DEF and ENTITY_NAME have a size of three.

Now, we need to identify the boundary condition for each of the nodestrings and their entity name (which is the id number of the type of boundary condition). For example, there are in total five nodestrings for the dam-break tutorial. Then the vectors BC_ID_ENTITY and ENTITY_NAME_DISPLAY will have a size of five for the dam-break tutorial. BC_ID_ENTITY vector will store the id of each nodestring and ENTITY_NAME_DISPLAY will store the entity name for each nodestring.

We will compare the BC_ID_ENTITY vector (which stored the boundary condition id declared by BC_DEF) to the BC_ID_TEMP vector (which is declared by BC_VAL and stores the boundary condition id associated to a nodestring). Then, if those two vectors are equal then the ENTITY_NAME (which is defined in the BC_DEF) gives its content to another vector called ENTITY_NAME_DISPLAY_TEMP which has the size of the number of nodestrings.

It is possible that the order of the nodestrings found in the nodestrings list is different to the one found in BC_VAL. Hence, new vectors such as BC_ID_ENTITY_DISPLAY and ENTITY_NAME_DISPLAY are created so that the boundary conditions id and the entity name have the same order.

ENTITY_INDEX is a vector that will store the seven different boundary condition used in the SF_Fluent. If the vector ENTITY_NAME_DISPLAY is equal to one of the boundary condition ENTITY_INDEX, then a new vector called ENTITY_INDEX_DISPLAY will store the id of the index entity with the same order as the other vectors.

B.4 Input File

STR2D will ask questions whether the user wants to generate a new input file or if the user has already a file the user wants to use. If the user wants to generate a new input file, STR2D will ask some questions that the user must answer in order for the code to generate an input file as shown in Figure B.31.

Figure B.31 Elements

APPENDIX C MATHEMATICAL PROOF OF THE COMPUTATION OF REAL CONCENTRATION

$$S_{e,k} = \frac{1}{L_{t,k}} \left(q^{\star}_{t,k} - \beta V_t h C_k \right) \tag{C.1}$$

$$S_{e,k} = \frac{(hC_k)^{n+1} - (hC^{int}_k)}{\Delta t} \tag{C.2}$$

$$\frac{1}{L_{t,k}} \left(q^{\star}_{t,k} - \beta V_t h C_k \right) = \frac{(hC_k)^{n+1} - (hC^{int}_k)}{\Delta t} \tag{C.3}$$

$$C^{n+1}_k = \frac{\frac{\Delta t \times q^{\star}_{t,k}}{L_{t,k}} + C^{int}_k h^{int}}{\left(1 + \frac{\beta_k V_t \Delta t}{L_{t,k}}\right) h^{n+1}} \tag{C.4}$$

When the real concentration is higher than the intermediate concentration it means there is erosion, and when the real concentration is less than the intermediate concentration, it means there is deposition.